

ORGANISATION EUROPÉENNE POUR LA RECHERCHE NUCLÉAIRE
CERN **EUROPEAN ORGANIZATION FOR NUCLEAR RESEARCH**

**The PS Complex as Proton Pre-Injector for the LHC –
Design and Implementation Report**

M. Benedikt, A. Blas, J. Borburgh, R. Cappi, M. Chanel, V. Chohan, G. Daems, A. Fowler,
R. Garoby, J. Gonzalez, D. Grier, J. Gruber, S. Hancock, C.E. Hill, A. Jansson, E. Jensen,
A. Krusche, P. Maesen, K.D. Metzmacher, R. Losito, J. Olsfors, M. Paoluzzi, J. Pedersen,
U. Raich, J.P. Riunaud, J.P. Royer, M. Sassowsky, K. Schindl, H. Schönauer, L. Sermeus,
M. Thivent, H. Ullrich, W. Van Caeter, F. Völker, M. Vretenar.

CERN, Geneva, Switzerland.

M. Barnes, E. Blackmore, F. Cifarelli, G. Clark, S. Koscielniak, F. Mammarella, A. Mitra,
R. Poirier, K. Reiniger, T. Ries.

TRIUMF, Vancouver, Canada.

Editor: M. Benedikt

ORGANISATION EUROPÉENNE POUR LA RECHERCHE NUCLÉAIRE
CERN **EUROPEAN ORGANIZATION FOR NUCLEAR RESEARCH**

**The PS Complex as Proton Pre-Injector for the LHC –
Design and Implementation Report**

M. Benedikt, A. Blas, J. Borburgh, R. Cappi, M. Chanel, V. Chohan, G. Daems, A. Fowler,
R. Garoby, J. Gonzalez, D. Grier, J. Gruber, S. Hancock, C.E. Hill, A. Jansson, E. Jensen,
A. Krusche, P. Maesen, K.D. Metzmacher, R. Losito, J. Olsfors, M. Paoluzzi, J. Pedersen,
U. Raich, J.P. Riunaud, J.P. Royer, M. Sassowsky, K. Schindl, H. Schönauer, L. Sermeus,
M. Thivent, H. Ullrich, W. Van Caeter, F. Völker, M. Vretenar.

CERN, Geneva, Switzerland.

M. Barnes, E. Blackmore, F. Cifarelli, G. Clark, S. Koscielniak, F. Mammarella, A. Mitra,
R. Poirier, K. Reiniger, T. Ries.

TRIUMF, Vancouver, Canada.

Editor: M. Benedikt

GENEVA

2000

ABSTRACT

The LHC will be supplied with protons from the pre-injector chain comprising Linac2, PS Booster and PS. These accelerators have undergone a major upgrading programme during the last five years so as to meet the stringent requirements of the LHC. This implies that many high-intensity bunches of small emittance and tight spacing (25 ns) be available at the PS extraction energy (26 GeV/c). The upgrading project involved an increase of Linac2 current, new RF systems in the PS Booster and the PS, raising the PS Booster energy from 1 to 1.4 GeV, two-batch filling of the PS, and the installation of high-resolution beam profile measurement devices. With the project entering its final phase and most of the newly installed hardware now being operational, the emphasis switches to producing the nominal LHC beam and tackling the associated beam physics problems. This report describes all the hardware changes related to the upgrading project.

FOREWORD

The LHC will be supplied with protons through the existing PS / SPS injector chain. In order to achieve the very special beam properties, a major upgrade was needed, particularly in the PS complex, where hardware modifications were required in the Linac, Booster and in the PS itself. This upgrade project was started in 1995 and all major hardware modifications are now complete and on schedule. The next phase of commissioning the beam with the required properties for the LHC is well advanced.

This project has been carried out by the PS team with major contributions from colleagues at the TRIUMF laboratory in Canada. I would like to thank them all and congratulate them for this first important step towards obtaining luminosity in the LHC.

Lyn Evans (LHC Project Leader)

CONTENTS

FOREWORD.....	V
ABBREVIATIONS.....	IX
INTRODUCTION AND SUMMARY.....	1
1. BEAM REQUIREMENTS AND FUNDAMENTAL CHOICES.....	3
1.1 LHC AND SPS REQUIREMENTS.....	3
1.2 SCHEME TO PRODUCE THE LHC PROTON BEAM IN THE PS COMPLEX.....	5
1.3 OVERVIEW OF HARDWARE CHANGES, RECENT BEAM TESTS.....	6
2. PROTON LINAC FOR LHC INJECTION.....	8
2.1 PROTON SOURCE OPTIMISATION.....	9
2.2 REPLACEMENT OF THE COCKROFT-WALTON INJECTOR BY RFQ2.....	9
2.3 LINAC RF IMPROVEMENTS.....	9
2.4 BUNCH SHAPE MEASUREMENTS AND OPTIMISATION OF THE LINAC SETTING.....	10
2.5 BEAM TRANSPORT TO THE PSB.....	10
2.6 LINAC2 PERFORMANCE.....	10
3. UPGRADING THE PSB TO 1.4 GEV – POWER SUPPLIES.....	11
3.1 MAIN MAGNET POWER SUPPLY AND REACTIVE POWER COMPENSATOR.....	11
3.1.1 <i>Topology of the upgraded main magnet supply.....</i>	<i>11</i>
3.1.2 <i>The reactive power compensation.....</i>	<i>13</i>
3.1.3 <i>The power converter groups.....</i>	<i>13</i>
3.1.4 <i>Regulation and control electronics.....</i>	<i>14</i>
3.1.5 <i>Quadrupole correction power supplies QFO and QDE.....</i>	<i>14</i>
3.2 MAIN BENDING MAGNETS “TRIM” POWER SUPPLY.....	15
3.3 PSB-PS/ISOLDE BEAM-LINE POWER SUPPLIES.....	15
3.3.1 <i>Requirements.....</i>	<i>15</i>
3.3.2 <i>Performance specification.....</i>	<i>16</i>
3.3.3 <i>Technical solution.....</i>	<i>16</i>
3.3.4 <i>Project wind up.....</i>	<i>18</i>
3.4 PULSED POWER CONVERTERS FOR THE SEPTUM MAGNETS IN THE TRANSFER LINE PSB-PS.....	18
3.4.1 <i>Operational requirements.....</i>	<i>19</i>
3.4.2 <i>Pulsed capacitors discharge power converters.....</i>	<i>19</i>
3.4.3 <i>Matching transformer and strip-line.....</i>	<i>19</i>
3.4.4 <i>Regulation and active filter.....</i>	<i>19</i>
3.4.5 <i>Characteristics of the power supplies.....</i>	<i>19</i>
4. UPGRADING THE PSB TO 1.4 GEV – OTHER SYSTEMS.....	20
4.1 PSB-PS LINE SEPTUM MAGNETS.....	20
4.1.1 <i>Vacuum tanks.....</i>	<i>21</i>
4.1.2 <i>Magnets.....</i>	<i>21</i>
4.1.3 <i>Displacement system.....</i>	<i>22</i>
4.1.4 <i>Beam screen.....</i>	<i>22</i>
4.1.5 <i>Vacuum equipment.....</i>	<i>22</i>
4.1.6 <i>Calculations.....</i>	<i>22</i>
4.1.7 <i>Measurement results and conclusions.....</i>	<i>23</i>
4.2 PSB-PS TRANSFER LINE MAGNETS.....	23
4.3 FAST KICKER SYSTEMS.....	26
4.3.1 <i>PSB ejection BE.KFA14L1 and recombination kickers BT.KFA10 and BT.KFA20.....</i>	<i>26</i>
4.3.2 <i>PSB ejection dipoles.....</i>	<i>28</i>
4.3.3 <i>PS injection and ejection kickers.....</i>	<i>29</i>
4.4 MORE POWERFUL WATER AND AIR COOLING SYSTEMS FOR THE PSB.....	29

5.	NEW RF HARMONICS TO ENABLE PS TWO-BATCH FILLING.....	31
5.1	NEW PSB RF CAVITIES $h=1$ (0.6 – 1.8 MHz).....	31
5.1.1	<i>Cavity design</i>	32
5.1.2	<i>RF amplifier chain</i>	33
5.1.3	<i>System electronics layout</i>	33
5.2	CONVERTED PSB $h=2$ CAVITIES (1.2 – 3.9 MHz).....	33
5.3	PSB BEAM CONTROL MODIFICATIONS	35
5.3.1	<i>Hardware layout</i>	35
5.3.2	<i>The transition to $h=1$</i>	36
5.4	PS BEAM CONTROL	37
5.5	REPERCUSSIONS ON OTHER PS BEAMS	38
6.	NEW RF CAVITIES IN PS TO PRODUCE LHC BUNCH SPACING.....	39
6.1	DEBUNCHING, REBUNCHING AND BUNCH ROTATION IN THE PS	39
6.1.1	<i>Low-level RF</i>	39
6.1.2	<i>Beam dynamics</i>	40
6.2	40 MHz AND 80 MHz CAVITIES.....	42
6.2.1	<i>Requirements</i>	42
6.2.2	<i>Power considerations</i>	42
6.2.3	<i>Cavity geometry</i>	43
6.2.4	<i>Fast RF feedback</i>	44
6.2.5	<i>Higher order mode damping</i>	44
6.2.6	<i>Mechanical short circuit</i>	45
6.2.7	<i>Amplifier</i>	45
6.2.8	<i>40 MHz: electric coupling</i>	46
6.2.9	<i>80 MHz: magnetic coupling</i>	47
6.2.10	<i>Tuner</i>	47
6.2.11	<i>Parameters</i>	47
6.2.12	<i>Overall system design</i>	48
7.	TRANSVERSE EMITTANCE CONSERVATION AND MEASUREMENT	49
7.1	EMITTANCE CONSERVATION ISSUES	49
7.1.1	<i>Transfer PSB to PS:</i>	50
7.1.2	<i>PS injection damper</i>	51
7.1.3	<i>Transfer PS to SPS:</i>	51
7.2	BEAM DIAGNOSTIC UPGRADES IN VIEW OF LHC BEAMS	51
7.2.1	<i>SEM-grids at PSB injection</i>	51
7.2.2	<i>The PSB fast wire scanners</i>	52
7.2.3	<i>The fast blade scanner</i>	52
7.2.4	<i>The PSB measurement line</i>	53
7.2.5	<i>The PS measurement targets</i>	53
7.2.6	<i>Non destructive profile measurement in the PS</i>	53
7.3	OTHER BEAM DIAGNOSTICS: NEW, IMPROVED, MODIFIED	53
8.	POSSIBLE FUTURE DEVELOPMENTS.....	55
8.1	MEANS TO ACHIEVE THE SPECIFIED LONGITUDINAL BEAM PARAMETERS	55
8.1.1	<i>Status of performance</i>	55
8.1.2	<i>Multiple splitting</i>	55
8.2	OTHER IMPROVEMENTS.....	57
8.2.1	<i>Bunching factor at low energy</i>	57
8.2.2	<i>Special beam time structure for handling electron clouds in the LHC</i>	57
	ACKNOWLEDGEMENTS	57
	APPENDIX: LIST OF RELEVANT PARAMETERS	59
	REFERENCES.....	61

ABBREVIATIONS

AC	Alternating Current
AD	Antiproton Decelerator
ADC	Analogue to Digital Converter
CAMAC	Computer Automated Measurement And Control (IEEE standard)
DC	Direct Current
DCBCT	DC Beam Current Transformer
DCCT	DC Current Transformer
DDS	Direct Digital Synthesiser
DSC	Device Stub Controller
DSP	Digital Signal Processor
FODO	Focusing lattice structure
HF	High Frequency
HLM	High Loss Mode
HOM	Higher Order Mode
HV	High Voltage
IGBT	Insulated Gate Bipolar Transistor
LHC	CERN Large Hadron Collider
Linac2	CERN 50 MeV proton linear accelerator
MD	Machine Development
MP	MultiPactor
PA	Power Amplifier
PFN	Pulse Forming Network
PLC	Programmable Logic Controller
ppb	protons per bunch
PPM	Pulse to Pulse Modulation
ppp	protons per pulse
PS	CERN Proton Synchrotron
PSB	CERN Proton Synchrotron Booster
QDE	Defocusing quadrupole magnets of the PSB
QFO	Focusing quadrupole magnets of the PSB
RF	Radio Frequency
RFQ	Radio Frequency Quadrupole
SEM	Secondary Emission Monitor
SMPS	Switch Mode Power Supply
SPS	CERN Super Proton Synchrotron
TCR	Thyristor Controlled Reactor
VME	VERSAmodule Eurocard (industrial standard computer bus)

INTRODUCTION AND SUMMARY

CERN's Large Hadron Collider (LHC) [1] will be supplied with protons from the injector chain Linac2 - Proton Synchrotron Booster (PSB) - Proton Synchrotron (PS) - Super Proton Synchrotron (SPS), shown in Fig. 1. These accelerators are in the process of being upgraded so as to meet the very stringent needs of the LHC: many high intensity proton bunches (2835 per LHC ring) with small transverse and well defined longitudinal emittances. The main challenges for the PS complex are (i) the unprecedented transverse beam brightness (intensity/emittance), almost twice the one the PS was able to produce so far, and (ii) the production of bunches with the LHC spacing of 25 ns before extraction from the PS (26 GeV/c). A scheme was proposed [2] which implies new Radio Frequency (RF) harmonics in the PSB (1, 2) and PS (8, 16, 84), an increase of the PSB energy from 1 to 1.4 GeV, and two-batch filling of the PS. After a successful (partial) test of the scheme's main ingredients in 1993, a project of converting the PS complex for LHC was started in 1995 and its completion is scheduled for early 2000. Major parts of this project are (i) new $h=1$ RF systems in the PSB, (ii) upgrading of the PSB main magnet supply from 1 to 1.4 GeV operation, (iii) new magnets, septa, power supplies, kicker pulsers for the PSB-PS beam transfer, (iv) new 40 and 80 MHz RF systems in the PS, (v) beam profile measurement devices with improved resolution. About one quarter of the project resources (funds, manpower) is provided by TRIUMF under the Canada-CERN Co-operation Agreement on the LHC.

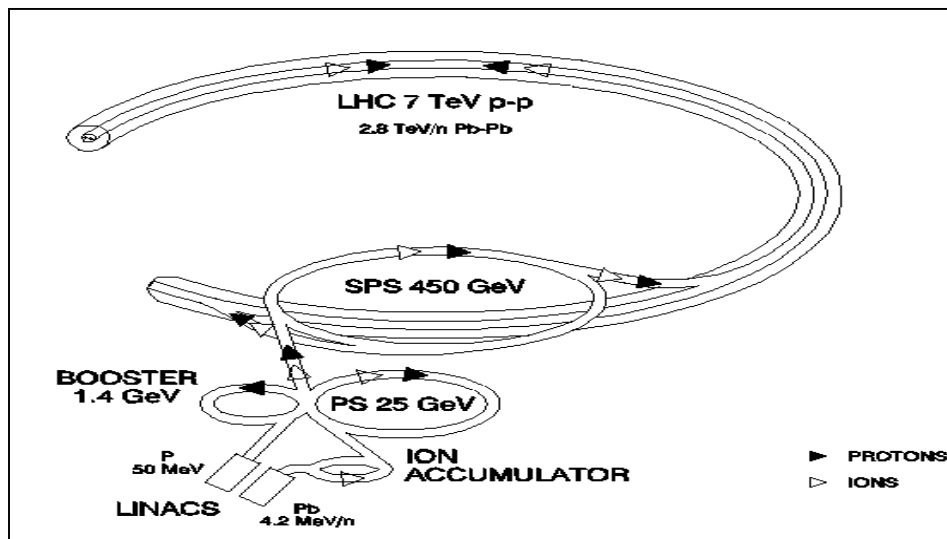


Fig. 1 The LHC injector complex.

The SPS, LHC's injector synchrotron, has to deal with two major issues: (i) maintaining the high-density bunches stable during acceleration, implying an elaborate programme for impedance reduction, (ii) keeping the transverse emittance blow-up within very tight tolerances. The upgrading of the SPS as LHC injector has been presented in a Design Report [3] and the project has been launched recently. Yet, some of the basic decisions depend on studies still to be done with LHC-type beams from the PS, which was the main reason to get the PS conversion started so much earlier.

An overview of the PS conversion as well as the beam dynamics issues involved are presented in Chapter 1 together with older (1993) and more recent results of beam tests. Note that upgrading of the PS complex as a heavy ion pre-injector for LHC is not treated in this Design Report.

Measures to even further improve the proton beam intensity (aiming at 180 mA) and brilliance from Linac 2 are outlined in Chapter 2.

Increasing the beam energy of the PSB by 40 % (momentum by 26 %) to 1.4 GeV calls for renewal or overhaul of several systems and components, such as the main magnet supply (including transformers and chokes), the PSB-PS 4-level recombination and transfer line magnets and their DC or pulsed power supplies, the pulsed magnetic septa and fast kicker pulsing systems, and the water and air cooling system to tackle the increased power dissipation. Chapter 3 deals with the

new/upgraded power supply systems, whereas new magnets, septum magnets, kicker pulsers and water cooling are discussed in Chapter 4.

Operating each of the four PSB rings with just one bunch opens up the way for PS two-batch filling. The new $h=1$ and converted $h=2$ cavities as well as the digital beam control systems dealing with the new harmonic numbers in PSB ($h=1, 2$) and PS ($h=8, 16$) are presented in Chapter 5, which also touches upon the repercussions of these changes on other operational beams of the complex.

Short (< 4 ns) bunches with 25 ns spacing are produced in the PS by fixed-frequency RF cavities (one at 40 MHz with 300 kV, and two at 80 MHz with 300 kV each) which have to withstand the beam loading of much higher intensity beams without perturbing them. The cavities, their driving systems as well as the elaborate non-adiabatic procedure to achieve the short bunch length (including results of extensive beam tests) are dealt with in Chapter 6.

The LHC beam features transverse emittances which are unusually small and have to stay so through the injector chain. Small amounts of mis-steering and mismatch between the accelerators of the chain, virtually negligible for normal operation, are becoming increasingly important, and their effect has to be measurable, calling for high-resolution beam profile monitors. Moreover, various position measurement systems are modified to deal with the new harmonics (rings) or to allow bunch-by-bunch observation (TT2). The new or modified diagnostic devices are summarised in Chapter 7 which also deals with work on an injection oscillation damper for the PS.

Finally, Chapter 8 gives a glimpse of possible future developments which may avoid some of the difficulties which have already been identified in beam tests.

A comprehensive parameter list of the PS complex as LHC proton injector is compiled in the Appendix.

1. BEAM REQUIREMENTS AND FUNDAMENTAL CHOICES

1.1 LHC and SPS requirements

The figure of merit for colliders such as the LHC is the luminosity

$$L = \frac{k_b N_b^2 f_{\text{rev}} \gamma}{4\pi \epsilon_n \beta},$$

with k_b the number of bunches per ring, N_b the number of protons per bunch, f_{rev} the revolution frequency, ϵ_n the normalised rms transverse beam emittance (same in both planes), β the beta-function at the interaction point. L is proportional to the number of events per second and has thus to be maximised. But more conditions are to be satisfied: (i) the beam emittance has to fit into the small aperture of the superconducting LHC magnets; (ii) the total intensity $k_b N_b$ is limited by the thermal energy produced by synchrotron radiation which must be absorbed by the cryogenic system; (iii) the beam-beam effect – proportional to the transverse beam brightness N_b/ϵ_n - causing a spread in betatron tunes (“footprint”) when the beams are colliding has to be kept below a certain limit; (iv) the space-charge limit in the injectors, which also scales with N_b/ϵ_n . Conflicting requirements also determine the longitudinal emittance ϵ_L which has to be small at injection (small $\Delta p/p$ to ease beam transport from the SPS through the two ~ 2.5 km long lines), but large at collision to avoid transverse emittance blow-up by intra-beam scattering.

An elaborate optimisation procedure, taking into account these boundary conditions, has resulted in the LHC beam parameter set [1] compiled in Table 1. The “ultimate” performance level corresponds to the LHC beam-beam limit, whereas the “nominal” performance combines high luminosity with operational margin. Moreover, during the first year of physics running the LHC will be operated at a much lower intensity and luminosity level (“initial”).

Table 1
LHC nominal, ultimate, initial proton beam parameters.

			Injection	Collision	
Energy		[GeV]	450	7000	
Luminosity	nominal ultimate initial	[cm ⁻² s ⁻¹]		10 ³⁴ 2.5 10 ³⁴ 10 ³³	
Number of bunches			2835		3564 bunch places
Bunch spacing		[ns]	24.95		
N_b intensity per bunch	nominal ultimate initial	[p/b]	1.1 10 ¹¹ 1.7 10 ¹¹ 1.7 10 ¹⁰		
Beam current	nominal ultimate initial	[A]	0.56 0.87 0.087		
ϵ_n (transverse emittance, rms, normalised), nominal & ultimate		[μm]	3.6	3.75	Emittances equal in both planes. small blow-up allowed in LHC
ϵ_n (transverse emittance, rms, normalised), initial		[μm]	0.9	1.0	
Longitudinal emittance, total		[eVs]	1.0	2.5	Controlled blow-up during accel. has to fit into 400 MHz buckets
Bunch length, total (4σ)		[ns]	1.7	1.0	
Energy spread, total (4σ)		[10 ⁻³]	1.9	0.45	

Much like the PS complex, the SPS is an “old” machine and was not optimised for its future function as LHC injector. The intensity the SPS is able to accelerate ($\sim 4 \cdot 10^{13}$ protons/cycle, particularly difficult if concentrated on 3/11 of its circumference) limits the number of PS pulses per

SPS cycle to three. The momentum spread acceptance of the PS-SPS line (TT2, TT10) is about $\pm 0.2\%$ in $\Delta p/p$, while the total bunch length has to be below 4 ns to fit into the buckets of the SPS 200 MHz accelerating system, that is a longitudinal emittance of 0.35 eVs per PS bunch. Owing to the SPS's large longitudinal broad-band impedance, such bunches are intrinsically unstable (longitudinal micro-wave instability) when injected: an SPS impedance reduction programme is in progress. While the longitudinal emittance will be increased (hopefully in a controlled way) from 0.35 to 1 eVs during SPS acceleration, there is little margin for (undesirable) transverse emittance blow-up in this machine.

Table 2
Beam characteristics at extraction from the PS.

Proton momentum	[GeV/c]	26	
Number of PS batches to fill SPS		3	Limited by SPS peak intensity
PS repetition time	[s]	3.6	PS 2-batch filling from PSB
Number of bunches in PS		84	81 to SPS, 3 "killed" by extr. kicker
Bunch spacing	[ns]	24.97	
Number of protons/bunch N_b –			
<i>ultimate</i>		$1.7 \cdot 10^{11}$	
<i>nominal</i>		$1.1 \cdot 10^{11}$	
<i>initial</i>		$1.7 \cdot 10^{10}$	
Transverse normalised rms emittance ϵ_n	[μm]	3.0 0.8	Brightness N_b/ϵ_n of <i>initial</i> beam smaller than <i>nominal</i> and <i>ultimate</i>
Bunch area (longitudinal emittance) ϵ_L	[eVs]	0.35	
Bunch length (total)	[ns]	4	Limited by SPS 200 MHz buckets
Relative momentum spread $\Delta p/p$ total (4σ)		0.004	Limited by TT2-TT10 acceptance

The LHC and SPS requirements define the beam characteristics at PS extraction (Table 2). The filling sequence PS-SPS-LHC is sketched in Fig. 2.

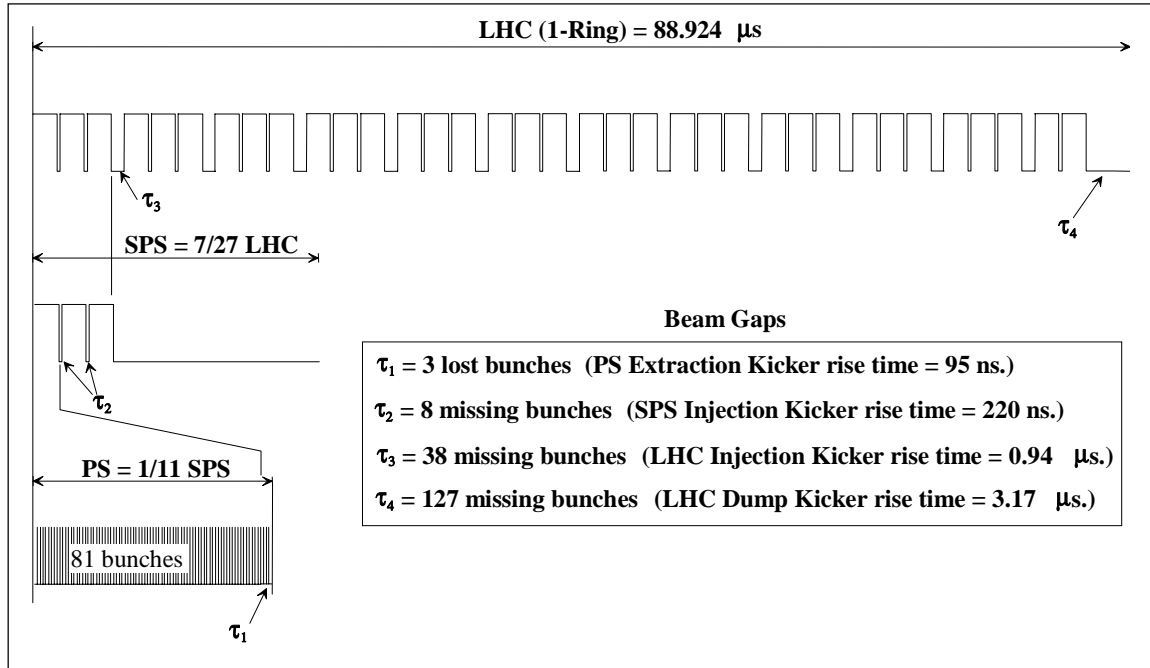


Fig. 2 Proton bunches in the PS, SPS and one LHC ring. Note the partial filling of the SPS (3/11) and the holes due to kicker rise-times. One LHC ring is filled in 3 min.

1.2 Scheme to produce the LHC proton beam in the PS complex

While the intensity required for LHC is well within the capabilities of the PS complex, the transverse emittance is very small, yielding a beam brightness N_b/ϵ_n about 1.6 times higher than was hitherto achievable. Low-energy synchrotrons suffer from space charge which can be quantified by the tune shift

$$\Delta Q \propto -\frac{N}{(\beta\gamma^2)_{\text{rel}} \epsilon_n},$$

where N is the number of protons in the synchrotron. This tune shift would become unmanageable in the PSB at 50 MeV (almost -1) and in the PS at 1 GeV. The measures to overcome this fundamental limitation are (i) filling the PS with two PSB pulses, thus halving the intensity per pulse and thus ΔQ at 50 MeV; (ii) raising the PS injection energy from 1 to 1.4 GeV, thus decreasing ΔQ in the PS by a factor 1.5 ($1/\beta\gamma^2_{\text{rel}}$).

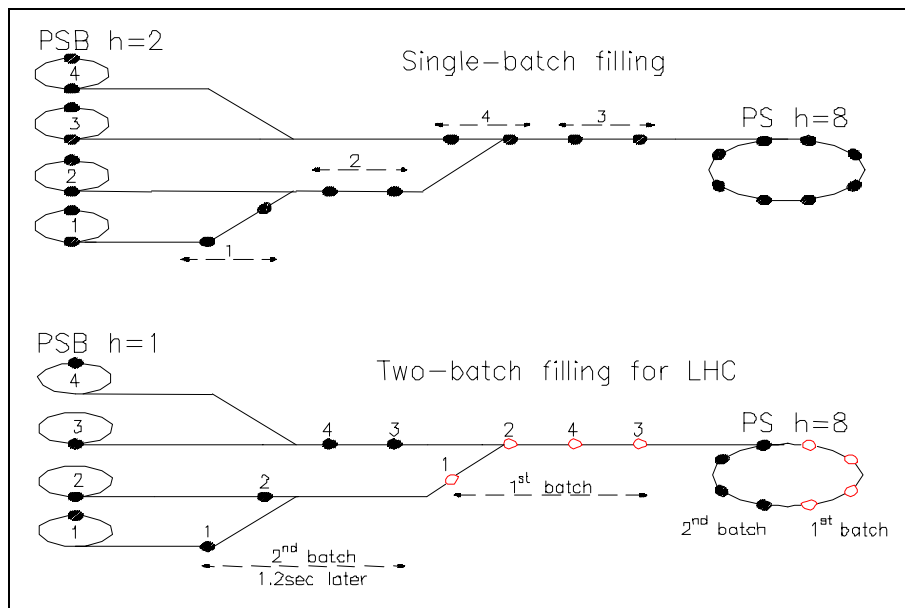


Fig. 3 PSB-PS transfer schemes: PS single-batch filling for SPS physics (top), PS two-batch filling for LHC (bottom).

The four PSB rings, $1/4$ of the PS circumference each, are normally ejected and transferred sequentially to fill the PS in one go, e.g. for the SPS Physics beam with two bunches per ring (5 bunches per ring until 1997). However, with only one bunch per ring, the four bunches can be squeezed into $1/2$ of the PS, thus leaving space for a second PSB batch 1.2 seconds later (Fig. 3).

To operate with RF harmonic 1 instead of the former 5, the PSB is now equipped with new RF cavities featuring a frequency range of 0.6 to 1.7 MHz, and the former $h=5$ systems have been modified to work on $h=2$. Also the PS has to cope with new RF harmonics (8, 16) – an opportunity to equip both machines with Digital Beam Control.

For raising the PSB ejection/PS injection energy from 1 to 1.4 GeV (+26.3 % in momentum), the PSB main power supply has been upgraded to cope with the higher magnet currents. The elements of the PSB-PS beam transport have to provide higher field levels, which meant renewal of most of the magnets (dipoles, quadrupoles, septa, kickers) and their power supplies.

The LHC bunches with 25 ns spacing are generated at the 26 GeV/c ejection flat top in the PS: sixteen bunches are adiabatically debunched, followed by recapture on $h=84$ by a new 40 MHz cavity. Two 80 MHz systems finally shorten the bunches to 4 ns so as to fit into the SPS 200 MHz buckets. Out of the 84 bunches, 81 are transferred to the SPS, 3 are supposed to be lost due to the extraction kicker rise-time.

A partial test of the main ingredients of the upgrading project was carried out in 1993 [4]. One single bunch ($h=1$) was accelerated in ring 3 to 1.4 GeV, transferred to the PS, accelerated in the PS on $h=8$ to 26 GeV/c, and ejected to the TT2 line. Also two-batch filling of the PS was tried. Already earlier, the proton current from Linac2 had been increased to unprecedented 160 mA by installation of a 750 keV Radio Frequency Quadrupole (RFQ). For this test, the hardware has been prepared as prototypes and low magnet cycling rates were used to avoid undue heating. The transverse emittances were measured along the chain, for both *nominal* and *ultimate* intensities, and both 1 GeV and 1.4 GeV PSB energies (Table 3).

Table 3
Normalised rms emittances measured at PS transfer energy of 26 GeV/c in the ring (wire scanner) and in TT2 (SEM-fils) during the 1993 test.

p/bunch before debunching	p/LHC bunch	PS Injection Energy [GeV]	$(\epsilon_{n,x}+\epsilon_{n,y})/2$ in PS at 26 GeV/c [μm]	$(\epsilon_{n,x}+\epsilon_{n,y})/2$ ejected beam in TT2 [μm]
1.15 10^{12} (<i>nominal</i>)	1.1 10^{11}	1	2.1	1.8
		1.4	1.7	1.6
1.80 10^{12} (<i>ultimate</i>)	1.7 10^{11}	1	3.3	3.0
		1.4	2.7	2.5

The higher PS injection energy clearly yields smaller emittances, in particular for the ultimate intensity. The transverse emittance is well below 3 μm for the nominal beam, but only marginally for the ultimate beam. One expects a somewhat less favourable situation with beams from four PSB rings. Note the differences between the two devices, showing that improving/adding of beam profile monitors is an issue of major importance for the small-sized LHC-type beams.

1.3 Overview of hardware changes, recent beam tests

Encouraged by this conclusive test, a project to convert the PS complex to an LHC pre-injector was launched in 1995, based on a project proposal which included budget and manpower estimates [5]. Also in 1995, Canada offered in-kind contributions for the LHC machine (via TRIUMF/Vancouver), which soon developed into an efficient collaboration, with TRIUMF providing $\sim 1/4$ of the resources needed for the PS upgrading project. Major systems and their hardware components are compiled in Table 4, together with Canadian contributions and installation dates. The project will be finished by 2000.

Already in 1999, beams with the LHC intensity and bunch spacing were made available, enabling the SPS to be investigated under LHC conditions. Albeit very useful, these beams are not yet completely nominal:

- transverse emittances are somewhat too large at nominal intensity; double-batch filling is indispensable to reach them;
- the debunching-rebunching procedure suffers from excessive blow-up in momentum spread at nominal intensity, resulting in bunch length > 4 ns.

Nevertheless, a series of machine studies in autumn 1999 dealt with producing an LHC beam with nominal intensity and transverse beam emittances (but not the bunch spacing) by using all four PSB rings and two-batch filling of the PS at 1.4 GeV. Meaningful profile measurements for these small-size beams were available in the PS machine and the TT2 line, but not in the PSB (new instruments to be installed in 2000). The PS beam intensity accelerated and ejected was $9.2 \cdot 10^{12}$, corresponding to 84 LHC bunches, that is $1.1 \cdot 10^{11}$ p/bunch, the nominal LHC bunch intensity. Figure 4 illustrates the evolution of the normalised rms emittances $\epsilon_{n,x}$ and $\epsilon_{n,y}$ along the acceleration in the PS machine. The beam is virtually round (as it should be) and emittances vary between 1.9 and 2.4 μm , well below the PS limit of 3 μm . This result is rather consistent with those of 1993, allowing for some emittance increase in the intricate recombination of four levels to one level in the PSB-PS line when working with all rings. Residual transverse injection errors of 1-2 mm were observed in the

PS, but they will be corrected to a large extent by the transverse dampers (both planes) which are being fabricated.

Table 4
Major hardware components of the “PS Conversion for LHC” project.

System	Components	Installation	TRIUMF contribution	Comments
Linac	Inter-tank beam shape monitors (2)	1999, 2000		study very high intensities (180 mA)
50 MeV line	laminated quadrupoles	1997	two magnets	correct optics for protons and ions
PSB RF $h=1$	rf cavities “C02” (4), tune range 0.6-1.7 MHz	1998	ferrites, HV power supplies	one cavity per ring
PSB RF $h=2$	rf cavities “C04” (4), tune range 1.2-3.9 MHz	1998		bunch flattening and/or splitting
PSB main magnet supply	double-transformers (5), VAR compensator, quadrupole trim supplies, control circuitry	1998	all transformers, VAR compensator	26 % increase of magnet current on PSB main magnets
PSB water cooling	closed-circuit demineralised water	2000		cope with more heating at 1.4 GeV
PSB instrumentation	fast wire scanners (4 rings, H+V, + 2 spares)	2000?	design, fabrication of 10 units	standard PS beam profile meas. device
	fast blade profile monitor prototype	2000	design and fabrication	measures amplitude profile
	Q-measurement: electronics, kicker pulser	1999/2000		all four beams are kicked
PSB-PS beam transport	ejection/recombination kicker pulsers (6)	1998, 1999		26 % more kick to cope with 1.4 GeV
	ejection, recombination, PS injection septa + power supplies (8)	1997, 1998, 1999		half-sine-wave pulses of 3.5 ms
	15 laminated magnets (vertical bending magnets, quadrupoles, correction dipoles)	1997, 1998	all 15 magnets all (+spare) power supplies	allow pulse-to-pulse modulation between 1.4 GeV (PS) and 1 GeV
PS RF $h=84$	300 kV fixed-frequency (40 MHz) cavities (1+1 spare installed) “C40”	1996, 1999	model studies, tuners, higher-order-mode dampers, HV supplies	for generating LHC bunch spacing of 25 ns at 26 GeV/c
PS RF $h=168$	300 kV fixed-frequency (80 MHz) cavities (2+1 spare installed) “C80”	1998, 1999		for shortening the LHC bunches to 4 ns
PS transverse feedback	new amplifiers, deflector, electronics	2000/01		damping injection oscillations and instabilities
PS instrumentation	wide-band position monitors (2) in line TT2	1998		bunch-by-bunch position measurement

All beams need further studies, in particular the “initial” beam and the conservation of its small emittance throughout the chain (encouraging results have been obtained in the PSB in 1999).

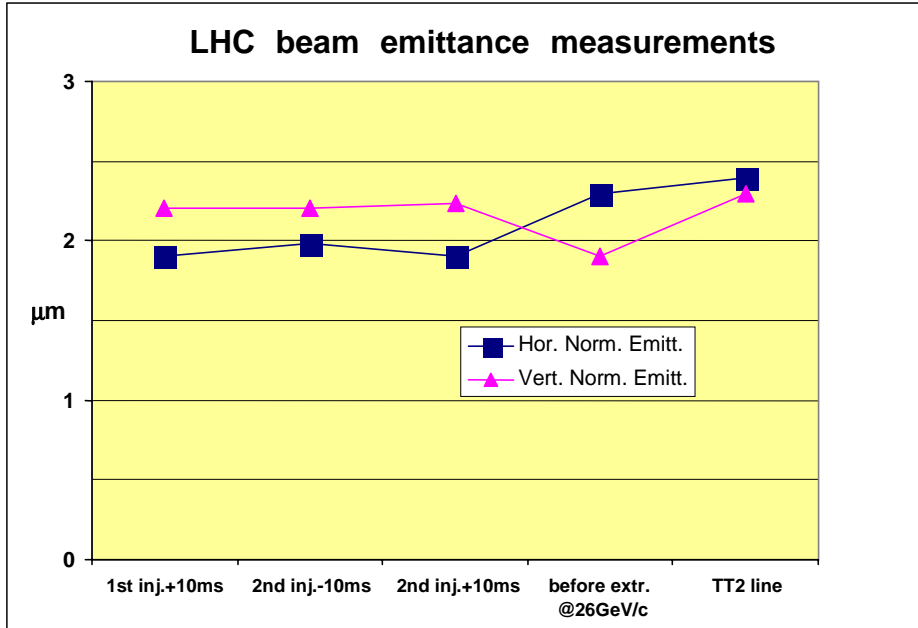


Fig. 4 LHC beam with nominal intensity ($9.2 \cdot 10^{12}$ p, that is $1.1 \cdot 10^{11}$ p/LHC bunch) in the PS, November 1999: Transverse normalised emittances at various stages of acceleration and in TT2. Nominal emittance at PS extraction: $3 \mu\text{m}$.

2. PROTON LINAC FOR LHC INJECTION

Linac2 has been the primary source of protons for the CERN accelerator complex for the last 20 years, and over the past few years the machine performance has been steadily improved in anticipation of the demands that will be made on it in the LHC era [6]. The nominal LHC requirement will be for a beam of 180 mA by $30 \mu\text{s}$, i.e. 20 % higher proton current than the Linac2 design value of 150 mA, inside the same emittances. Figure 5 shows the increase of the Linac2 operational current and of the high intensity test current delivered to the PSB over recent years, with the corresponding steps taken. A description of these improvements is presented in the following paragraphs.

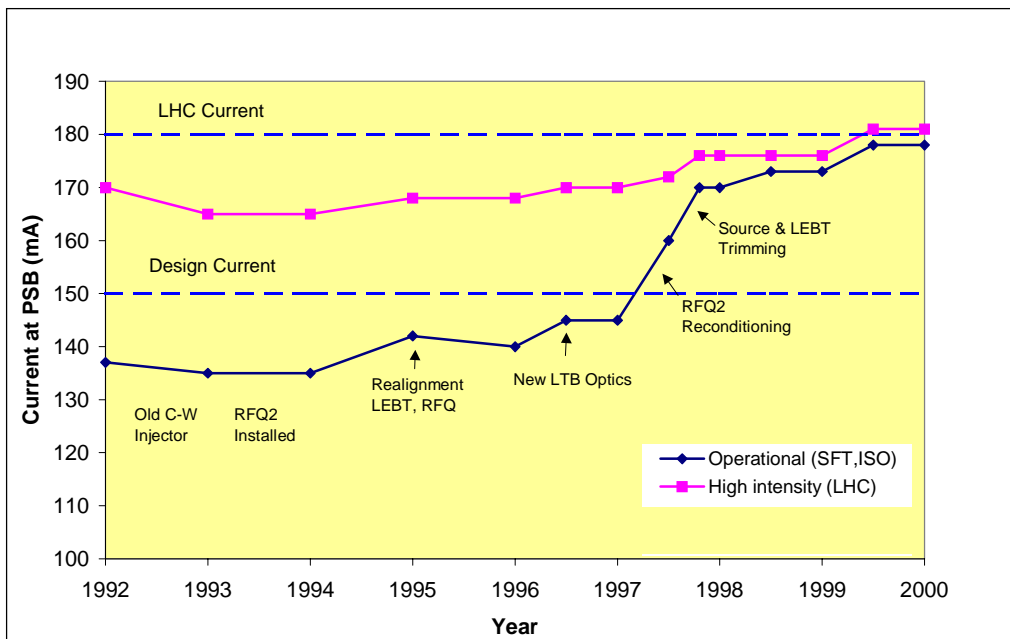


Fig. 5 Evolution of Linac2 operational and high intensity beam current measured at PSB entry.

2.1 Proton source optimisation

The total beam out of the Linac2 duoplasmatron source is around 300 mA with a hydrogen consumption of about 6 ml/min. The gauge pressure of approximately $3.5 \cdot 10^{-5}$ mbar in the source housing falls to the high 10^{-7} level in the RFQ. With this relatively high pressure in the beam transport section between source and RFQ neutralisation is very high, making the effective focusing strength of the solenoids in the line highly dependent on the gas flow from the source. Once this process was understood, gains in intensity of around 10 % were obtained by iterative re-optimisation of source parameters and solenoid focusing strengths.

2.2 Replacement of the Cockroft-Walton injector by RFQ2

The main intensity bottlenecks in the original layout of Linac2 were the space charge limited 750 keV Cockroft-Walton injector and the long transfer line to the linac. In 1993 they were replaced by a new 90 kV platform and a 750 keV RFQ2 with compact (<1 m long) beam matching lines, designed for 200 mA current. After the RFQ installation, the linac was immediately able to provide 135 mA for the normal operation and a beam of 165 mA with standard emittances for high intensity studies [7].

A first increase in the RFQ2 current was obtained in 1995 with a careful realignment of the system. After a complete set of source emittance measurements, the source was re-aligned on the measured beam axis instead of the mechanical axis, and then the solenoids between the source and the RFQ were as well aligned on their magnetic, not on their mechanical axes [8]. After this, the RFQ could be properly aligned, its transmission was increased by about 5 % and the number of RF breakdowns (induced by ions hitting the electrodes) was reduced.

The next step towards higher RFQ current was a slow re-conditioning of the RFQ cavity during operation at the linac. In order to accelerate a space charge dominated beam of 200 mA, the RFQ was designed for a high electrode voltage, 178 kV, resulting in a peak surface electric field of more than twice the Kilpatrick limit [9]. The operation at this high field level was initially plagued by a high RF breakdown rate, which let the RFQ operate reliably only up to 92 % of the design level, resulting in a 10 % reduction in beam transmission. The origin of the breakdowns was finally traced to backstreaming oil vapours from a defective drag pump in the RFQ vacuum system that enhanced field emission from the electrodes and finally started the breakdowns. After replacement of the pump, steady operation at high field level in the following years slowly eliminated the hydrocarbon from the electrodes and the RFQ was reconditioned in small steps from 92 % up to 100 % of the nominal level during normal operation [10]. As a result, the current delivered by the linac increased from 145 to 160 mA.

2.3 Linac RF improvements

Allowing for 5 % beam losses in the transfer line, 180 mA at the PSB entry correspond to 190 mA out of the linac. Adding up the beam power corresponding to this current, the copper power and a margin for phase and amplitude control, tuning precision and amplifier balancing, about 2.7 MW per Linac2 final RF amplifier will be needed, i.e. 10 % more than their design power. An upgrade programme has been gradually applied to the RF chains to increase their output power. In fact, the final amplifier tubes (TH170R), rated at 2.5 MW for a duty cycle greater than that used at Linac2, can deliver more provided that enough drive power is available. For this, an additional amplifier stage was added in the Tank 1 chain, which suffers the heaviest beam loading, and modern 4.5 kW solid state amplifiers replaced ageing tube pre-amplifiers in all chains. These more reliable transistor amplifiers also contribute to a decrease in the linac fault rate. Great attention has also been given to the correct adjustment of the feedback loops, which have not only to compensate for an increased beam loading but also have to stabilise amplifiers that are often working in the non-linear region close to saturation.

2.4 Bunch shape measurements and optimisation of the linac setting

Particular care was given to minimising the losses inside the linac tanks. This required a complete set of measurements for the re-optimisation of the working point (phase and amplitude setting) for the three linac tanks. These measurements were performed using the longitudinal emittance measurement line and the new bunch shape monitors that give the bunch density distributions in the three geometrical planes and their variations along the beam pulse [11]. Some careful optimisation of the quadrupole setting was also necessary.

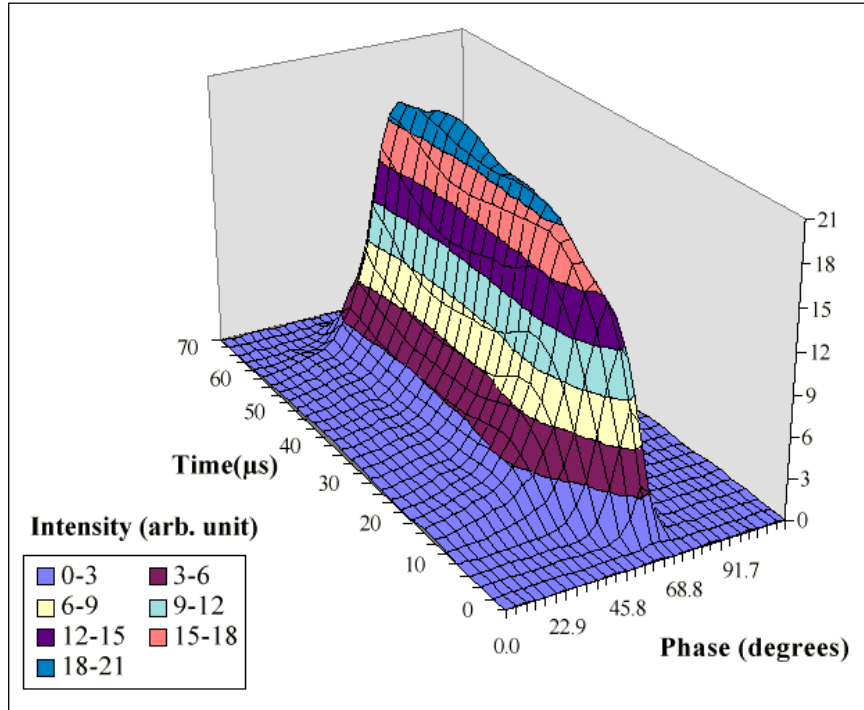


Fig. 6 Bunch shape evolution along the beam pulse as measured by the Bunch Shape Monitor.

2.5 Beam transport to the PSB

The 80 metres long high current beam line between the Linac2 and PSB uses 20 quadrupoles, 2 bending magnets, 8 steering magnets, and a debuncher cavity together with eight position pick-ups and two emittance measurement lines. For the needs of the high current beam, this line has been simulated and re-optimised. The beam is strongly space charge dominated at the beginning of the line and becomes emittance dominated after about 50 metres. The focusing of the line was modified to provide a “quasi” FODO system with constant phase advance per focusing period, an arrangement that turned out to be the most convenient for optimising transmission and beam qualities whilst minimising the sensitivity to steering by the stray field of the PS.

2.6 Linac2 performance

The result of the installation of the new injector and of many improvements to the source, RF, optics and diagnostics of Linac2 and its transfer lines is the achievement of test currents up to 183 mA and the parallel improvement of the operational current (for SPS and ISOLDE) up to 178 mA. This makes Linac2 the highest intensity ion linear accelerator in the world (peak current). No limitations are observed in the pulse length, making it possible for the linac to produce high intensity beams of up to 120 μs. The transverse emittances at high intensity are about the same as at low intensity (140 mA). A summary of Linac2 beam parameters at 180 mA current is reported in Table 5, while Table 6 shows the measured beam currents and transmissions for the different elements of the Linac2 accelerator.

The losses, mainly concentrated in the RFQ and the first tank of the Linac, are due to space charge effects, as predicted by beam dynamics simulations.

Table 5
Characteristics of LHC proton beam from Linac2.

Parameter	LHC Specification	Achieved	
Current during pulse	180	182	mA
Pulse length	30	>100	μ s
Transverse norm. rms emittance	1.2	1.2	μ m
Momentum spread ($\pm 2\sigma$)	± 0.15 %	± 0.15 %	

Table 6
Output beam current and transmission at high intensity (180 mA) for the different elements of Linac2.

	Output Current	Transmission
Source	360 mA (p^+, H_2^+)	
RFQ	204 mA	~ 86 %
Linac tank 1	194 mA	95 %
Linac tanks 2 and 3	190 mA	98 %
Transfer line to PSB	180 mA	95 %

3. UPGRADING THE PSB TO 1.4 GEV – POWER SUPPLIES

3.1 Main magnet power supply and reactive power compensator

The output energy of the PSB is increased from 1 to 1.4 GeV. This implies an increase of the magnetic field by about 26 % to 0.87 Tesla, which is obtained by raising the coil current of the main magnets. The rms current is raised from 2000 A to 2300 A and the peak current from 3300 A to 4050 A at a maximum magnet voltage of nearly 3500 volts (the magnet circuits are tested up to 10 kV).

The main magnets power supply has to cope with a significant increase of the peak power (from 8 to 14 MVA for the LHC cycle) making the redesign of the rectifier transformers and the reactive power compensation system necessary in order to keep the line voltage variations to a minimum.

The upgrade [12] allowed the phasing out of the old polychlorinated biphenyl filled transformers and reactors in compliance with Swiss legal requirements.

3.1.1 Topology of the upgraded main magnet supply

The PSB main magnets are powered from the 18 kV line directly without energy storage. A high power fast-pulsed power supply (14 MVA peak power, 1.2 s repetition rate) feeding an inductive load and operated directly from the utility power lines presents a dynamic load that causes voltage and phase variations in the transmission system. The amount of disturbance is directly proportional to the dynamic load and inversely proportional to the short circuit capacity of the power system.

To minimise these effects on the AC lines and to increase the DC performance of the load, the PSB power supply is built as a series connected group of four 12-phase rectifier modules with freewheeling thyristors connected to the star point of the transformers. This circuit arrangement has the advantage of requiring less reactive power on the AC side. With respect to a normal 12-phase-bridge, it significantly reduces the output ripple on the DC load. Therefore, a smaller passive ripple filter can be used. The power system scheme is shown in Fig. 7 and the 1.4 GeV magnet cycle in Fig. 8.

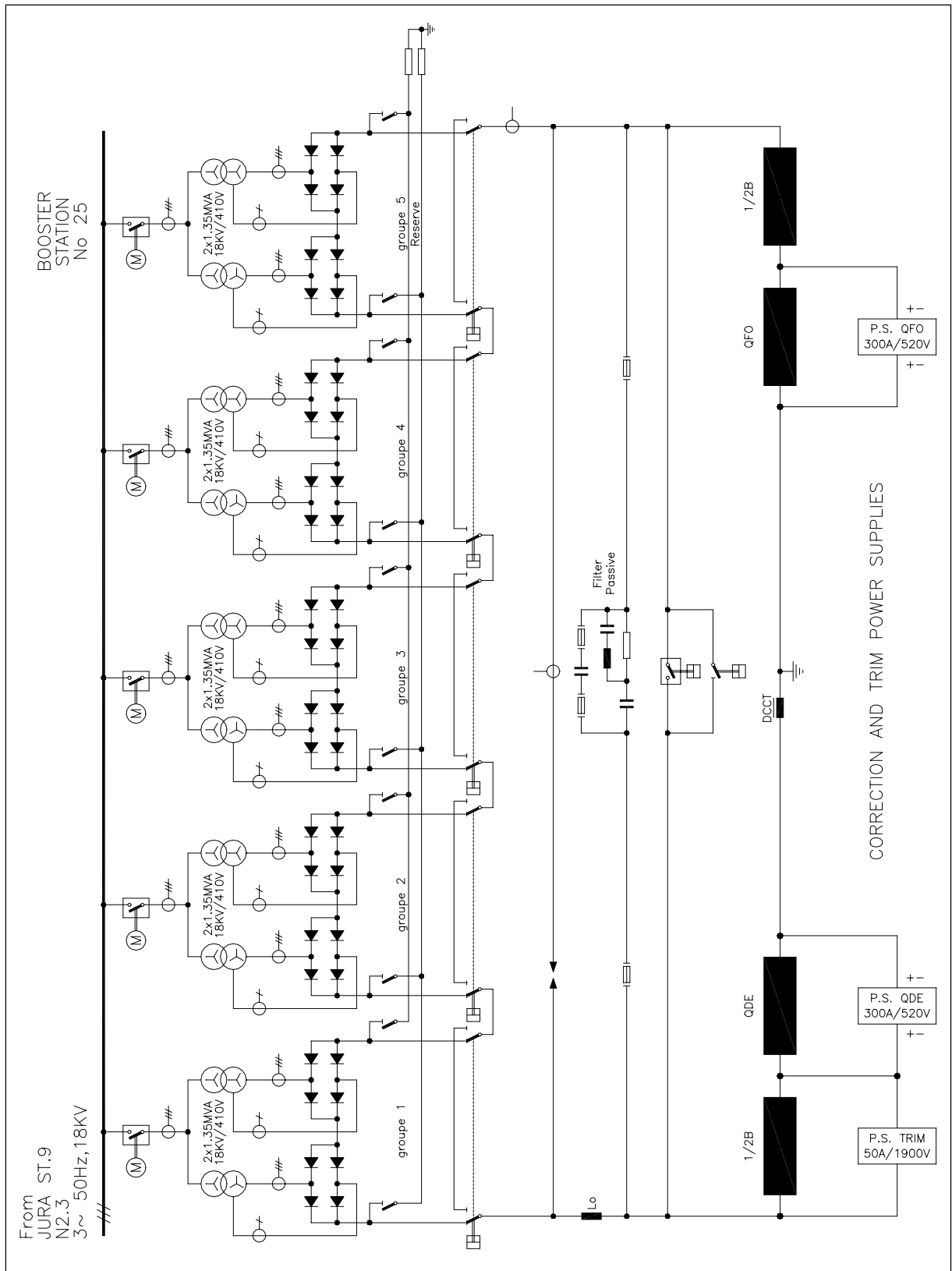


Fig. 7 Main magnet supply electrical diagram.

3.1.2 The reactive power compensation

The scheme described in Section 3.1.1 reduces the line harmonics on the 18 kV side and minimises the reactive power variations, but not sufficiently.

To obtain a satisfactory reactive power compensation and a sufficiently low total harmonic distortion, an existing 18 MVAR capacitor bank and harmonics filter on the 18 kV level near the Jura substation at the Meyrin site is used [13]. The dynamic compensation is assured by a set of Thyristor Controlled Reactors (TCR) installed next to the filter. All the filtering and compensating equipment is connected to the power distribution system at the 18 kV level.

Particular care has been taken of the TCR control circuitry to ensure that variations of the network voltage are kept to a minimum. The TCR was specified [14] and installed by the CERN power distribution group and ordered within the Canadian collaboration with TRIUMF.

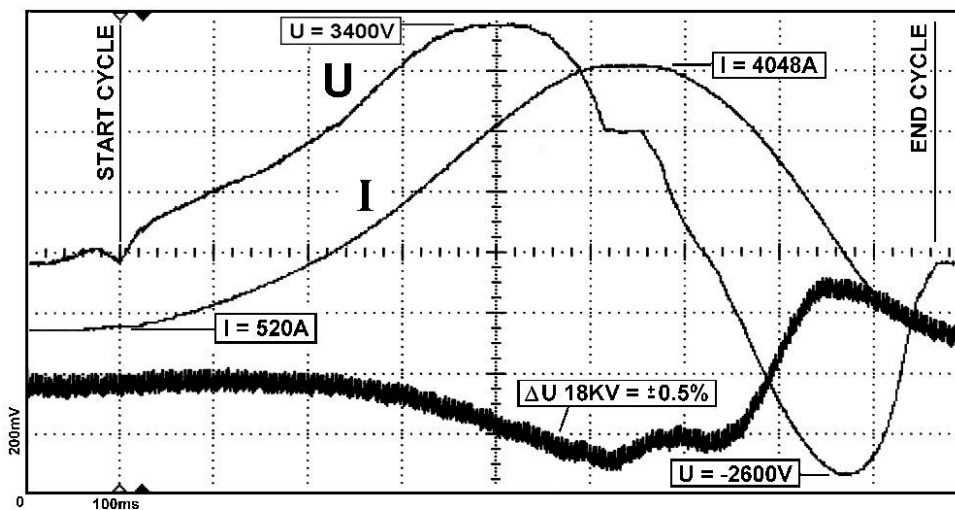


Fig. 8 Voltage (U) and current (I) of the 1.4 GeV cycle, and voltage excursion (ΔU) on the 18 kV network. 100 ms/div.

During the 1.4 GeV cycle the variation of the line voltage on the 18 kV network is of the order of 2.3 % without and 0.5 % with compensation. The latter figure contains other variations in the network, as it is impossible to do measurements with an ideally stable network (see Fig. 8). The installation has been in service for more than one year and, so far, no other users claim to be perturbed by the PSB magnet cycles.

3.1.3 The power converter groups

The original rectifier groups (four plus one spare) have been refurbished to deal with the increased rms and peak power for the LHC cycle. However, the water cooling of the freewheeling thyristors had to be upgraded and additional heat sinks for the fuses were installed to decrease their temperature.

The CERN power distribution group installed a complete, new 18 kV switch gear with the connection to the primary of ten new rectifier transformers (two units in one tank, rated 18kV/390V/2x 1.34 MVA). The latter were ordered as part of the Canadian collaboration with TRIUMF. The transformers were specified to be housed in the same position as the former transformers in order to retain the same phase symmetrical connections to the rectifier bridges.

For the transformers a polygon primary to star secondary coupling was specified in order to connect the freewheel thyristors to the neutral point and to have a higher turns ratio for the accuracy of the phase angle ($\pm 15^\circ$ el. with a tolerance of 0.03°). Also much care was taken to ensure that the absolute impedance (4 %) of all ten transformers had limited spread within phases and units ($\pm 5\%$). Both efforts were necessary to keep subharmonics (50, 100 Hz) as low as possible [15].

The over-voltage protection circuits on the secondary of the transformers were redesigned and adapted to the new layout.

The DC output connections of the rectifier modules (1000 V / 2300 A rms / 4050 A peak), the DC switching circuitry for the series connection of up to four groups, the passive filter and the connections to the magnets have been taken over from the old system.

3.1.4 Regulation and control electronics

A magnet cycle editor running on the controls system allows the creation and storage of cycles for different beam requirements. These cycles are sent to the main magnet supply via the local Device Stub Controller (DSC).

Input to the current regulation electronics is the base current from the PS control interface MIL1553 bus and, via a serial digital function generator, the Ldi/dt function. By measuring the magnet current by a DC Current Transformer (DCCT) and using a Digital Signal Processor (DSP) the IR component is added to the Ldi/dt component to calculate the reference voltage for the magnet. By integration of the Ldi/dt function a current reference is created and compared to the actual current. The difference corrects the reference voltage signal and eliminates the influence from the resistive (thermal) variations of the magnet [16]. A block diagram of the regulation is shown in Fig. 9.

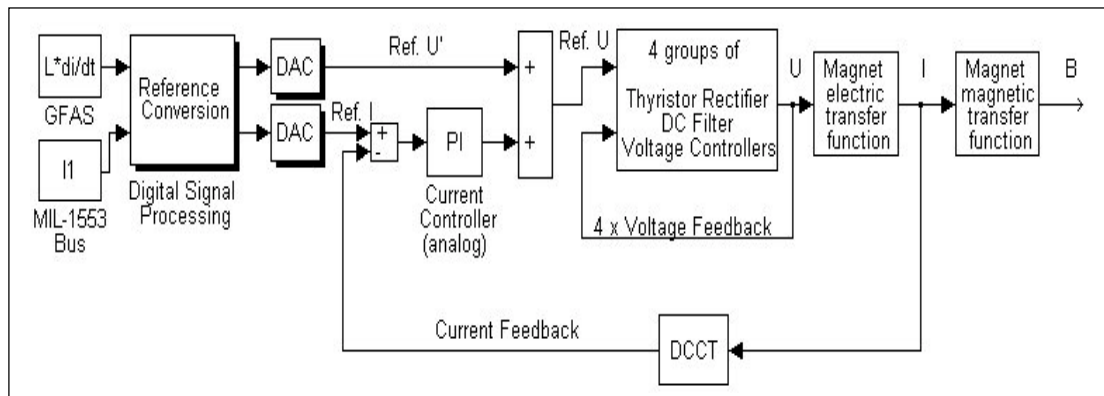


Fig. 9 Block diagram of voltage and current regulation using digital reference processing.

The magnet voltage reference signal is distributed to the four rectifier groups and controls successively the groups from zero to full voltage. Each rectifier group has its dedicated voltage feedback loop. This enables the variation of the reactive power consumption to be reduced and to keep the ripple of the voltage of the modules in series as low as possible.

The control of the 12 pulse rectifier-inverter bridges is done by high precision linearised gate control sets with a resolution of 0.1° el.. There are two separate functions for each group: bridge mode and freewheel mode. During start up the firing pulses of the selected groups have to be synchronised and switched from freewheel to bridge mode. In case of a major fault the freewheel thyristors act as a crowbar and thus protect the main magnet.

On the current and field measurements disturbances with harmonics of the supply's commutation frequency have been observed. The modification of the grounding of the magnet circuit and the installation of a common mode filter at the output of the power supply improved the situation [18].

Most of the control and interlock functions as well as the digital part of the power supply interface to the controls system are performed by decentralised Programmable Logic Controllers (PLCs) interconnected by a serial fieldbus. Some vital functions (e.g. overcurrent) are hard wired in parallel to the PLC. The Mimic diagram and local and remote control are also integrated in the PLC system.

3.1.5 Quadrupole correction power supplies QFO and QDE

All bending and quadrupole magnets of the PSB machine are connected in series. To control the quadrupole magnets separately within a span of 8 % of the main current, two correction power supplies are connected in parallel to the quadrupoles (see Fig. 7). These power converters are 12-

phase thyristor-controlled rectifiers with passive and active fast filters in series with a current precision and tracking error better than 10^{-3} of nominal current and high dynamic capability (4 kA/s). Nominal ratings are 300A/520V/150kW. The insulation to ground withstands 10 kV as the entire main magnet circuit [17].

3.2 Main bending magnets “Trim” power supply

During the running-in period (in 1998) after the upgrade of the PSB to 1.4 GeV it became clear that the main bending magnets showed more effects of saturation than had been anticipated. The field values for the outer rings (rings 1 and 4) were slightly smaller as the magnet had been shimmed [19] to equalise field values at the former ejection energy of 800 MeV.

To equalise the bending fields the idea of the installation of a trim power supply was developed. Investigations of the cabling of the coils of the bending magnet string showed that the coils for rings 1 and 4 as well for rings 2 and 3 are in series with connection points accessible from the power supply equipment room.

A switch-mode power supply was specified, ordered, constructed, installed and commissioned in a record time of 4 months [20, 21]. The main characteristics are:

- bipolar 1900 V
- current 0 – 50 A with 10 A_{rms}
- total precision ± 0.2 % (ripple, tracking error, disturbance) relative to the maximum current of the main supply
- stable operation at zero current
- radiated and conducted switch noise below 50 mA_{pp}
- insulation to ground 10 kV, as the whole main magnet circuit.

To anticipate a step increase of the main current, the bending magnets voltage signal is used as a feed-forward voltage reference for the trim supply. This allows to reduce the tracking error of the trim supply to nearly zero.

Control and interlocks of the trim supply are integrated as the QFO- and QDE- supplies (focusing and defocusing quadrupole magnet trim supplies) into the PLC system of the main power supply and controlled by the same knobs as the main supply.

3.3 PSB-PS/ISOLDE beam-line power supplies

The PSB-PS beam transfer line was designed in the late sixties for 800 MeV protons. In mid 1980 the PSB was upgraded to 1 GeV without modifying the transfer line equipment. More recently it was decided to upgrade further to 1.4 GeV for future LHC operation while also making available 1 or 1.4 GeV beams to the ISOLDE facility. Consequently, a number of magnets and power converters of the PSB transfer lines had to be replaced and this work was carried out in co-operation with TRIUMF, taking advantage of the Canadian in-kind contribution to the LHC project.

3.3.1 Requirements

The characteristics of the transfer line magnets and the related power supplies, as well as the operational requirements at 1.4 GeV, are shown in Tables 7 and 8. Some of the magnets are DC while others require to be modulated in 600 ms between field values corresponding to 1 and 1.4 GeV or even zero, 1 and 1.4 GeV. One magnet (BT.BHZ10), which directs the particles almost symmetrically either to the PS or to the ISOLDE / PSB measuring-line, has to perform a full current reversal at 1 or 1.4 GeV within < 750 ms. To allow a certain flexibility during operation in the years to come, a suitable margin in voltage and current was provided when specifying the new power supplies.

3.3.2 Performance specification

The critical specifications for the new power supplies (Refs. [22, 23]) concern:

- the operational DC precision/stability of current referred to nominal set-point, to be better than $1 \cdot 10^{-4}$ over 8 hours;
- the capability of changing, on subsequent PSB cycles, the current by $\pm 25\%$, or by 100% in some cases, within 600/750 ms regulation transients included;
- the conformity to the PS control interface (MIL-1553) and to the operator interface in use in the PS complex;
- the use of state of the art circuit topologies so as not to become obsolete once the LHC starts operation.

With the view of simplifying the design of the power parts, the operational requirements of the transfer line magnets were met by two sets of power supply ratings: a lower range up to 35 kW (Batch-1) and a higher one up to 250 kW (Batch-2).

Consequently the following types of power converters have been specified, (Tables 7 and 8):

- Batch-1 (38 units): type a1=15 kW (300 A, 50 V) with mechanical output current polarity selector; a2=31.5 kW (350 A, 90 V) and a3=35 kW (500 A, 70 V).
- Batch-2 (8 units): type b1=100 kW (500 A, 200 V) and b2=250 kW (450 A, 550 V).

Table 7

Main operational parameters of power converters up to 35 kW and of related magnets ("B" means bending magnet, "D" correction dipole, "Q" quadrupole. "PPM" stands for "Pulse to Pulse current Modulation" every 1.2 s).

Function	Item	Identification	Magnet Type	DC Resistance (w. cables) (Ω)	Operation at I_{max} (1.4GeV)		Power Supply Type	Remarks	Notes	
					Current (A)	Voltage (V)			Magnets: mH / m Ω / ms	
PSB Injection Line	1	BI-BVT	B5 (*)	0.175	250 (*)	44	a2	ppm1	B : 43 / 221 / 194	
	2	BT1-BVT10	B	0.246	281	70	a2	ppm	B1: 92 / 422 / 218	
	3	BT4-BVT10	B	0.246	281	70	a2	ppm	B4: 205 / 94 / 2180	
	4	BT-BVT20	B1	0.442	244	109.5	268 A -118 V	ppm	B5: 31 / 160 / 194	
	5	BT2-DVT10	D	0.09	147	13.5	a1	ppm (+/-)	B6: 11 / 85 / 130	
	6	BT3-DVT10	D	0.09	147	13.5	a1	ppm (+/-)	B7: 15 / 110 / 136	
	7	BT2-DVT20	D	0.09	248	22.5	a1	ppm (+/-)	D : 3.2 / 80 / 40	
PSB Transfer Line	8	BT3-DVT20	D	0.09	248	22.5	a1	ppm (+/-)	Q : 48 / 160 / 300	
	9	BT3-DVT40	D	0.09	124	11.5	a1	ppm (+/-)	Q1: 160 / 260 / 615	
	10	BT2,3-QNO10	2 X Q	0.35	199	71.5	a2	ppm	Q2: 240 / 200 / 1200	
	11	BT2,3-QNO20	2 X Q	0.35	189	68	a2	ppm	(Bold = new TRIUMF magnet)	
	12	BT-QNO30	Q	0.18	88	16.5	a1	ppm	Power Converters:	
	13	BT-QNO40	Q	0.18	259	48	a2	ppm	Type a1: 300 A - 50 V (18)	
	14	BT-QNO50	Q1	0.27	197	60	a2	ppm	Type a2: 350 A - 90 V (9)	
	15	BTP-QNO10	Q (*)	0.185	150	28	a1	dc (**)	Type a3: 500 A - 70 V (2)	
	16	BTP-QNO20	Q (*)	0.185	145	27	a1	dc (**)	Batch1: 21xa1+11xa2+6xa3	
	PS Injection Line	17	BTP-QNO30	Q (*)	0.2	139	28	a1	dc (**)	Operations:
		18	BTP-QNO40	Q (*)	0.2	177	35.5	a1	dc (**)	ppm : 1 / 1.4 GeV
		19	BTP-QNO50	Q	0.2	152	30.5	a1	dc (**)	ppm1: protons / ions
		20	BTP-QNO60	Q (*)	0.215	176	38	a1	dc (**)	I7 : 17.4 = 0.79 : 1
	ISOLDE Line	21	BTY-BVT116	B4	0.11	410	45	a3	dc	I (ions) = 1.12 x I (protons)
22		BTY-QDE209	Q2 (*)	0.23	174	40	a1	dc	Δt available for ppm: 600 ms	
23		BTY-QFO210	Q2 (*)	0.23	221	51	a2	dc		
GPS Line	24	BTY-DHZ212	D	0.1	243	24.5	a1	dc (+/-)	(+/-) = mechanical - remote	
	25	BTY-DVT212	D	0.1	243	24.5	a1	dc (+/-)	controlled - polarity changer	
HRS Line	26	BTY-BHZ308	B4	0.13	410	53.5	a3	dc	(*) : Ions injection into the PSB	
	27	BTY-QDE321	Q2 (*)	0.23	174	40	a1	dc	(**): ΔI in ppm < 5%	
	28	BTY-QFO322	Q2 (*)	0.23	221	51	a2	dc	(*) : Solid yoke	
	29	BTY-DHZ324	D	0.1	243	24.5	a1	dc (+/-)	(**): Secondary beam	
	30	BTY-DVT324	D	0.1	243	24.5	a1	dc (+/-)	Location: BHP - ISOLDE Hall	

3.3.3 Technical solution

Using today's state of the art technology, Switch Mode Power Supplies (SMPS) have been specified, which have excellent precision/stability, low losses and fast regulation response [24].

Table 8

Main operational parameters of power converters with 100 and 250 kW ratings and of related magnets (“m1-4” means magnet. Other symbols as in Table 7).

Function	Item	Identification	Magnet	DC Resistance		Operation at I _{max} (1.4 GeV)		Power Supply	Remarks	Magnets: mH / m! / ms
				Type	(with Cables) (Ω)	Current (A)	Voltage (V)			
										m1: 92 / 480 / 192
										m2: 470 / 200 / 2350
										m3: 370 / 400 / 925
PSB Transfer Line	1	BT-BVT20	m1	0.5	244	123	b1	ppm		m4: 205 / 94 / 2180
										Power Converter types:
	2	BT-BHZ10	m3	0.42	(+/-) 381	488 (398)	b2	ppm		Type b1: 500 A - 200 V (4)
Switchyards	3	BTY-BVT101	m4	0.11	397	158.5	b1	ppm2		Type b2: 450 A - 550 V (1)
	4	BTY-BHZ301	m4	0.13	397	163.5	b1	ppm3		Batch-2: 6xb1 + 2xb2
										ppm2: 0 / 1 or 1.4 GeV
Measuring Line	5	BTM-BHZ10	m2	0.22	446	161	b1	ppm		ppm3 = ppm2 for GPS / HRS
										Δt available for ppm: 600 ms (0.75 s for BT-BHZ10)
										(+/-): bipolar power supply b2

As an illustration of the design, a block diagram of the power section of the 100 kW converter is shown in Fig. 10. Specifically, the power section of the converter consists of an AC series-parallel input filter to reduce current harmonics and rise the power factor; a rectifier and filter forming the DC link; an Insulated Gate Bipolar Transistor (IGBT) full H-bridge operating at a switching frequency of 16-18 kHz and a ferrite HF transformer with centre tap secondary, feeding a high current rectifier followed by two LC passive filter stages. To achieve a 600 ms current fall time despite of a load time constant of over 2 s in some case an optional regeneration thyristor bridge provides the required negative voltage on the magnet, and an IGBT switch isolates the converter from the load when the current is requested to decrease to zero.

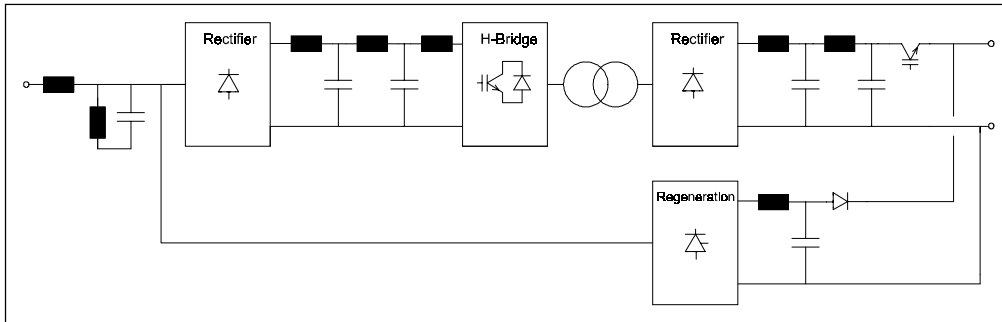


Fig. 10 Block diagram of a 100 kW switch-mode power converter.

The 250 kW converter has three IGBT H-bridges working in parallel and feeding the HF transformer whose secondary is connected to a Graetz-bridge rectifier followed by two LC filters. In addition to the regeneration section this converter has a thyristor selector of the DC current polarity which allows an inversion of the field which directs the protons either to the PS or to the ISOLDE/measuring line. The semiconductor switches and some of the magnetics are water cooled to remove the losses and to obtain a compact assembly as required by this type of converters for electromagnetic compatibility reasons.

All the voltage and current measurement systems used for monitoring, protection or feedback are insulated. The power supply output current is measured via high precision magnetic sensors (DCCTs).

As shown in Fig. 11, the regulation of such a SMPS consists of several cascaded feedback loops:

- a first loop balances the current in the two arms of each IGBT H-bridge to avoid saturation of the HF transformer by any DC component.
- A second loop controls and limits the current I_p on the primary of the HF transformer.
- A third fast loop controls the voltage U_r at the rectifier output.

A new electronic crate has been developed at CERN to facilitate the maintenance and to respect different criteria: standardisation, protocol, timing and regulation with active filter. The power parts have been designed at CERN and built in collaboration with industry.

3.4.1 Operational requirements

In the common part of the transfer line between PSB and PS, the kinetic energy is either 1 GeV (ISOLDE) or 1.4 GeV (PS). The PS supercycle is made of basic cycles (1.2 s length) dependent on the use of different beams. Consequently, pulsed power converters must work with an irregular pulse repetition and with pulse to pulse modulation of their current.

The recombination of the beam in the PSB transfer line uses: four superimposed horizontal septa (BE.SMH with the four magnets in series), three vertical septa (BT1.SMV10, BT4.SMV10, BT.SMV20) and a horizontal septum for the injection in the PS (PI.SMH42).

3.4.2 Pulsed capacitors discharge power converters

The principle is based on the charge and discharge of capacitors through a resonant circuit between capacitors and the load. The charging current of the capacitors is controlled via thyristors on the primary side of a high voltage transformer. The DC voltage and current are measured by voltage dividers and shunt. Once charged, the capacitors are discharged in the magnet via a power thyristor. In order to obtain a better flat top current than the basic sinusoidal discharge current, a third harmonic with parallel LC circuit is added. A choke, in series with the discharge circuit, is used for the active filter. The discharge is adapted with a matching transformer whose secondary delivers 4 to 12 times the primary current to the septum magnet.

3.4.3 Matching transformer and strip-line

The matching transformer is a special manufacture with air gap and a very low stray inductance. It is installed in the ring, and the secondary of the transformer is connected to a magnet vacuum feedthrough via a high current strip-line made of copper plates to minimise the value of inductance and to keep the resistance small relative to the magnet. The current in the septum is monitored by a current transformer between the pulse matching transformer and the high current strip-line.

3.4.4 Regulation and active filter

The capacitors voltage is regulated with a charging current internal loop. Temperature variations and magnetic effects caused by irregular repetition rate are regulated by special electronics which increases or decreases slightly the capacitors voltage.

A current flat top stability of 10^{-4} is achieved by an active filter power circuit with a regulation control loop. The principle is to charge the main capacitors slightly higher than the value necessary to give the current wanted. The excess current is then pulled through the inductance of the active filter, and the system acts in a closed loop through the matching transformer. More details may be found in Refs. [25, 27] and in the specification document [26].

3.4.5 Characteristics of the power supplies

The principal characteristics of the power converters are resumed in Table 9: Typical discharge and filter currents are shown in Figs. 12 and 13, with a current of 33 kA in the PI.SMH42 septum magnet [27].

Installation of the pulsed power supplies for the septum magnets is now completed. They entirely fulfil the operational requirements: higher and repetitive currents for 1.4 GeV, pulse to pulse modulation, irregular pulsing, high reliability so far.

Table 9
Main parameters of the pulsed septum magnet power supplies.

		BE.SMH	BT1.SMV10	BT4.SMV10	BT.SMV20	PL.SMH42
Peak current septum	A	6000	30000	30000	30000	40000
Transformer turn ratio	n1/n2	4	12	12	12	12
Charging voltage	V	1200	2100	2100	2100	2100
Peak current primary	A	1500	2500	2500	2500	3333
Total storage capacitors	μF	2500	2000	2000	2000	3000
Energy storage capacitors	J	1800	4410	4410	4410	6 615
Total inductance secondary	μH	22	3	3	3	2.03
Total resistor secondary	$\mu\Omega$	4020	660	660	660	620
Current pulse half period	ms	3.6	3.5	3.5	3.5	3.6
Current pulse flat top	μs	500	500	500	500	500
Current flat top precision	ppm	< 100	< 100	< 100	< 100	< 100
Pulse to pulse modulation		yes	yes	yes	yes	yes
Irregular pulse repetition		yes	yes	yes	yes	yes
Max. pulse repetition rate	Hz	1	1	1	1	1
Third harmonic choke	μH	248	370	370	370	280
Active filter choke	μH	50	50	50	50	50
Inductance seen by primary	μH	432	503	503	503	372
Power transformer 3 ph.	kVA	20	63	63	63	63
Prim./second. voltage effective	V	400/1000	400/2000	400/2000	400/2000	400/2000

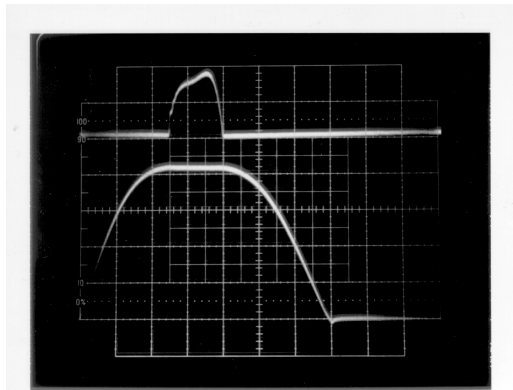


Fig. 12 Magnet and active filter current measured at 33 kA
Upper trace: active filter current, 100 A/div,
Lower trace: magnet current, 10 kA/div, 0.5 ms/div.

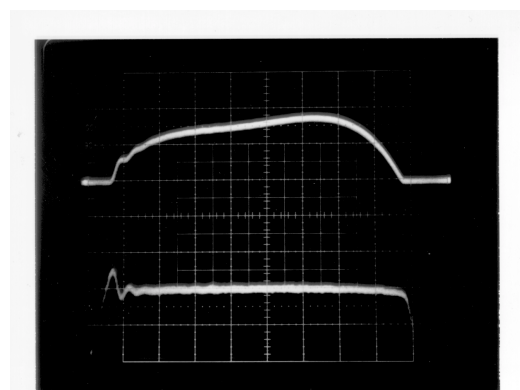


Fig. 13 Zoom on the flat top at 33 kA with active filter current. The current flat-top precision is in the 10^{-4} range.
Upper trace: active filter current, 100 A/div,
Lower trace: magnet current, 40 A /div, 0.1 ms/div.

4. UPGRADING THE PSB TO 1.4 GEV – OTHER SYSTEMS

4.1 PSB-PS line septum magnets

In the PSB, DC septum magnets, that were originally designed for 800 MeV beams, have been used for 1 GeV beams, since 1986, without modification. When the PSB energy needed to be increased to 1.4 GeV this implied redesigning all PSB ejection and transfer septa because of the thermal limit of the DC magnets. For the construction of these septum magnets, a single turn pulsed magnet approach has been adopted, which requires less energy hence less cooling power. This way they are also less prone to erosion in the cooling circuits. To attain the required vacuum, the laminated yoke of these pulsed magnets must first be baked at 200°C, despite the fact that these magnets are installed in non-bakeable accelerators. Therefore, the connecting flanges of the magnet tanks should not exceed 50°C when the magnets are being baked.

To reach the objectives stated in the introduction, the entire conception of the magnets has been revised. In the following paragraphs, the most outstanding details will be described per component.

4.1.1 Vacuum tanks

To reduce the risk of a leak developing during a bake out, cylindrical tanks have been fitted with circular ultra high vacuum flanges for diameters < 200 mm and “Wheeler” flanges with copper seals for the bigger diameters (>375 mm). The connecting flanges of the tanks to the accelerator vacuum chamber are of a conical “quick disconnect” type with aluminium seals, as standard in the CERN PS accelerators.

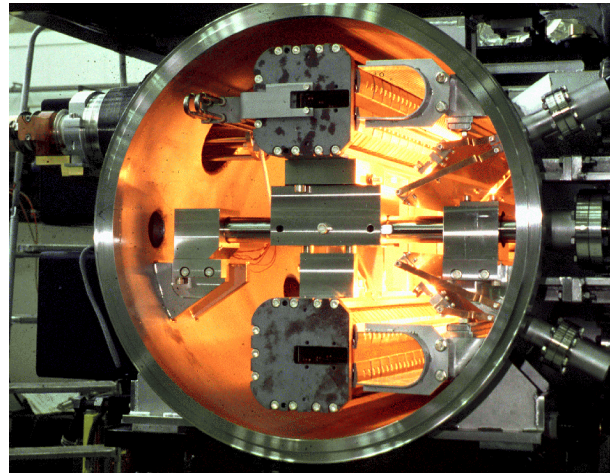


Fig. 14 Vacuum tank containing 2 ejection magnets.

4.1.2 Magnets

The new septum magnets, being of a pulsed type, are constructed with laminated yokes. Standard 0.35 mm thickness steel laminations with a 3 % silicon content have been used, which are insulated on both sides with a “Carlite” inorganic insulating coating. This solution provides a good inter-laminar resistance, and is still bakeable up to 200°C. The laminated yoke is held together in a stainless steel support by ceramic coated endplates, while sitting on ceramic bars, to ensure the electrical insulation between the yoke and the support.

The single-turn coils have been made of “OFHC” copper. The cooling circuit comprises two thin-walled stainless steel tubes, embedded (and brazed) in pre-machined slots in the septum conductor. This reduces erosion of the cooling circuit due to the high water speeds of up to 10 m/s. To increase the mechanical strength of the 60 mm gap septa conductors, a 0.5 mm thick stainless steel plate is brazed onto the outside of the septum conductor. To reduce the fringe field of the magnets, insulation has been eliminated between magnet yoke and septum conductor, while the return conductor of the coil is insulated with several layers of 0.06 mm and 0.12 mm thermally pre-formed “Kapton” sheet (see Fig. 15).

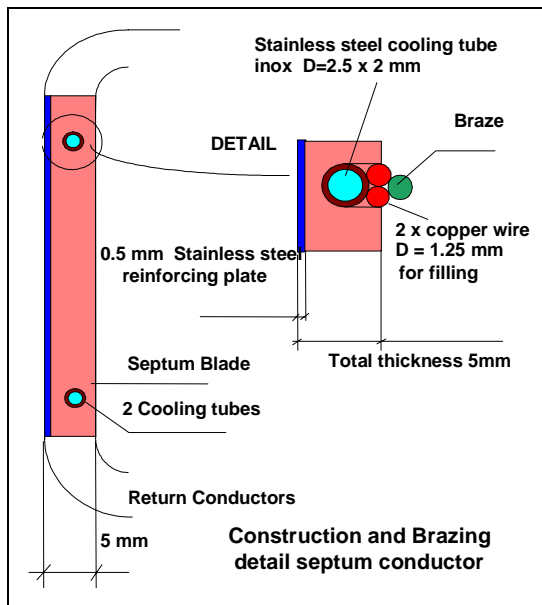


Fig. 15 Cross section of septum conductor.

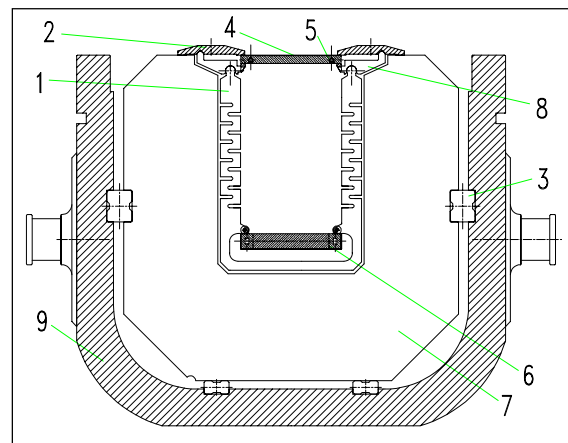


Fig. 16 Cross section of magnet yoke assembly.

1. Damping Spring
2. Clamping Plate
3. Ceramic Support
4. Septum Conductor
5. Cooling Tube
6. Rear Conductor
7. Lamination
8. Lever
9. Stainless Steel Support.

The complete magnet coil is held in the gap by clamping plates located outside of the magnet yoke. These insulated clamps retain the septum conductor in the gap, while a spring between the septum and rear conductor applies a mechanical force on the return conductor equal to the electromechanical force at the peak current.

The springs, spaced every 45 mm, are made of beryllium copper (5 % Be) suitably annealed to obtain the necessary modulus of elasticity (see Fig. 16).

A water-cooled coaxial power feedthrough, developed for use at $10 \text{ kA}_{\text{rms}}$, is used for all new pulsed septum magnets. The coaxial configuration provides the best possible symmetry in mechanical forces, (see Fig. 17)

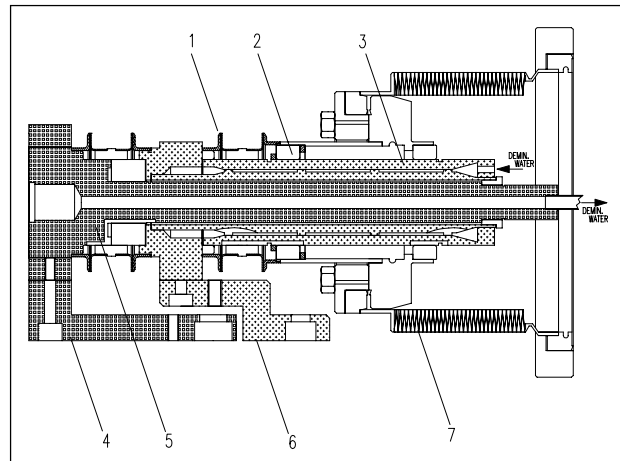


Fig. 17 Cross section of power feedthrough.

1. Dilver / Stainless steel weld
2. Ceramic support
3. External conductor
4. Main connection
5. Central conductor
6. Main connection
7. Vacuum bellows

4.1.3 Displacement system

All septum magnets can be moved remotely in the radial (or vertical, in the case of the septa in the transfer line) and angular directions, while their vacuum tanks remain fixed. A variable potentiometer, linked to the mechanical displacement system, provides a measurement of the position of the magnet inside the tank. The resolutions of the radial and angular systems are 0.1 mm and 0.1 mrad, respectively. For the initial installation, the magnet tank is aligned in all directions. In the event of a failure, the entire vacuum tank with septum magnet can be replaced without the need for realignment.

4.1.4 Beam screen

All septum magnet tanks (except transfer lines) are equipped with RF beam screens for the orbiting beam. These screens insure the continuity of the RF impedance of the vacuum tanks, to avoid unwanted harmonics during acceleration. The beam screens are made of perforated stainless steel sheet to improve vacuum pumping speed, and are linked with the connecting flanges of the tank by means of RF contacts.

4.1.5 Vacuum equipment

The vacuum tanks are kept under vacuum with a dedicated set of ion pumps, additional pumping being provided by titanium sublimators for the tanks installed in the accelerator rings. In view of the large surface of the magnet laminations under vacuum, and the pressure level to be obtained, it is necessary to bake out the magnets before commissioning. Standard off-the-shelf infra red lamps are used inside the vacuum tank, with reflectors of electro-polished stainless steel. By connecting two in series, the power consumption is reduced by a factor four, while their expected life time is dramatically increased. The temperature of the magnet is measured with ordinary Cu/Cn (Cn-Constantan) thermocouples, and the control and regulation utilises standard temperature regulators.

4.1.6 Calculations

For the first rough estimation of the septum magnet parameters, a program was used running under Microsoft Excel developed in the CERN/PS/SEPTA section. To finalise the cross sectional design of the magnet a finite element based program called "FLUX2D" from Cedrat/Magsoft was used. The longitudinal design was determined using the finite element based program "OPERA3D/TOSCA" from Vector Fields, using a model developed in house to simplify the magnet model without significant loss of precision. For mechanical and thermal calculations the finite element program

ANSYS from Swanson Analysis Systems was used, while the cooling requirements were checked with the CERN developed program TUBE, running under Microsoft Excel.

4.1.7 Measurement results and conclusions

Measurements of magnetic length of the septa confirm theoretical predictions to within 0.5 % of the model. The fringe fields measured are less than 1/1000 of the gap field at a 50 mm distance from the septum conductor, or better in case of the BE.SMH, (PSB Ejection) where a very low fringe field was required. After a bake out cycle, consisting of a quasi linear temperature increase of 200°C over 12 hours, a 24 hour period at 200°C, and an exponential temperature decrease of approximately 48 hours, a vacuum of $6 \cdot 10^{-10}$ to $4 \cdot 10^{-9}$ mbar is achieved. Since the bake out lamps are installed with reflectors, the connecting flanges of the vacuum tanks never exceed 50°C, allowing the use of aluminium seals for connecting to the accelerator vacuum chambers.

The new septum magnets constructed show that it is possible to achieve a vacuum in the low 10^9 mbar range, even with laminated yokes under vacuum. In order to reach the low pressures specified, it is imperative to perform a pre-commissioning bakeout at 200°C. The bakeout is performed using commercially available infra red lamps operated below nominal power to avoid excessive temperatures on the vacuum chamber connecting flanges.

For completeness, the technical specifications of the septum magnets are listed in Table 10.

Table 10
Technical specifications of the septum magnets.

	BESMH	BTSMV10	BTSMV20	PISMH42
L_{eq} (m)	0.95	1.00	1.00	0.57
B_0 (T)	0.354	0.569	0.525	0.689
$\int B \cdot dl$ (T.m)	0.336	0.566	0.523	0.390
I (kA) single turn coil	7.0	27.3	25.2	33.1
E (GeV) protons	1.4	1.4	1.4	1.4
Deflection Angle (mrad)	47	79	73	55
Gap height (mm)	25	60	60	60
Gap width (mm)	89	116	116	116
Septum Thickness (mm)	3.8	5	5	5
Rear conductor thickness (mm)	7.6	8.8	8.8	8.8
1/2 sine pulse width (ms)	3.1	3.1	3.1	3.2
Water flow (l/min.)	1.9	3.5	3.5	4.25
Year of installation	1998	1999	1997	1996

4.2 PSB-PS transfer line magnets

Most of the magnets in the transfer line from the PSB to the PS had to be replaced, for two different reasons. Some of the replaced magnets were not laminated, thus the induced eddy currents would have hindered pulse to pulse modulation. For some other magnets, the cooling power was no longer sufficient at the higher currents necessary for 1.4 GeV operation. The magnets are part of the Canadian in-kind contribution to the LHC project.

All the magnet yokes are laminated using low carbon steel sheets of 1.5 mm thickness stacked between non-laminated low carbon steel end plates. The coils are built from rectangular copper conductor with a circular cooling hole. The inter-turn and mass insulation is made from half-lapped glass fibre tape. The coils are vacuum impregnated using radiation resistant epoxy resin.

The BVT10 dipoles are window frame magnets with a single bedstead coil. A yoke extension block compensates the asymmetry caused by the coil head. The BVT20 magnet is similar to the BVT10, but with an aperture of twice the width and two symmetrical bedstead coils which are identical to the BVT10 coils. The DVT correction dipoles are window frame magnets with a smaller

bending power. They have two bedstead coils. The yokes of the BT.QNO quadrupoles use a “figure of eight” design. The doublet version is built from two single yokes separated by appropriate spacers. Details about the magnet design and excerpts from the construction drawings can be found in Refs. [28, 29] and the references herein.

The quadrupoles were magnetically measured at TRIUMF with a newly built rotating coil system [30] and an existing Hall probe system. The dipoles were field mapped at TRIUMF using a Hall probe system. Details of the measurements, comparisons between different measurement methods and comparisons to magnetic field calculations can be found in Refs. [29-31] and the references herein.

Table 11 lists the magnet characteristics. The values given for cooling flow, temperature rise, and pressure drop are measured values. Higher currents are possible by increasing the inlet water pressure, the maximum permissible value being 25 bar. Table 11 also contains the coefficients $\int Bdl/I$, $\int Gdl/I$; the value for the BVT10 dipoles corresponds to the linear part up to 200 A. At the field necessary for 1.4 GeV operation, a saturation of 0.7 % can be seen for this magnet, see Fig. 18. The polynomial coefficients to describe this curve can be found in [29]. For all other magnets saturation effects are negligible at this field level. All values are averaged over a given magnet type, individual measurements for each magnet can be found in [29].

Table 11
Magnet characteristics: $\int Bdl$ and deflection angle correspond to the current given in this table.

	BVT10	BVT20	DVT	BTQNO singlet	BTQNO doublet	
Deflection angle Elements	78.5 BT1.BVT10 BT4.BVT10	70.0 BT.BVT20	max. 11.1 BT2.DVT10 BT3.DVT10 BT2.DVT20 BT3.DVT20 BT3.DVT40	- BT.QNO30 BT.QNO40	- BT2.QNO10 BT3.QNO10 BT2.QNO20 BT3.QNO20	mrad
Overall length	985	980	445	590	590	mm
Overall height	460	460	280	500	1000	mm
Overall width	340	530	440	700	700	mm
Yoke length	800	800	250	430	430	mm
Horizontal aperture	62	120	102	-	-	mm
Vertical aperture	124	124	124	-	-	mm
Aperture diameter	-	-	-	150	150	mm
Weight	500	650	100	650	1400	kg
Cooling flow	7.7	13.5	3.5	5.3	9.7	l/min
Temperature rise	35	28	20	30	30	°C
Pressure drop	4.2	3.5	3.5	4.5	4.3	bar
I (for given $\int Bdl / \int Gdl$)	275	234	250	260	260	A
R at 20 °C	212.3	416.5	74.6	147.1	296.5	mΩ
R at 45 °C	235.3	460.8	82.4	162.9	328.2	mΩ
L at 100 Hz	39.8	86.5	2.68	39.0	78.4	mH
L at 1000 Hz	32.6	72.7	2.16	34.3	69.2	mH
Dissipated power	17.8	25.3	5.2	11.0	22.0	kW
B	0.6189	0.5476	0.1971	-	-	T
$\int Bdl$	0.5611	0.5003	0.07957	-	-	Tm
G	-	-	-	6.612	6.614	T/m
$\int Gdl$	-	-	-	3.082	3.082	Tm/m
$\int Bdl/I$ (BVT10: $I < 200A$)	$2.0555 \cdot 10^{-3}$	$2.1370 \cdot 10^{-3}$	$3.1830 \cdot 10^{-4}$	-	-	Tm/A
$\int Gdl/I$	-	-	-	$1.1854 \cdot 10^{-2}$	$1.1854 \cdot 10^{-2}$	T/A
Effective length	906.6	913.6	403.8	466.1	466.0	mm

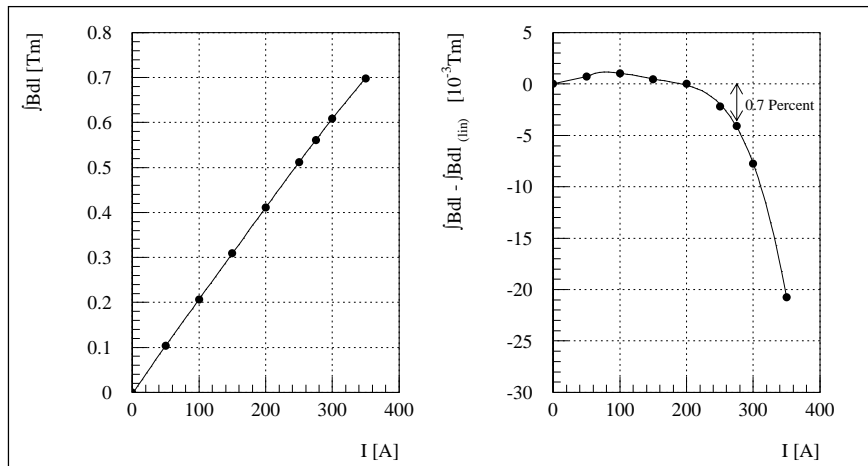


Fig 18 BVT10 magnetisation curve.

Figs. 19 and 20 show the homogeneity of $|Bdl|$ of BVT10#1, BVT20 and DVT#1. X corresponds to the horizontal, Y to the vertical direction with respect to the beam. Fig. 21 shows the homogeneity of G and $|Gdl|$ of BTQN0#6, calculated from the harmonics measured with the rotating coil system. As a comparison, the direct measurements using a gradient flip coil system are shown.

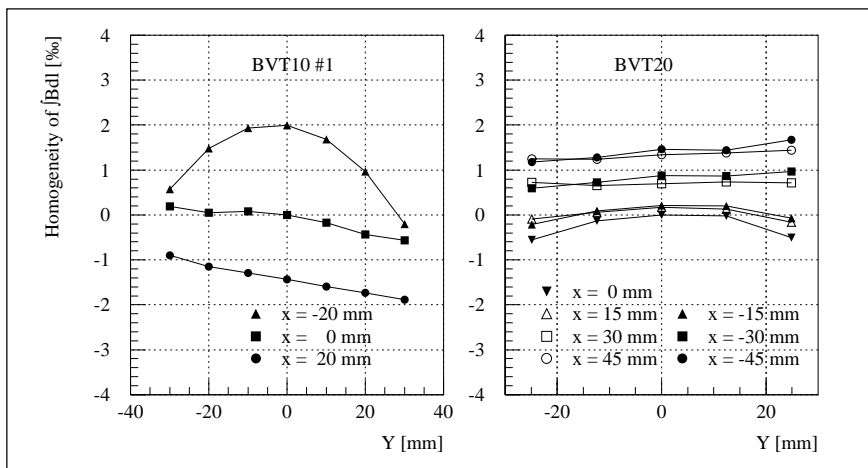


Fig. 19 Homogeneity of $|Bdl|$ of BVT10#1 and BVT20.

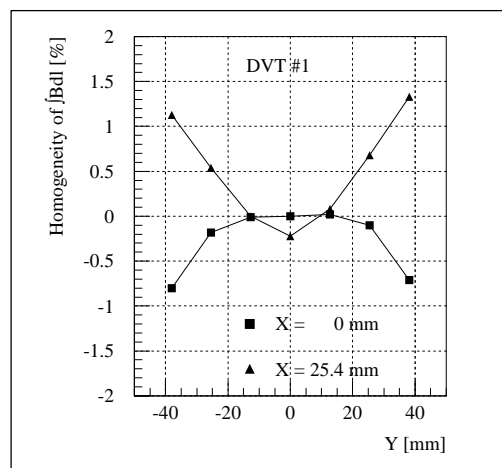


Fig. 20 Homogeneity of $|Bdl|$ of DVT#1.

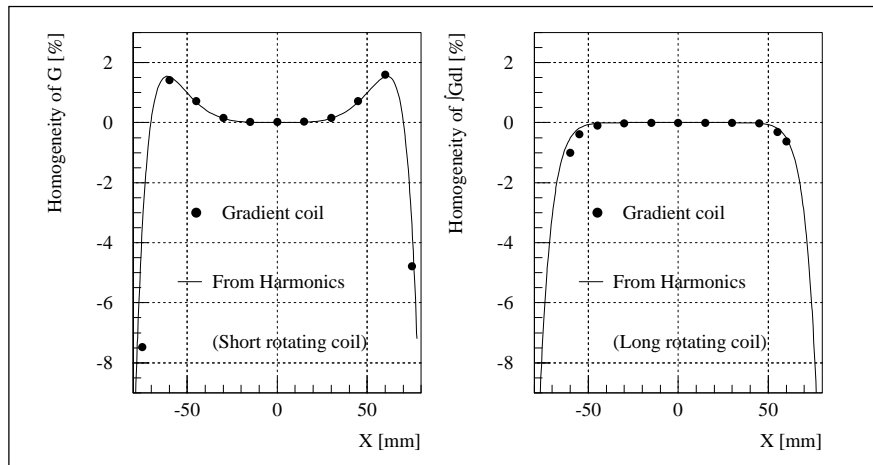


Fig. 21 Homogeneity of G and $|GdI|$ of BTQNO#6.

4.3 Fast kicker systems

4.3.1 PSB ejection BE.KFA14L1 and recombination kickers BT.KFA10 and BT.KFA20

The PSB kicker magnets are used for the horizontal ejection and sequential vertical recombination of the beams from the four PSB rings into one string of bunches, which is being guided to the PS. The magnets are of cellular, closed aperture, C-ferrite loaded, transmission line type; they are inserted in the machine vacuum. Ejection and recombination magnets have different apertures to best match the beam dimensions. Given the constraints of the PSB ring and transfer line layout, the original magnets and vacuum tanks were re-used. The particularity of the original PSB kicker system configuration [32] was the insertion of the magnets between the Pulse Forming Network (PFN) and transmission cables, as sketched in Fig. 22, below.

The principal advantage of this extremely tailored layout is that the magnets are used in virtual short-circuit mode. The short-circuit current is provided immediately by the thyatron switch and its leading edge travels only once through the magnet. This configuration yields the fastest kick rise-time and highest kick strength for a given PFN voltage. Although the PFNs are resonantly charged in milliseconds, the crucial disadvantage of this configuration, however, is the relatively long exposure of the magnet to the PFN charging voltage, which may precipitate magnet sparking for charging voltages larger than ~ 35 kV. Because of the increase of PSB energy, (the charging voltage for the kicker pulse generators is 26 % higher), this original air-insulated generator configuration could not be retained, except for the second recombination kicker BT.KFA20, which operates far below the magnet voltage hold-off. This minimal cost system has other disadvantages:

- The impedance at the main thyatron switch is low (6.25Ω), thus increasing the relative importance of unavoidable inductive mismatches present in such systems.
- Timing and transmission cable length adjustments, possible with independently powered modules, which are very effective to reduce the influence of individual magnet kick rise-time and ripple on the sum kick of the magnets, cannot be made.

At previous occasions of PSB energy upgrades and consolidations, the initially effective, but cumbersome ferrite loaded pulse-steepening lines [33] (Fig. 22) were removed. High voltage thyratrons, vacuum feedthroughs and the magnet ferrites were upgraded (except for BT.KFA10), and all PFN and transmission cables were replaced by low loss, SF_6 pressurized high voltage cables.

For the present LHC upgrade the PSB kicker equipment (hardware and software), was completely replaced, except for the magnets, vacuum tanks and high voltage cables, previously dealt with.

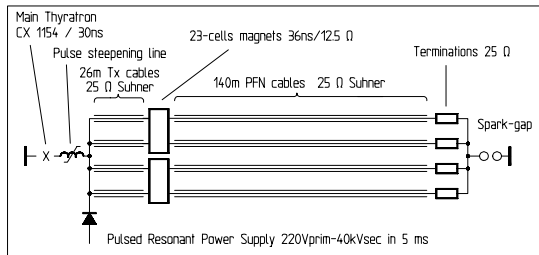


Fig. 22 Original BT.KFA20 configuration.

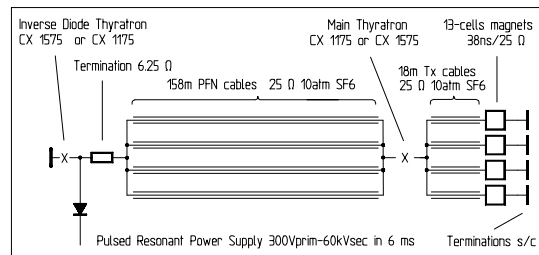


Fig. 23 BE.KFA 14L1 (1 of 4 rings) for LHC era.

New, oil-insulated pulse generators using two multistage thyratrons, each capable of operating at 60 kV and in two-shot Pulse to Pulse Modulation (PPM), were developed and installed together with their associated electronics and controls for BE.KFA14L1 and BT.KFA10, systems which are very similar. These magnets are now hard short-circuited and pulsed in the more classical configurations of Figs. 23 and 24. For BT.KFA20, the new hardware developed for the above systems is also used, but the original configuration has been retained in order to achieve the short rise-time without the need of bulky artifices, Fig. 25.

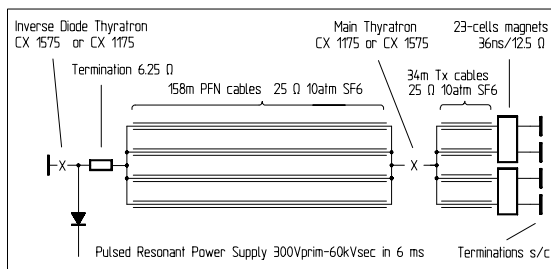


Fig. 24 BT.KFA 10 configuration for LHC era (1 of 2 lines).

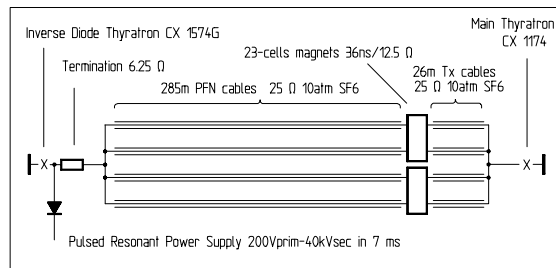


Fig. 25 BT.KFA 20 configuration for LHC era.

The principal advantage of the new layout is that the short-circuited magnets (and their electrical feed-throughs) are exposed to high voltage for the minimum possible duration, largely obviating the problem of sparking. The intrinsic disadvantage of this new configuration with respect to the previous layout is that the initial switch current has to traverse the magnet twice before the total kick is established, leading to a longer rise-time (~90 ns instead of ~60 ns). However, because of the PSB harmonic number change from 5 to 2 or 1, this longer rise-time can be accepted.

Development work is actually in progress to improve the rise-time, including the eventual use of small saturable ferrite loaded inductors, and to reduce flattop ripple by adequate compensation of the various unavoidable mismatches. Other complications inherent in this configuration are different lengths of transmission cables to compensate for particle flight time from magnet to magnet.

The main parameters of the PSB kickers can be found in the Table 12 and more information is on the web via <http://nicewww.cern.ch/psdata/www/Kickers/psparam.htm>.

Table 12
PSB and PS Kicker main parameters and performances (kick strengths for I_{max})

Element	No.of Generators	V PFN (kV)	Magnet Z_o (Ω) nominal	Termination Z (Ω)	Magnet I_{max} (kA)	No. of turns	Magnet Aperture w×h (mm)	Magnet length (mm)	Kickstrength in SS/ring (G.m)	rise-time 2-98 %	Flattop length (μ s)
BE.KFA14L1	4	60	25	s/c	2.4	1	115x70	450	775	102 ns	1.5
BT.KFA10	2	60	12.5	s/c	4.8	1	53x110	786	862	86 ns	1.5
BT.KFA20	1	30	12.5	s/c	2.4	1	53x110	786	431	80 ns	2.7
PL.KFA45	4	80	26.3	26.3/0	.5 / 3	1	150x53	222	314.2 / 601.5	49 ns	0 - 2.6
PR.KFA71-79	12	80	15	15	2.6	1	147x53	221	1673	85 ns	0 - 2.1
BE.BSW14L4	1	0.5	-	-	0.765	36	141x144	540	946	5.25 ms	100
BE.BSW15L1	1	0.5	-	-	0.845	24	144x72	378	1336	5.25 ms	100
BE.BSW15L4	1	0.5	-	-	0.765	36	141x144	540	946	5.25 ms	100

4.3.2 PSB ejection dipoles

For ejection at 1.4 GeV it was necessary to increase the bumper magnet peak current from 500 A to 630 A. Whilst it was possible to conserve the existing magnets, their associated pulse generators were limited to 550 A peak current. In addition, the bumpers are now required to operate in PPM between 1 GeV and 1.4 GeV. In view of these new operating conditions, the necessity to interface to a new DSC-based control system and their advanced age, it was decided to completely replace the existing pulse generators [34].

The existing magnets, in use since 1970, are retained. BE.BSW14L4 and BE.BSW15L4 are PSB type 5 magnets, BE.BSW15L1 is a type 6 magnet. The magnets are connected in a series/parallel configuration which presents an effective impedance equivalent to that of a single magnet. This arrangement is identical for the three straight sections. Each bumper pulse generator excites four vertically superimposed magnets. The relevant parameters for the three sections are given in Table 12. For operational purposes, I_{max} is hardware limited to 690 A for all twelve magnets.

The operating principle is based on a resonant semi-sinusoidal current discharge into the bumper magnet with a freewheel diode/inductor circuit providing a partial recharge of the primary capacitor C1. Figure 26 shows a simplified electrical circuit for one bumper magnet group and its associated power supply.

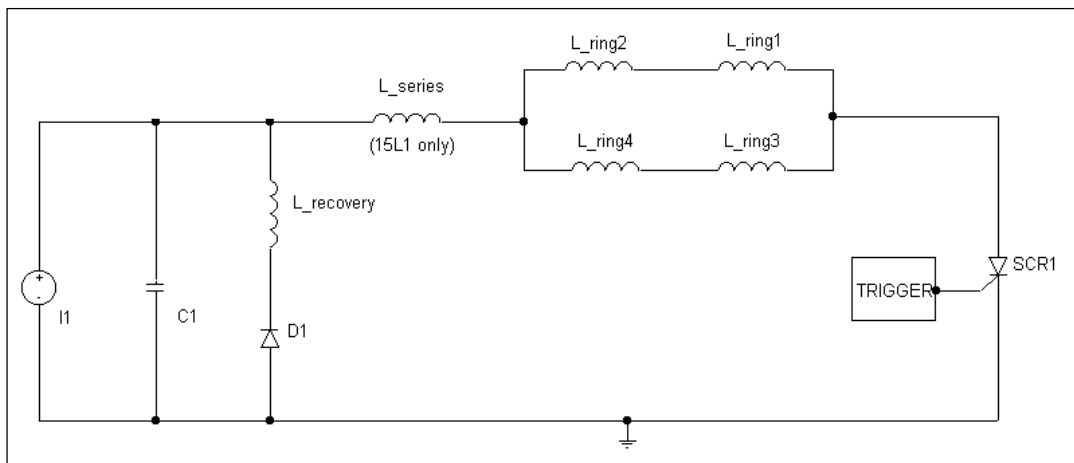


Fig. 26 Simplified circuit diagram of one bumper magnet group (four superimposed magnets).

C_1 is charged to a voltage V by a current source I_1 . When the semiconductor switch, SCR_1 , is triggered on, a resonance is excited between C_1 and the magnet inductances L_{ring1} , L_{ring2} , L_{ring3} and L_{ring4} . This slightly-damped sinusoidal current is interrupted by the opening of SCR_1 at the instance of zero-crossing. Time to peak of the current pulse is 5.25 ms. The free-wheel circuit

comprising D1 and L_recovery begins to conduct when the voltage on C1 goes negative; a secondary, lower-frequency resonance then occurs between L_recovery and C1 which ends when the current in D1 starts to become negative. This results in C1 completing the cycle with a positive charge thereby reducing both the power losses and the post-cycle recharge period. An additional series inductance is required in the 15L1 circuit to compensate for the lower inductance of the type 6 magnet compared to the type 5 magnets.

4.3.3 PS injection and ejection kickers

The present PS injection and ejection kickers will be re-used in their actual configuration because they are sufficiently powerful. The PS injection Kicker PI.KFA45 works in a particular configuration (Fig. 27), which permits the doubling, in PPM, of the kick duration by short-circuiting the magnets and using timing shifts for use with ions. However, as proton injection for LHC is performed in two-batch filling mode, the present kick rise-time must be shortened to ~95 ns. This improvement will be done with saturable inductors and matching elements, which will also be effective for the flatness and fall-time of the kick.

The improvement required for the PS ejection kicker KFA 71-79 (Fig. 28) is more dramatic. In the nominal scheme, 3 out of 84 bunches have to be discarded, leading to the specified rise-time of 95 ns. However, even if 4 bunches are discarded, the resulting kick rise-time of 120 ns (0.5 - 99.5 %) and flat-top stability of $\pm 0.5 \%$ are very difficult to achieve. So far extensive computer modelling indicates that this requested performance could be obtained. At present, preparations are underway to experimentally verify the predictions on full-scale laboratory equipment.

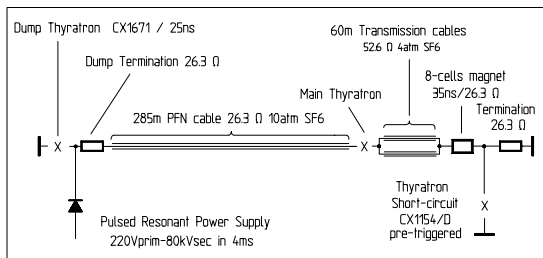


Fig. 27 PS injection kicker KFA45 (1 of 4 modules).

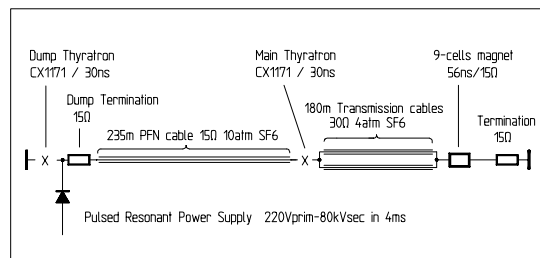


Fig. 28 PS ejection kicker KFA71-79 (1 of 12 modules).

4.4 More Powerful Water and Air Cooling Systems for the PSB

The elements of the PSB (mainly magnets and power supplies) are cooled with demineralized water, distributed in three separated circuits: “Anneau”, “Zones”, and “Locaux Techniques”. While each circuit has a different inlet cooling water pressure, the temperatures are equal. Moreover, they have a common return circuit.

Operating the PSB at 1.4 GeV raises the power dissipation of the main magnets (dipoles and quadrupoles) by about 60 % which the present cooling system can not tackle.

The demineralised water is circulating in a closed loop and cooled in heat exchangers whose primary coolant is industrial town water, sent to the drain after use. To avoid this waste of precious resources at considerable cost, CERN has decided on a policy to gradually replace town water by closed-circuit water systems using atmospheric coolants (cooling towers). For these reasons, a complete renovation of the PSB water cooling and air conditioning systems was launched (see Table 13 for the system’s key parameters).

The upgrading of the water cooling system implied (Fig. 29):

- Concentration of all system components in a new building (Nr. 237).
- Construction of a closed-circuit cooling plant based on cooling towers, thus avoiding the waste of about 100 m³/h town water.

- Increase of the installed cooling power from 4 to 5.2 MW.
- Matching of the cooling requirements to just one single demineralised water supply with common temperature and pressure.
- Installation of a new device to generate demineralised water in adjacent building 141, with a capacity of 6 m³/h, aiming at a water conductivity below 2 µS. It is based on reverse osmosis and does not any more require periodic in-situ regeneration of chemical products, except for the final ion exchangers.

Table 13
PSB water cooling system, old and new: key parameters.

	Old system			New system	
Installed cooling power [MW]	4			5.2	
Demineralised water circuit	Anneau	Locaux Techn.	Zones	Anneau + Loc.techn. and TT2	Zones
Flow rate [m ³ /h]	90	57	22	270	35
Max. inlet temperature [°C]	20	20	20	27	27
Inlet pressure on magnets [bar]	10.5	10	18	13	14.7
Outlet pressure on magnets [bar]	5	5	6	4.4	3.7
Press. difference available [bar]	5.5 ¹	5	12	8.6 ¹	11
Primary water circuit	Town water to drain			Water recycled via cooling towers	
Total flow rate [m ³ /h]	120 ²			465	
Average temperature [°C]	13			24	
Water pressure [bar]	6			2.5	
Replacement town water [m ³ /h]	-			20 ²	

Note that the primary water temperature of the new system will be subject to seasonal changes of the atmospheric coolant (air temperature, humidity), with concomitant variations of the PSB magnet temperature of up to 7°C. An extensive Machine Development (MD) session in July 1996 has demonstrated that this temperature increase does not impair at all the PSB machine performance [35].

The present air conditioning system, with an installed power of 1.8 MW, is also being adapted to atmospheric coolants, thus saving further 90 m³/h of industrial town water (Table 14). The new device will also be accommodated in building 237.

Table 14
PSB air cooling system, before and after upgrading.

	Old system	New system
Installed cooling power [MW]	1.8	3
Primary water circuit		
Flow rate [m ³ /h]	100	258
Average temperature [°C]	13	24
Town water consumption [m ³ /h]	100 (to drain)	10 (replacement)
Saving in town water consumption [m ³ /h]		90

¹ The higher pressure difference on the magnets copes with the increased dissipation power at 1.4 GeV.

² Thus the saving in town water consumption is 100 m³/h.

More detailed information on this upgrading programme may be found in [36]. The overall saving in town water consumption (both systems) amounts to 190 m³/h, with a concomitant cost saving (1999 prices) of some 170 kCHF/year. The renovated systems become operational for the accelerator start-up in March 2000.

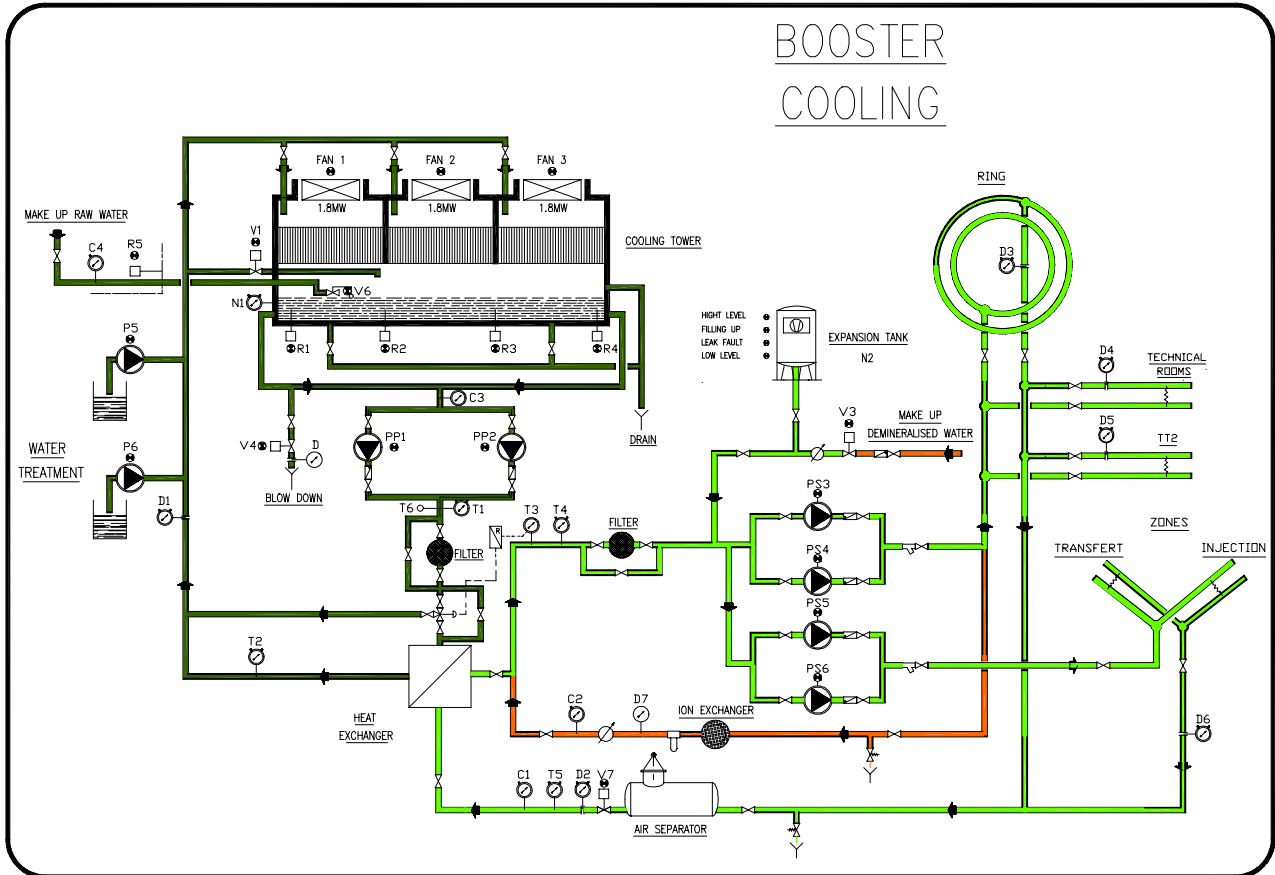


Fig. 29 Demineralised water cooling system of the PSB after upgrading.

5. NEW RF HARMONICS TO ENABLE PS TWO-BATCH FILLING

5.1 New PSB RF cavities $h=1$ (0.6 – 1.8 MHz)

The addition of cavities accelerating on RF harmonic $h=1$ and supplemented with a $h=2$ system, contributes to reduce harmful space charge effects and avoids the coupled bunch instabilities observed with the former acceleration scheme on $h=5$ [2]. These advantages are exploited equally well for all other proton beams handled in the PS accelerator chain [37]. System properties are summarised in Table 15.

A nominal peak RF voltage of 8 kV with ample margin is required, since high-intensity beams beyond 10^{13} particles per pulse and per PSB ring are to be handled. Vertical installation space is scarce due to the particular PSB construction with four superimposed rings restricting the vertical size of any equipment. For this reason the idea to squeeze four cavities in one PSB straight section was abandoned, and a second section had to be sacrificed to allow usage of large size ferrite rings.

Table 15
Main parameters of C02 RF system.

Frequency Range Cav. Equiv. Capacitance ³	MHz pF	0.6 - 1.8 700	Permeability at remanence		~600
Quality Factor ³ @			Tuning Bias	A*turn	0-500
0.6MHz		6.5	Power density	mW/cm ³	64
1.2MHz		16	Magn. RF Flux Density	mT	4-12
1.8MHz		28	Cooling Air Flow	m ³ /s	1
Cav. Shunt Res. ³ @	kΩ		Ferrite Ring Size	cm	48x24x3
0.6MHz		2.5	Total Ferrite Length	cm	1500
1.2MHz		3.0	Nominal Gap Voltage	kVp	8.0
1.8MHz		3.4	Max. Gap Voltage	kVp	10.0
Beam Impedance at resonance (with FB)	Ω	~300	Power Loss	kW	13.0
Ferrite Type (Philips)		4A11	Peak Power	kW	50
			CW Power	kW	20
			RF Feedback Loop Gain	dB	20

5.1.1 Cavity design

A classical and conservative NiZn ferrite-based design was chosen, replicating essentially the one-gap design with virtual ground symmetry in the gap mid plane of the other two PSB RF system cavities (Fig. 30) [38]. Air cooling of the ferrite through 1 mm spacing between rings gives the best ferrite filling factor, keeps the mechanical construction simple and is very cost effective compared with water cooling. The choice of Philips ferrite material grade 4A11 was made after tests on several small size ring samples, with the absence of resonant absorption phenomena in the required working area as main criterion.

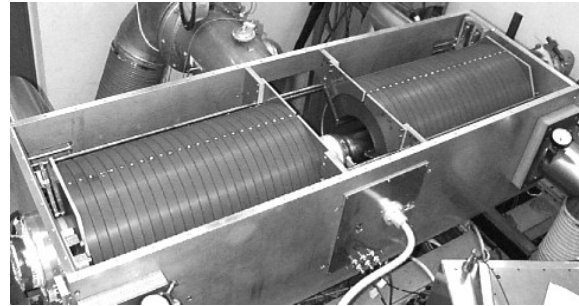


Fig. 30 Ferrite loaded cavity C02.

PSB operation implies synchronisation of the four rings with the PS cycle on a magnetic flat top (duration up to 60 ms) at constant or very slowly changing RF frequency around 1.8 MHz. It is known that under such conditions ferrite can jump into the so-called High Loss Mode (HLM) at critical excitation and disturb the servo control of the RF voltage amplitude [39]. The onset of HLM appears to arrive earlier at higher DC saturation of the ferrite, i.e. towards the high frequency end of the tuned cavities. Figure 31 shows the measured effect. The ferrite volume and cross section was chosen to stay safely below HLM onset at nominal RF voltage (8 kV_p). The selected ferrite grade exhibits a smooth and fairly stable transition into HLM and experience has shown that safe operation well beyond nominal voltage is possible. A temperature check of the individual rings in the operational cavities replaced laborious ferrite reception testing.

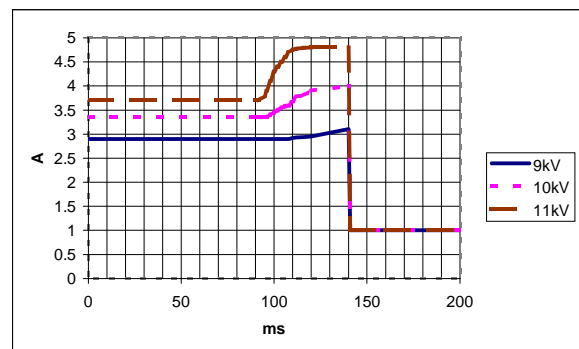


Fig. 31 Final cathode current vs. time and gap voltage
at $f = 1.8$ MHz.

³ As seen across the gap at nominal voltage, with final amplifier and all accessories connected.

5.1.2 RF amplifier chain

A conservatively-rated power amplifier was developed using the tetrode RS1084CJ, already widely used in the PS 10 MHz RF systems. Two newly developed wide-band transistor amplifiers plus a

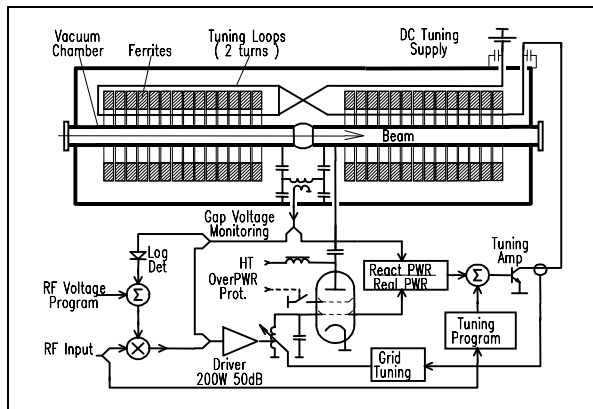


Fig. 32 C02 system layout.

power combiner (100 kHz...100 MHz) serve both as driver and fast feedback amplifier. The whole unit is water-cooled. Feedback of the gap RF signal provides reduction of the cavity impedance to the beam by about 20 dB. Higher values are possible when needed. A particularity of the design is the use of a tuned low Q resonant grid circuit [40] synchronised with the DC tuning current of the cavities. Advantages are higher gain, smaller drive power and the possibility to program phase response for increased feedback loop stability. The movable amplifiers are placed near to the cavities and can be easily replaced in case of a repair. The system layout is sketched in Fig. 32.

5.1.3 System electronics layout

The system electronics were developed to cover the frequency range of 0.5-20 MHz and are used in all PSB RF systems. Servo control of RF voltage amplitude is provided by logarithmic detector and modulator electronics (Fig. 32). The detector has a 70 dB dynamic range and ~ 0.5 dB absolute precision in the working range. Frequency response to modulation is 200 kHz for the detector and 40 kHz for the voltage control loop. The cavity tuning uses a novel IGBT linear current amplifier, which is controlled by a reactive power detection module. Maximum current is 400 A and tuning loop response to small perturbations extends to 500 Hz. The frequency to tuning current relationship is pre-programmed in a memory; fine tuning is handled in the analogue feedback loop which automatically turns on when the gap voltage exceeds ~ 100 V. An RF overpower detector acts rapidly on the final tube screen grid to prevent system trips. Two such systems as shown in Fig. 33 are installed in PSB straight sections 10L1 and 7L1.

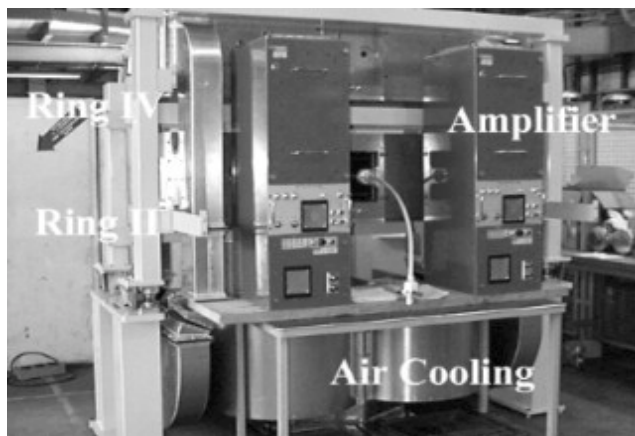


Fig. 33 C02 test mount for PSB rings II and IV.

5.2 Converted PSB $h=2$ cavities (1.2 – 3.9 MHz)

With the abandoning of RF harmonics $h=5$ it became possible to modify the existing equipment for $h=2$ operation at little cost. Cavities modifications mainly consisted in increasing the gap equivalent capacitance, so as to shift the working frequency to 1.2 - 3.9 MHz, and replacing the gap voltage divider with a calibrated, wide-band unit.

Although the gap voltage required for $h=2$ operation is only $2/3$ of the previously used voltage at $h=5$ (8 kV instead of 12 kV), the frequency decrease by a factor $2/5$ results in an RF induction increase given by the ratio of the two factors (~ 1.7). This pushes the ferrite (Philips 4L2) more to its limits, and the nominal RF voltage is reached without much margin. Ferrite entering into HLM, which with this ferrite grade appears to be unstable, is the critical parameter. Operation at constant frequency (~ 3.5 MHz) for synchronisation of the four rings with the PS RF system, has to be limited in duration as shown in Fig. 34.

The existing push-pull power amplifiers, using two RS2012CL tetrodes, have been retained without modifications. They are air-cooled and share the cooling system with the cavities (Fig. 35).

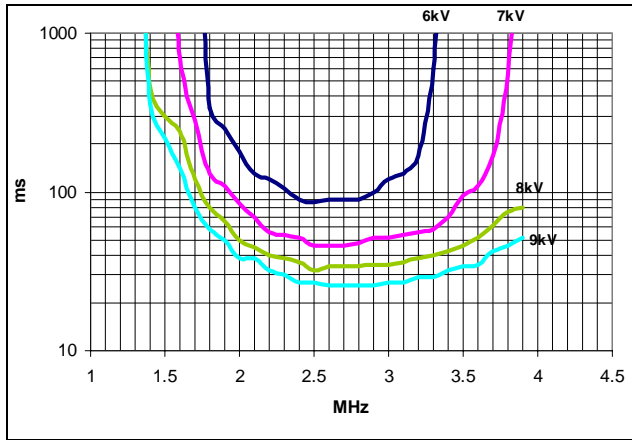


Fig. 34 High loss mode on-set time.

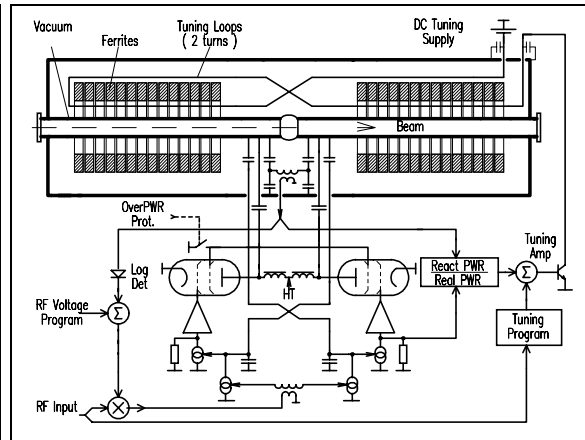


Fig. 35 C04 system layout.

Standard 100 W wide band amplifiers already used in the C02 systems have been added as fast feedback power drivers. Feedback of the gap RF signal provides reduction of the cavity impedance to the beam by 20-26 dB.

Although most of the heavy hardware has been retained, control and servo electronics have been replaced with the new, wide-band standard electronics developed for the C02 system. The system properties are therefore similar to those already described in the previous section. System properties are summarised in Table 16.

Table 16
Main parameters of C04 RF system.

Frequency Range	MHz	1.2 – 3.9	Tuning Bias	A*turn	0 - 1800	
Cav. Equiv. Capacitance ⁴	pF	650	Power density	mW/cm ³	31	
Quality Factor ⁴ @			Magn. RF Flux Dens	mT	3.2 – 9.4	
	1.2MHz	85	Cooling Air Flow	m ³ /s	1	
	2.5MHz	130	Ferrite Ring Size	cm	35x20x3	
	3.9MHz	190	Total Ferrite Length	cm	1500	
Cav. Shunt Res. ⁴ @	kΩ		Nominal Gap Voltage	kVp	8.0	
	1.2MHz	17.5	Max. Gap Voltage	kVp	9.0	
	2.5MHz	12.5	Power Loss	kW	3.0	
	3.9MHz	12.0	Peak Power	kW	20.0	
Beam Impedance (with FB):	kΩ		CW Power	kW	10.0	
	1.2MHz	0.88	Feedback Loop Gain @	dB		
	2.5MHz	0.79			1.2MHz	26
3.9MHz	1.07	2.5MHz			24	
Ferrite Type (Philips)		4L2			3.9MHz	21
Permeability at Remanence		~200				

⁴ As seen across the gap at nominal voltage, with final amplifier and all accessories connected.

5.3 PSB beam control modifications

The PSB is composed of four superimposed rings, each having three cavities described in Table 17.

The present beam control was installed in 1998 within the framework of the harmonic change from $h=5$ to $h=1$ and/or $h=2$. Its structure is based on one digital frequency synthesiser per cavity, each digital frequency word being directly derived from the main magnetic field measurement (B to f conversion). The present architecture is represented in Fig. 36. For one PSB ring, the parameters of the LHC beam are: one single proton bunch, 190 ns long, obtained with longitudinal blow-up (momentum spread $\Delta p/p = \pm 2.5 \cdot 10^{-3} (\pm 2\sigma)$).

Table 17
PSB cavities.

Cavity	Frequency range	Maximum voltage	Use (for protons)	Use (for ions)
C02	0.6 → 2 MHz	8 kV	Acceleration on $h=1$	Acceleration $h=4$ up to 1.8 MHz ($f_{rev}=450$ kHz)
C04	1.2 → 3.9 MHz	8 kV	Bunch flattening Bunch splitting ($h=1 \rightarrow 2$) at 1.4 GeV Acceleration on $h=2$	Acceleration on $h=4$ from 1.8 MHz ($f_{rev}=450$ kHz) up to 3.86 MHz ($f_{rev}=965$ kHz)
C16	5 → 16 MHz	6 kV	Controlled longitudinal blow-up ($h=9$) near 1.4 GeV	

5.3.1 Hardware layout.

Figure 36 shows that the measured value of the dipolar field (“B-train”) is used for generating the frequency words feeding all three cavities. The revolution frequency (f_{rev}) is obtained from a look-up table (typically a read only memory) and multiplied by the harmonic number aimed for C02 ($h=1$ for LHC beams). The resulting frequency is summed with the loop (phase and synchronisation) error signals, so as to obtain the actual C02 RF value sent to the cavities via a digital synthesiser.

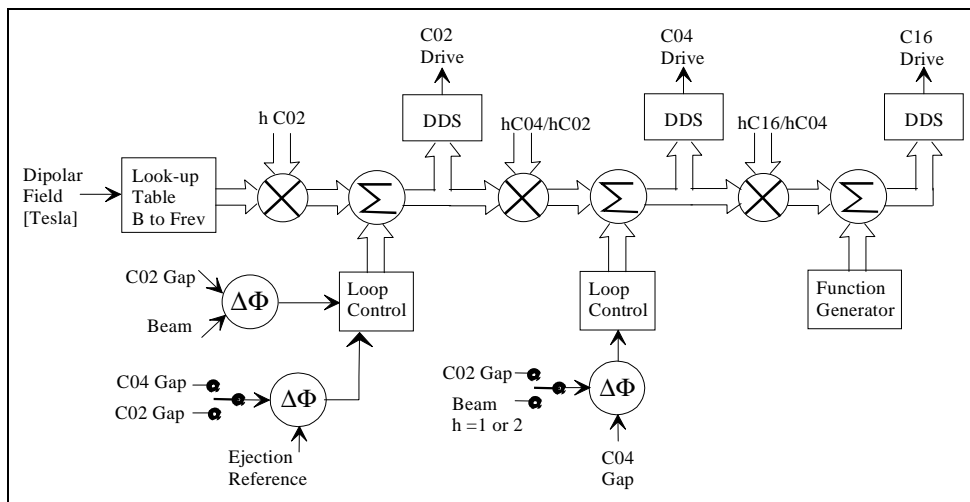


Fig. 36 PS Booster Beam Control layout.

The same principle applies for C04 and C16 cavities. Moreover, depending on the user, C04 is operated in single or dual harmonic mode. In the former case C04 is working on its own at $h=2$ (for some proton beams), whereas in the latter case it is tracking the C02 ($h=1$) cavity so as to obtain particular bunch shapes to improve for example the bunching factor.

C16 is used as a “controlled blow-up” cavity and therefore not included in any loop. Its frequency is modulated by a function generator. The blow-up principle is similar to the one used in the PS or SPS [41] and consists of a phase modulation (typically at $3f_s$) of a high harmonic signal ($h=9$).

The main advantages of the digital structure are:

- The look-up-table on the left-hand side of Fig. 36 sets the RF frequency so as to keep the beam on orbit for any magnetic field. This feature makes it possible to accelerate a beam with all loops open (albeit with some losses and instabilities). In the previous (analogue) version, only the radial loop could establish the required frequency to keep the beam centred but the position detectors were quite hard to run at low intensity beams (e.g. lead ions).
- All cavities are naturally locked in frequency even with loops open; this avoids the presence of an integrating type of corrector in the different phase loops (simplified correctors and more stability margins).
- In the old system, the loss of beam led to saturation of the different loops and erratic behaviour of the frequency and voltage programmes necessitating security interlocks, quite heavy to handle, to protect the power equipment. In the new system the loops just need to act on a small frequency range and do not provoke cavity trips.

5.3.2 The transition to $h=1$

Since its running-in period in 1972, the PSB machine was subject to many improvements. The most perceptible in 1983 consisted in the introduction of a second harmonic cavity on each ring. The peak accelerated intensity levelled off from that time at about $3.4 \cdot 10^{13}$ protons per pulse (ppp) with all four rings ($1.1 \cdot 10^{13}$ on ring 2). The introduction of a fast feedback on the cavities in 1985 consolidated the operation, but did not improve the record value.

During the first $h=1$ run in 1998, the operation was disturbed by the impedance of the vacuum flanges around the ring. The resonances of these flanges gave a total (integrated around the ring) longitudinal coupling impedance of 450Ω at 750 kHz [42] which is the RF frequency range at the beginning of the cycle. The return voltage generated by the beam current was coupling to different electronic devices which therefore had to be equipped with common mode rejection circuits. Some coupling between rings remained, implying adjustment of the radial position to avoid beating between cavities near the synchrotron frequency. After some flanges had been short-circuited [42] during the 1998-99 shutdown the total impedance was lowered to about 200Ω (still higher than the maximum value for $h=5$ which was 130Ω). This eliminated the frequency beating from one ring to the other as a source of trouble and helped to reach a new intensity record in September 99: $4.1 \cdot 10^{13}$ ppp accelerated in the PSB with $1.2 \cdot 10^{13}$ in ring 2. New RF decoupling flanges will be introduced in the 1999-2000 machine shut-down to further reduce the impedance.

The transition to $h=1$ eliminated the coupled bunch mode instabilities (inexistent with a single bunch) and thus made the complex feedback system as well as the “Hereward” damping system (tackling quadrupolar bunch-shape oscillations) superfluous. This last effect, not formally studied, might be explained by a criterion given in Refs. [43, 44] that relates the loss of Landau damping to the beam current. The current threshold, proportional to V_{RF}/h , has been improved by a factor 3.3 when moving from $h=5$ to $h=1$. The absence of the quadrupolar loop indirectly permitted an increase of the $h=2$ versus $h=1$ voltage ratio limited to 50 % in the former system where beam amplitude detection was misled by double peaked bunches.

Another improvement came from the C04 ($h=2$) cavities. These were obtained from the conversion of the older C08 cavities that were used as the main $h=5$ drive cavities. They have more voltage and power margin than the previous C16 cavities used at $h=10$ and thus run more reliably whenever the phase relationship between $h=1$ (C02) and $h=2$ (C04) is critical in terms of power demand from $h=2$.

All these improvements certainly contributed to the record intensity increase.

In summary, the main advantages of the $h=5$ to $h=1$ conversion are:

- Feasibility of two-batch filling of the PS as required for the LHC beam.
- Increase of longitudinal acceptance (proportional to $\sqrt{V_{rf}/h}$).
- No need of coupled bunch mode feedback system.
- Less longitudinal space charge effect \Rightarrow no need for Hereward damping at present intensities.

5.4 PS beam control

For the needs of the proton beam for LHC, the PS has been equipped with a beam control operating on harmonics 8 and/or 16 and capable of controlling bunch splitting with the beam phase loop closed. The basic block diagram of that beam control is sketched in Fig. 37. Similar principles have been used in the design of the low level RF systems of the PS [45] and PSB, and a large fraction of the electronic modules are the same.

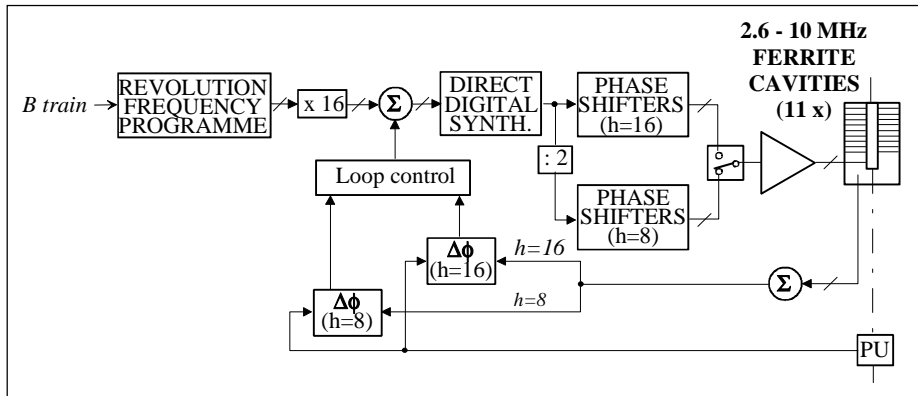


Fig. 37 Principle of the PS beam control for LHC.

The open loop revolution frequency is derived from a look-up table controlled by a real-time B -field measurement (B -train). After digital multiplication by the harmonic number, the RF on $h=16$ is generated by a Direct Digital Synthesiser (DDS). Dividing it by 2, $h=8$ is derived with a fixed phase with respect to harmonic 16. On these harmonics the distance between cavities differ from an integer number of RF periods so that phase shifters are implemented in the forward and return paths to and from each of the 11 ferrite cavities.

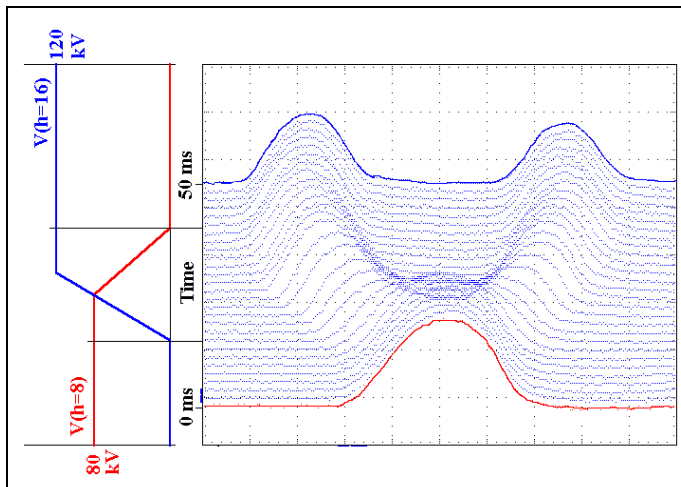


Fig. 38 Bunch splitting at 3.57 GeV/c in the PS
1 trace / 800 turns - $I_{beam} = 3 \times 10^{12}$ ppb.

Closed loop operation is obtained by modulating the control signal of the DDS as a function of the instantaneous phase of the beam with respect to the RF. That phase being simultaneously measured on harmonics 8 and 16, the loop can be kept closed during bunch splitting by smoothly changing from one harmonic to the next (Fig. 38). In these conditions the bunch splitting process has proven to be robust against drift up to the highest intensities required by operational beams.

5.5 Repercussions on other PS beams

The switch of the PSB from a systematic number of five proton bunches per ring to one or two bunches led to a redesign of all RF operations both in the PSB and the PS, and a renewal of the beam control equipment. In the PSB, each ring is now equipped with two beam control systems: one is used for protons and controls all three RF cavities (C02, C04, C16), whereas the lead ion system assures acceleration of four bunches by controlling C02 and C04.

Three beam control systems are available in the PS [45]: (i) medium and high intensity proton acceleration on $h=8$ & 16; (ii) acceleration of lowest intensity beams (protons, lead ions) on $h=16$; (iii) a system enabling the beam to undergo stepwise harmonic changes $h=8-10-12-14-16-18-20$ for p-bar production for the Antiproton Decelerator (AD). Adequate functions are implemented in the PS to handle the various modes of transfer from the PSB to the PS (one or two proton bunches per ring, in one or two batches).

More details on how to produce the various operational PS beams are compiled in Table 18. A four-weeks running-in period in March 1998 was entirely devoted to assuring the production of most of these operational beams; 1999 saw the commissioning of the increased PSB extraction/PS injection energy of 1.4 GeV.

Table 18
Typical operational beams after 1998, and ways to produce them.

	ISOLDE	LHC nominal	SPS physics	SPS ion physics	East Hall	AD p-bar production	AD test
Particle	p	p	p	Pb ⁸²⁺	p	p	p
PSB extraction				(Pb ⁵³⁺)			
Energy/nucl. [GeV]	1/1.4	1.4	1.4	0.145	1.4	1.4	1.4
Charges/ring	$8 \cdot 10^{12}$	$1.15 \cdot 10^{12}$	$8 \cdot 10^{12}$	$5 \cdot 10^9$	$\sim 3 \cdot 10^{11}$	$5 \cdot 10^{12}$	$4 \cdot 10^{10}$
Harmonic number	1	1	2	4	1	1	2
Bunch splitting.	no	no	yes	no	no	no	no
Rings used	4	4	4	4	1	4	1
PSB batches	1	2	1	1	1	1	1
Bunch spacing at PS inject.[ns]		286	286	259		286	
Bunch length [ns]	190	190	176	90	50-120	190	140
Kicker rise/fall time max. [ns]	382	96	110	169		96	
PS injection							
Charges		$9.2 \cdot 10^{12}$	$3 \cdot 10^{13}$	$2 \cdot 10^{10}$	$\sim 3 \cdot 10^{11}$	$2 \cdot 10^{13}$	$2 \cdot 10^{10}$
Harmonic number		8	8	16	8	8	16
Number of bunches		4 + 4	8	16	1	4	1
Bunch splitting at 3.56 GeV/c		yes	yes	no	no	no	no
PS extraction							
Momentum/charge [GeV/c]		26	14	20	24	26	3.56
Harmonic number		84	420	16	debunched	20	16
Number of bunches		84	420	16		4	1
RF gymnastics before extraction		debunch. rebunch. +rotation	debunch. rebunch.	none	debunching (+slow extraction)	h sweep from 8 to 20 and rotation	none
Comments			often lower intens.	in-flight transfer C02-C04 in PSB	lower intensity often required		1 bunch discarded at PS injection

These fundamental changes prove advantageous – rather than detrimental – to the quality of most of the beams; the main advantages are listed and commented below:

- With one bunch per PSB ring, schemes to fill a fraction of the PS with four PSB rings can be designed (LHC, p-bar production beam for the AD, maybe others).
- The RF harmonic 1 raises the PSB longitudinal acceptance, thus eliminating a long-standing bottleneck.
- One bunch in a ring cannot be driven unstable by coupled-bunch modes, resulting in more stability in the PSB.
- The longitudinal spectrum of very long bunches (50 to 100 m in both PSB and PS) is narrower, so they do not probe potentially harmful impedances at high frequencies.
- Bunch splitting – together with controlled longitudinal blow-up techniques – is now possible also in the PSB (the old 2nd harmonic cavity, C16, is employed for longitudinal excitation, while 200 MHz cavities are used in the PS, as before).
- The risetime of the PSB ejection, recombination, and PS injection fast kicker magnets is now relaxed to at least 90 ns (instead of 60 ns when PSB was operating with 5 bunches).
- All beams are now injected at 1.4 GeV, thus raising the space-charge limit for all high intensity beams in the PS, such as SPS fixed target physics, AD production, and certainly others to come. Moreover, beam losses between PSB and PS are reduced due to the smaller beam size of the highest intensity beams.

A more extensive analysis of the PS complex’ operational beams after the conversion to LHC may be looked up in [37]; not all parameters given therein are up-to-date.

6. NEW RF CAVITIES IN PS TO PRODUCE LHC BUNCH SPACING

6.1 Debunching, rebunching and bunch rotation in the PS

6.1.1 Low-level RF

After acceleration to 26 GeV/c on $h=16$ by the ferrite cavity system, the beam has to be tailored to meet the needs of the SPS and LHC before ejection [46], (Table 19). To this end, RF systems capable of delivering 300 kV at 40 MHz and 600 kV at 80 MHz have been built (see Section 6.2). The basic principle of the associated low-level RF system is illustrated in Fig. 39.

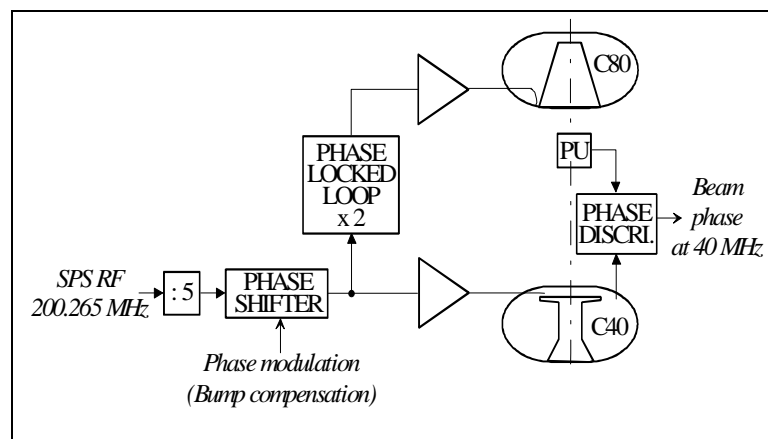


Fig. 39 Basic block diagram of the 40 and 80 MHz low-level RF system.

Both the 40 and 80 MHz frequencies are derived directly from the SPS RF frequency. The system is open loop because the beam is not held long enough to make use of a phase loop coupled to a synchronisation loop. The phase of the 40 MHz beam component with respect to the cavity voltage is available for observation purposes. A phase shifter serves to keep the beam energy constant while the orbit length is increased by the action of the pulsed extraction bump.

A sampling servo-loop (not represented in Fig. 39) has also been prepared to cancel slow drifts of the beam phase with respect to the SPS reference signal, but it has not yet been required.

6.1.2 Beam dynamics

The following operations are performed successively on a 26 GeV/c flat-top:

- Adiabatic debunching by a reduction, in 30 ms, of the RF voltage on $h=16$ from 200 to 1 kV. At the end of this process, just before the final step to 0 kV, the 16 bunches completely fill their buckets.
- Removal of density variations by letting the coasting beam drift for 100 ms.
- Adiabatic rebunching on $h=84$ by increasing, in 18 ms, the RF voltage on $h=84$ (40 MHz) from ~ 3 kV to 100 kV. Each of the 84 bunches is then shorter than 11 ns.
- Bunch rotation, 290 μ s before ejection, by first stepping the voltage on $h=84$ to 300 kV and, 180 μ s later, by applying 600 kV on $h=168$ (80 MHz). Ejection is triggered 110 μ s later when the bunches are at their shortest.

Figure 40a (bottom) shows the voltage on the three RF systems as functions of time. Figure 40b (top) is a spectrogram of the longitudinal Schottky signal at 394.82 MHz ($h=828$). The successive operations are clearly visible, as are:

- the imperfection of the debunching process, which is accompanied by a spurious displacement of the beam;
- a further displacement of the coasting beam, which is probably due to a slope of the main dipole field;
- a frequency shift, starting ~ 7 ms before ejection, caused by the orbit bump.

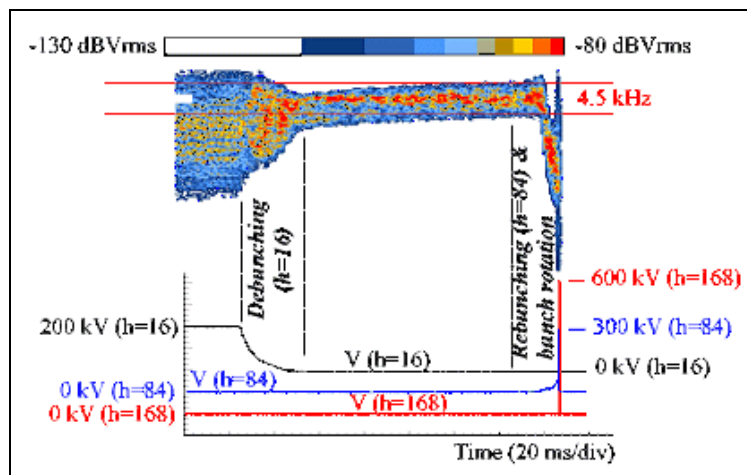


Fig. 40 Debunching, rebunching and bunch rotation at 26 GeV/c at the commissioning intensity of $2 \cdot 10^{12}$ ppp. a) Voltage programmes. b) Spectrogram of the longitudinal Schottky signal.

A controlled longitudinal blow-up (using some 200 MHz voltage) is applied during debunching to avoid any instability of the coasting beam. At an intensity of $2 \cdot 10^{12}$ ppp, the expected energy spread [46] is indeed achieved: $\Delta f = 4.5$ kHz, corresponding to $\Delta p/p = 4.5 \cdot 10^{-4}$. The evolution during the last 4 ms before ejection of the peak pick-up signal and the voltage programmes of the 40 and 80 MHz systems is shown in Fig. 41.

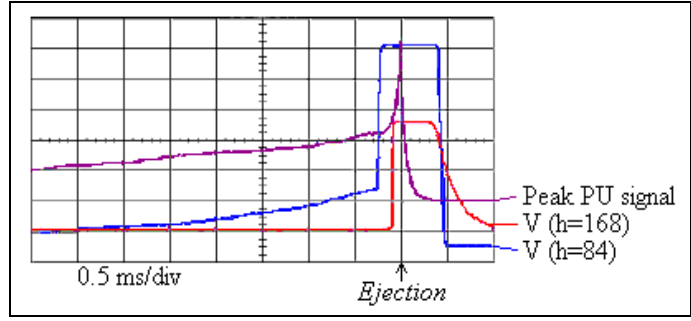


Fig. 41 Voltages and peak pick-up signal before ejection.

The orbit bump which moves the beam towards the extraction septum has a deleterious effect on the processes of rebunching and bunch rotation. This is compensated by programming the phase of the 40 and 80 MHz RF so that the buckets remain at constant energy while the phase at ejection is kept the same from cycle to cycle (phase modulation with a fixed point at ejection). If the mean radial excursion due to the bump reaches a maximum of ΔR in a time T , the orbit may be assumed to evolve according to

$$R(t) = R_{nom} + \Delta R \cdot \sin\left(\frac{\pi t}{2T}\right).$$

Hence, at constant energy, the (angular) RF frequency differs from its nominal value by

$$\Delta\omega(t) = -\omega_{nom} \cdot \frac{\Delta R}{R_{nom}} \cdot \sin\left(\frac{\pi t}{2T}\right).$$

Integrating gives

$$\Delta\phi(t) = \omega_{nom} \cdot \frac{\Delta R}{R_{nom}} \cdot \frac{2T}{\pi} \cdot \left[\cos\left(\frac{\pi t}{2T}\right) - 1 \right].$$

This is the form of the function with which the 40 and 80 MHz RF are phase shifted during rebunching and bunch rotation.

Figure 42 shows the result on the beam phase (top trace) of the compensation of the bump (middle trace) by a suitable phase modulation (bottom trace).

The bunches obtained at ejection at the nominal intensity of $1.1 \cdot 10^{11}$ protons per bunch (ppb) and at $3 \cdot 10^{10}$ ppb (roughly the commissioning intensity) are shown in Fig. 43. Longitudinal beam characteristics are summarised in Table 19.

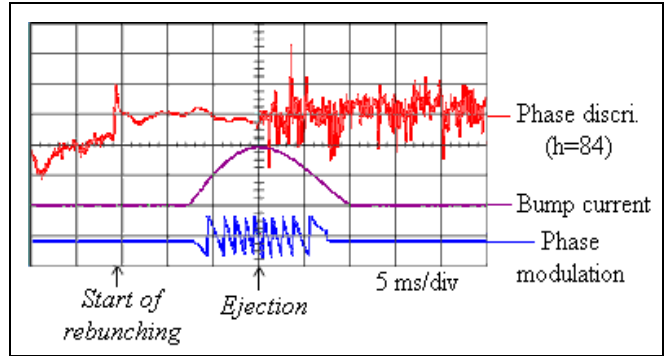


Fig. 42 Bump compensation.

Table 19
Longitudinal beam characteristics at ejection from the PS (25 ns bunch spacing).

Intensity (ppb)	$3 \cdot 10^{10}$ (achieved)	$1.1 \cdot 10^{11}$ (achieved)	$1.1 \cdot 10^{11}$ nominal
ϵ_L per bunch (eVs)	0.4 (± 0.05)	0.5 (± 0.05)	0.35
Bunch length (ns)	4.3 (± 0.2)	5 (± 0.2)	4
Total $\Delta p/p$	$4.3 \cdot 10^{-3}$	$4.5 \cdot 10^{-3}$	$4.1 \cdot 10^{-3}$

Because of the absence of margin in the original design of the RF gymnastics [47], the bunch length is too large at ejection. The problem is an instability of the coasting beam after adiabatic debunching. However, some improvement may be expected from one or more of the following actions [48].

- The removal from the PS ring of the 114 MHz cavities used for the acceleration of leptons. These cavities exhibit numerous higher order resonances which are strongly excited during the instability of the debunched beam. Their removal is planned for the shutdown of 2000-2001, i.e., after LEP stops.
- The use of more voltage at 40 and 80 MHz. The spare cavities (one at each frequency) can be activated simultaneously with the standard ones, making the bunches shorter at the cost of increasing their energy spread.
- The replacement of the debunching–rebunching process by a cascade of bunch splittings (see Chapter 8). This will also provide a gap in the train of bunches for the rise-time of the extraction kicker.

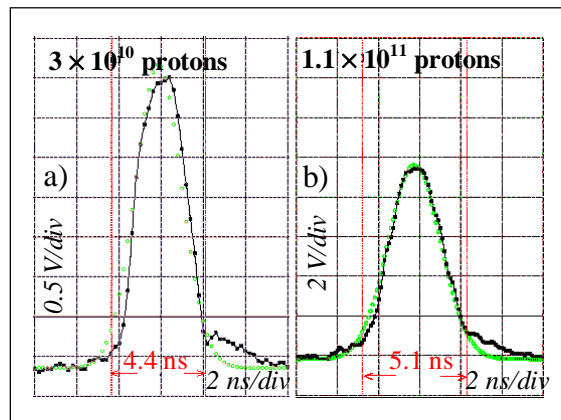


Fig. 43 Bunches at ejection from the PS at (a) commissioning and (b) nominal intensity.

6.2 40 MHz and 80 MHz cavities

6.2.1 Requirements

The bunch compression scheme utilises both adiabatic and non-adiabatic cavity gap voltage variations [37, 46, 49]. For the quasi-adiabatic part, smooth voltage variations must be possible, i.e. the dynamic range must be free of gap MultiPactor (MP). The dynamic range of the 40 MHz system is required to be 3...300 kV⁵. For the non-adiabatic part (bunch rotation), both the 40 MHz and the 80 MHz cavities should be able to be filled in $\sim 20 \mu\text{s}$. Small pulse lengths of up to 10 ns at duty cycles of below 1 % are required for the 40 MHz system – the 80 MHz systems is also capable of delivering long pulses. Beam loading is strong (nominal beam current at 40 MHz: 1.24 A). The impedance must be kept as small as possible in order not to perturb other beams.

6.2.2 Power considerations

Three somewhat competing requirements determine the power rating of the final amplifiers and the cavities:

- Power loss in the cavity walls, which favours a large shunt impedance. Since we need only short pulses and small duty cycles, this aspect is of minor importance for the 40 MHz cavities. Concerning the 80 MHz cavities, the design includes the option to accelerate leptons, which requires a high average power, so this argument gains importance.

⁵ Peak values are used for RF voltages and currents throughout.

- Instantaneous power needed to fill the cavity to full voltage in a short time. This favours small stored energy, i.e. a high R/Q . This short rise time requirement dominates the dimensioning of the Power Amplifier (PA) for the 40 MHz cavity.
- Reactive power due to transient beam loading: during the whole process of bunching, the voltages in both the 40 MHz and the 80 MHz cavities are kept in quadrature to the beam current. Seen from the amplifier, this is equivalent to an inductive reactance. At steady state, this could in principle be entirely compensated by a parallel capacitance, in other words by detuning the resonance frequency by

$$\frac{\omega - \omega_0}{\omega_0} = \left(\frac{R}{Q} \right) \frac{|I_B|}{2V_{\text{gap}}}.$$

- Note that the necessary detuning increases with R/Q . However, the detuning depends on both gap voltage and beam current. In order to compensate the reactance both before and after a non-adiabatic voltage variation, one would need a very fast tuner (μs !). The possibility to achieve this using perpendicularly biased ferrites has been thoroughly investigated, showing that such a tuner would not be a practicable solution [56].
- Without a fast tuner however, the output of the PA is strongly mismatched either before or after the gap voltage step. Even after balancing this mismatch to limit the absolute value of the generator current, a large complex power must still be delivered by the PA – it must operate as an “electronic tuner”. For a high Q cavity, the lowest maximum generator current (transformed to the gap) can be estimated to be slightly higher than half the beam current (0.7 A at nominal 300 kV). This is a strong effect and is taken into account in the design of the amplifier.

6.2.3 Cavity geometry

As a result of the above considerations, the ratio R/Q should be moderately small, requiring a strong capacitive load. For the actual parameters see Table 20 below. The optimum gap size was determined by MP and voltage breakthrough: The first order band of two point MP at the gap occurs around

$$V = (\omega g)^2 \frac{m_e}{2e},$$

higher order MP bands will have even lower resonance voltages [50]. Minimising the gap width g will bring the voltage V at which this condition is satisfied to very low values. This will determine the lower limit of the dynamic range of the gap voltage – with the 50 mm gap, this value is approximately 0.5 kV at 40 MHz, 2 kV at 80 MHz. The magnetic fringe field of the near-by ring dipoles increases these values: the measured MP band at 40 MHz was 300...1200 V at low magnetic field, 700...3300 V at high field. After conditioning, these bands became somewhat narrower.

The upper gap voltage is limited by vacuum breakdown, which can be conservatively estimated using Kilpatrick’s expression [51]. The voltage of 300 kV corresponds, with the chosen gap size of 5 cm, just to Kilpatrick’s limit at 40 MHz, and to 0.8 Kilpatrick at 80 MHz. Kilpatrick’s limit is known to be very conservative, and consequently, even at 470 kV, we have not observed any gap voltage breakdown.

The axially asymmetric, re-entrant cavities are machined from forged 316 L+N steel, galvanically copper plated on the inside. Many parts are identical for both systems – the main difference is the capacitive loading of the 40 MHz gap (see Fig. 44 below). The outside dimensions of the cavities are approximately: length 1 m, diameter 1.6 m. The asymmetry and the small gap helped accommodate the mechanical short circuit (Fig. 45). The 80 MHz cavities are water cooled for lepton operation.

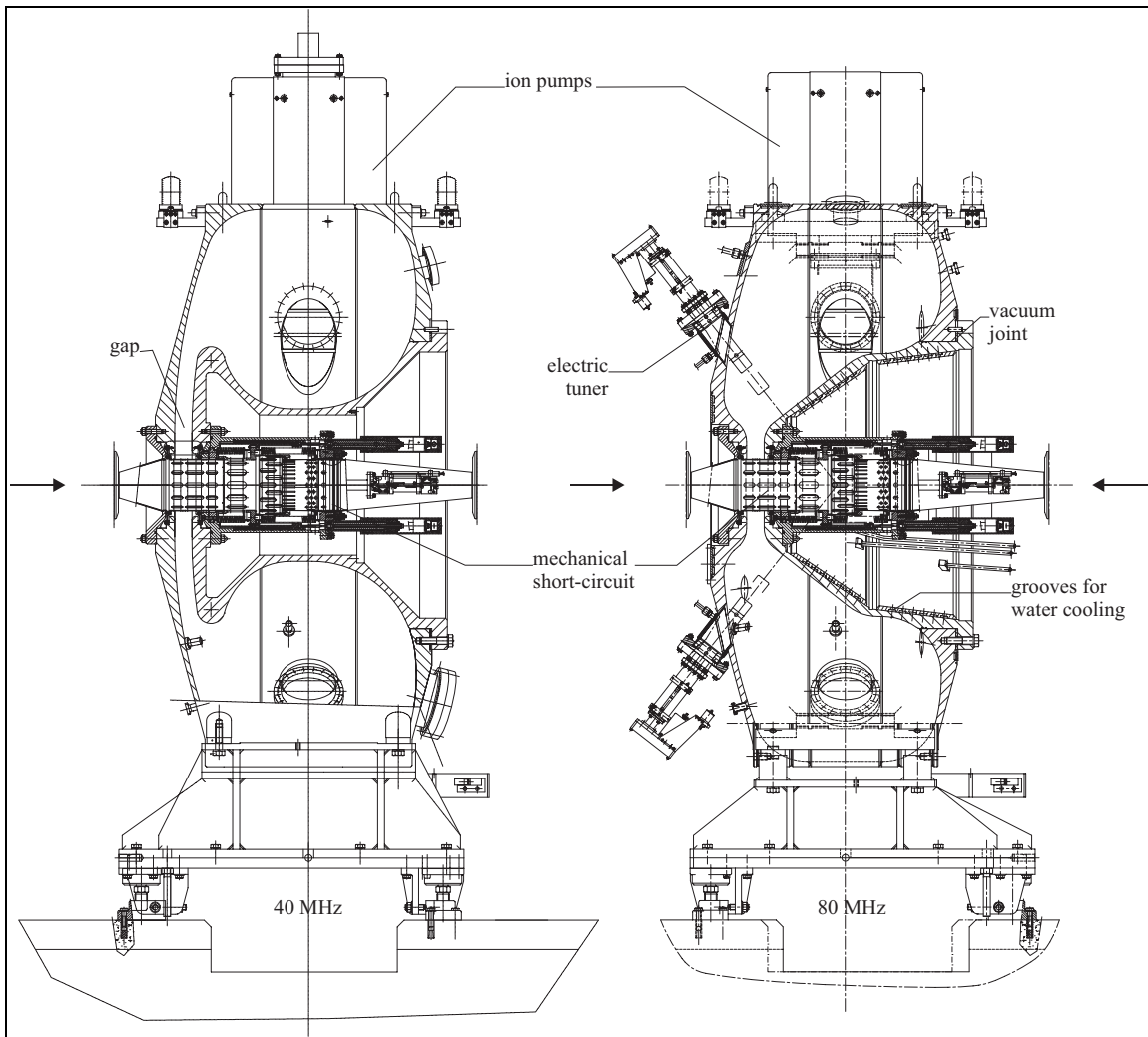


Fig. 44 Longitudinal section of the 40 MHz (left) and 80 MHz cavities (right).

6.2.4 Fast RF feedback

For beam stability reasons, the impedance seen by the beam (also other beams than for LHC) must be as small as possible. For the accelerating mode, this impedance can be drastically reduced with fast RF feedback. Detecting the gap voltage and feeding this signal back to the input of the amplifier chain will reduce both shunt impedance and Q by the loop gain. The gain characteristics have to be tailored to result in a large gain over a wide band around the operating frequency, a small group delay, and stability. We have obtained a gain of 43 dB (140) at 40 MHz, and 41 dB at 80 MHz. The group delay is 220 ns in both cases, the 3-dB-bandwidth approximately 600 kHz. The resulting longitudinal impedances per cavity are 2.3 k Ω at 40 MHz and 5.6 k Ω at 80 MHz, with equivalent Q 's of 70 and 100, respectively. To further increase the amplifier stability margin (12 dB), the cavities are currently operated with a reduced loop gain of 40 dB.

6.2.5 Higher order mode damping

While the beam impedance at the fundamental frequency is reduced electronically, potentially dangerous Higher Order Modes (HOMs) are passively damped. The strong capacitive loading of the cavities (low R/Q) has the positive side-effect that electric and magnetic energies are stored at separate locations inside the cavity volume, making the cavity behave more like a lumped-element circuit, pushing the frequencies of the first HOMs much higher. As a consequence, the first monopolar HOM of the 40 MHz cavity appears at 260 MHz, that of the 80 MHz cavities around

220 MHz. Also, the fundamental mode has virtually no electric field at the outer circumference of the cavity volume – electric couplers placed there thus do not couple to it, but they do couple to the HOMs.

The HOM dampers now consist of short antennas, each of them optimized to couple to the electric field of an individual HOM. The actual dampers are $50\ \Omega$ loads outside of the cavity, connected to the antenna via feed-throughs. Four HOM dampers are used in each cavity. All HOM dampers were studied, optimized and built at TRIUMF. Most of the study and optimization took place using a scale 1, copper lined wooden model of the cavity [53, 59]. For the 80 MHz cavity, the HOM dampers are water cooled.

6.2.6 Mechanical short circuit

The fast RF feedback reduces the cavity impedance seen by the beam significantly, but it requires the system to be switched on and running. When the system is switched off, the gap is closed by a pneumatically operated short-circuit.

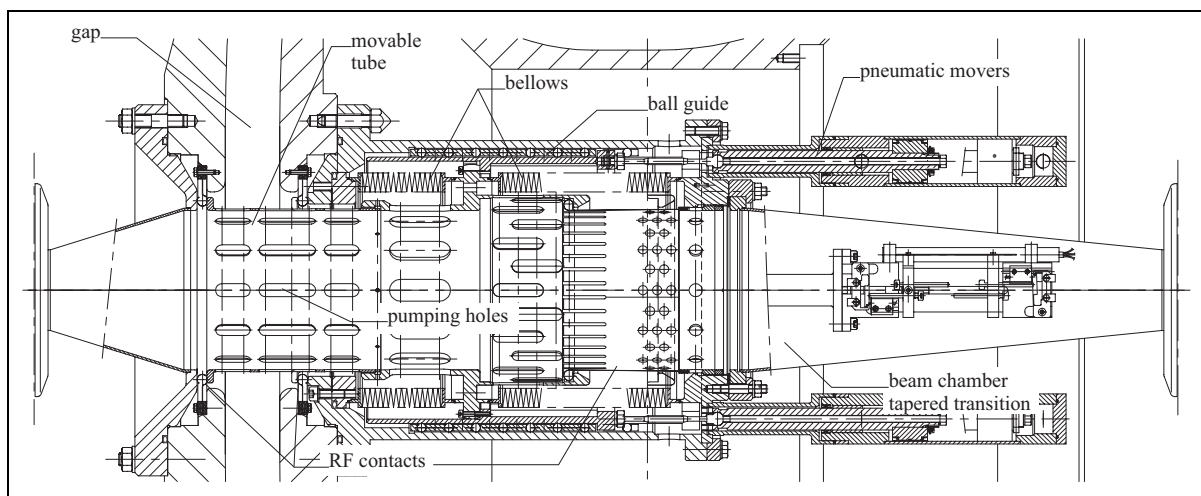


Fig. 45 Construction of the mechanical short circuit (shown in its closed position).

The short-circuit consists of a metallic tube which can be moved like a piston across the gap (stroke 78 mm). The tube has the diameter of the vacuum chamber and is constrained by a cylindrical ball guide, situated outside of the vacuum. A number of holes in this tube allow efficient vacuum pumping. RF contacts assure well defined current paths in both open and closed position, and two bellows assure vacuum tightness. The gap can be opened or closed in 0.6 s by two pneumatic arms, and end switches serve as indicators and interlocks. The short-circuit system has been carefully tested (some 10^5 cycles in a specially constructed test set-up) and proven very reliable [52].

6.2.7 Amplifier

The design of the amplifier chain is influenced by several major constraints. The output power must be of the order of 350 kW for rapid cavity filling at high cavity voltage. A forward gain from the chain input to the cavity of about 90 dB is necessary so that at 40 dB loop gain the cavity loop pickup and the feedback summing amplifier can operate at low level (about 2 W). The additional phase shift round the loop for frequency excursions either side of the resonance frequency of the cavity (f_0) must not exceed $\pm 90^\circ$ ($\pm 180^\circ$ total) at the points where the loop gain is -12 dB (the gain margin). This imposes a loop group delay of 230 ns maximum.

These last two considerations of gain and delay imply a solid state pre-driver amplifier (65 dB gain), situated at 10 m distance from the cavity to reduce irradiation, followed by a low gain 40 kW driver amplifier for the final stage input. The group delay of these amplifiers is 35 ns and 100 ns respectively, leaving about 95 ns for the connecting cables and hybrid summing amplifier.

A Thomson TH681 tube operated at 20 kV High Voltage (HV) in grounded grid mode provides the final output power. The tube anode is connected to the cavity coupler via a short (about 60 cm) coaxial line transformer (see Fig. 46), and the cathode is matched by an LC network to the $50\ \Omega$ line from the 40 kW driver amplifier.

Strong side resonances exist due to transformation of the cavity impedance by the line and coupler between anode and gap at frequencies near the cavity f_0 . The peaks and troughs of these resonances can provoke loop instability and strong frequency dependence of the anode to gap voltage step-up ratio respectively. Correct design of the line and coupler push these resonances away from, and situate them symmetrically about, f_0 . The line is composed of several sections of different impedances such that the low voltage/high current (350 A) at the coupler window is transformed to 16 kV/25 A in the plane of the anode [52].

In the case of the 80 MHz amplifier, the higher frequency causes a voltage zero to occur just above the top of the TH681 tube. This provided a convenient point to introduce the 20 kV HV via a $\frac{1}{4}$ -wave isolator. From this point on toward the cavity the line impedance is kept at $18\ \Omega$ so that the voltage at the small coupler window is nominally less than 8 kV [58].

When the mechanical gap short-circuit is open during normal LHC operation, the amplifier chain operates at greatly differing power levels for quiescent beam induced voltage reduction, cavity filling, or for lepton operation. The first of these three regimes requires low power and is quasi-continuous, and maintenance of the final amplifier bias level of 20 kV at 4 A would be undesirable. For lepton operation where the pulse length is long (800 ms), both the final and the driver tube dissipation must be reduced to a minimum. The final and driver anode HV supplies are therefore modulated according to the regime of operation, the final HV supply rising to 20 kV at 4 A bias current only during the short high power pulse for LHC bunching.

In the transient beam loading regime, the feedback is only required to reduce the induced gap voltage to the brink of the gap multipactor onset, whence the induced signal falls into the lowest multipactor level and the amplifier does very little work. This is an unforeseen but very fortuitous side effect of low voltage gap multipactor!

6.2.8 40 MHz: electric coupling

The 40 MHz cavity has a mushroom shaped gap electrode (cf. Fig. 44) which makes capacitive coupling possible. A coupling antenna with an asymmetric profile extends from the ceramic window coupler port towards the gap electrode, the capacity being adjustable, via the asymmetry, by rotation in a range of approximately 2...5 pF [52]. This allows to adjust the voltage step-up ratio – it was used to increase the gap voltage of the second 40 MHz cavity. The resulting detuning can be compensated for by means of the coarse tuner (see below). The ceramic coupling window is dimensioned to accept the final anode HV which is present on the coupling antenna so as to prevent any tendency to multipactor. During conditioning of the cavity gap (after venting), excessive multipactor may however occur, and the thus created electrons can induce a heavy discharge of the HV to ground.

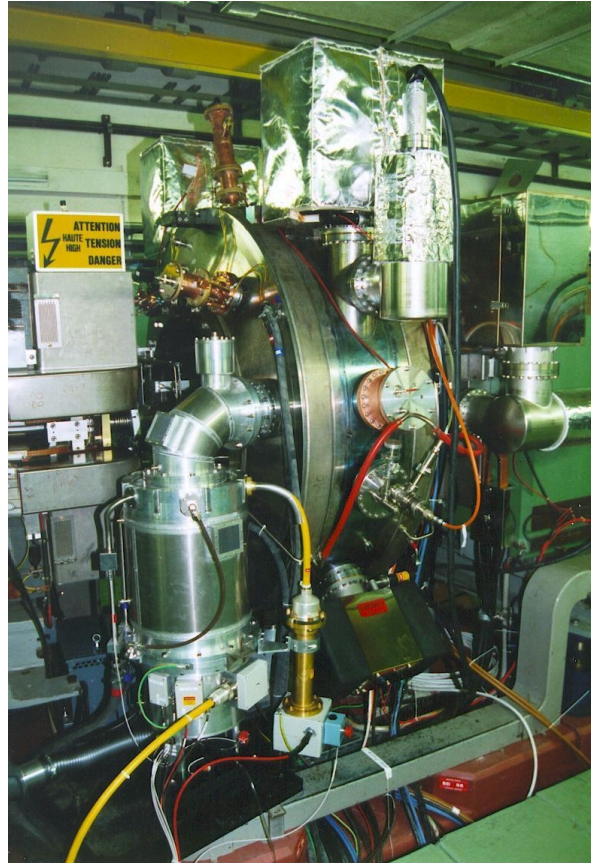


Fig. 46 Installed 80 MHz cavity. The final amplifier can be seen in the foreground.

6.2.9 80 MHz: magnetic coupling

Although less convenient, a magnetic coupling loop was adopted for the 80 MHz cavity since the gap electrode is much smaller, and a capacitive antenna would be excessively long. The self inductance of the coupling loop strongly affects the resonances in the line to the final anode. This inductance was kept down to 140 nH by making the loop from a wide (6 cm) strip, and by using the cavity wall for the loop return [58]. To prevent multipactor, the loop is DC isolated from the wall and kept at a potential of 1.2 kV; it is also water cooled for the long duty cycle lepton operation. The coupler step up ratio to the gap is 1:10 so that the equivalent coupler output is about 30 kV peak which further reduces to 8 kV at the ceramic window.

6.2.10 Tuner

Each cavity is equipped with two tuners, referred to as “coarse tuner” and “servo tuner”. The coarse tuners are manually adjusted in order to set the resonance frequency of the cavity to the centre of the tuning range of the servo tuner. This tuner compensates slow variations of temperature and atmospheric pressure, essentially during the high duty cycle lepton operation.

The tuners of the 40 MHz cavity consists of a large coupling loop, which is – for the servo tuner – coupled via a feed-through to a variable capacitor. For the coarse tuner, the loop is simply short-circuited – the tuning is obtained by the adjustment of the orientation of this loop in the magnetic field [54, 55].

The tuners of the 80 MHz cavity are capacitively coupled piston tuners. Coarse tuner and servo tuner are identical, but only the servo tuner is equipped with a motor drive [60]. For the obtained tuning ranges, refer to Table 20 below.

6.2.11 Parameters

The following Table 20 summarises some of the parameters obtained with the 5 realised cavities. All cavities are installed, but nominal operation requires only one 40 MHz and two 80 MHz systems, the others are considered “spare”. It should be noted that some of the given numbers are just indications; the loaded Q e.g. depends subtly on amplifier bias current and DC anode voltage, the step up ratio depends slightly on the tuning, etc.

Table 20
Parameters of the installed systems.

	40 MHz systems [52]		80 MHz systems [58]		
Cavity, location in PS, Installation date	“Susan”, SS 78, 9/96	“Tjitske”, SS 77, 3/99	“Lydia”, SS 89, 1/98	“Barbara”, SS 88, 2/98	“Anne”, SS 13, 2/99
Nominal DC beam current	40 MHz • 10 ¹¹ e = 0.64 A, (cf. [1], p. 169)				
Beam current (assumed Gaussian, $\sigma = 1$ ns)	0.97 · 2 · 0.64 A = 1.24 A		0.88 · 2 · 0.64 A = 1.13 A		
Operating frequency [MHz]:	84 · 0.476843 = 40.055		80.11		
Measured Q_0, Q_L :	18200, ~ 10000		22600, 11800		
Calculated R_s/Q_0 :	33 Ω		56 Ω		
Shunt impedance R_s, R :	600 k Ω , ~ 330 k Ω		1.26 M Ω , 660 k Ω		
Nominal gap voltage [kV]:	3...300		300		
Obtained gap voltage [kV]:	2...360	4...470	> 400		
Pulse length, duty cycle:	10 ms, 0.4 %		300 μ s, < 0.1 % @ 400 kV (LHC) 800 ms, 25 % @ 210 kV (lepton option)		
Zero to full voltage rise time:	25 μ s		15 μ s		
Feedback loop gain:	43 dB		41 dB		
Feedback group delay:	220 ns		220 ns		
Feedback reduced R, Q :	2.3 k Ω , 70		5.6 k Ω , 100		
Voltage step-up gap/anode	21	29	24		
Servo tuning range [MHz]	39.96...40.18	39.95...40.11	79.82...80.18	79.77...80.14	79.86...80.22

6.2.12 Overall system design

The following Fig. 47 shows a block diagram of the 40 MHz system. For simplification, the interlocks system is omitted. The 80 MHz system is conceptually similar.

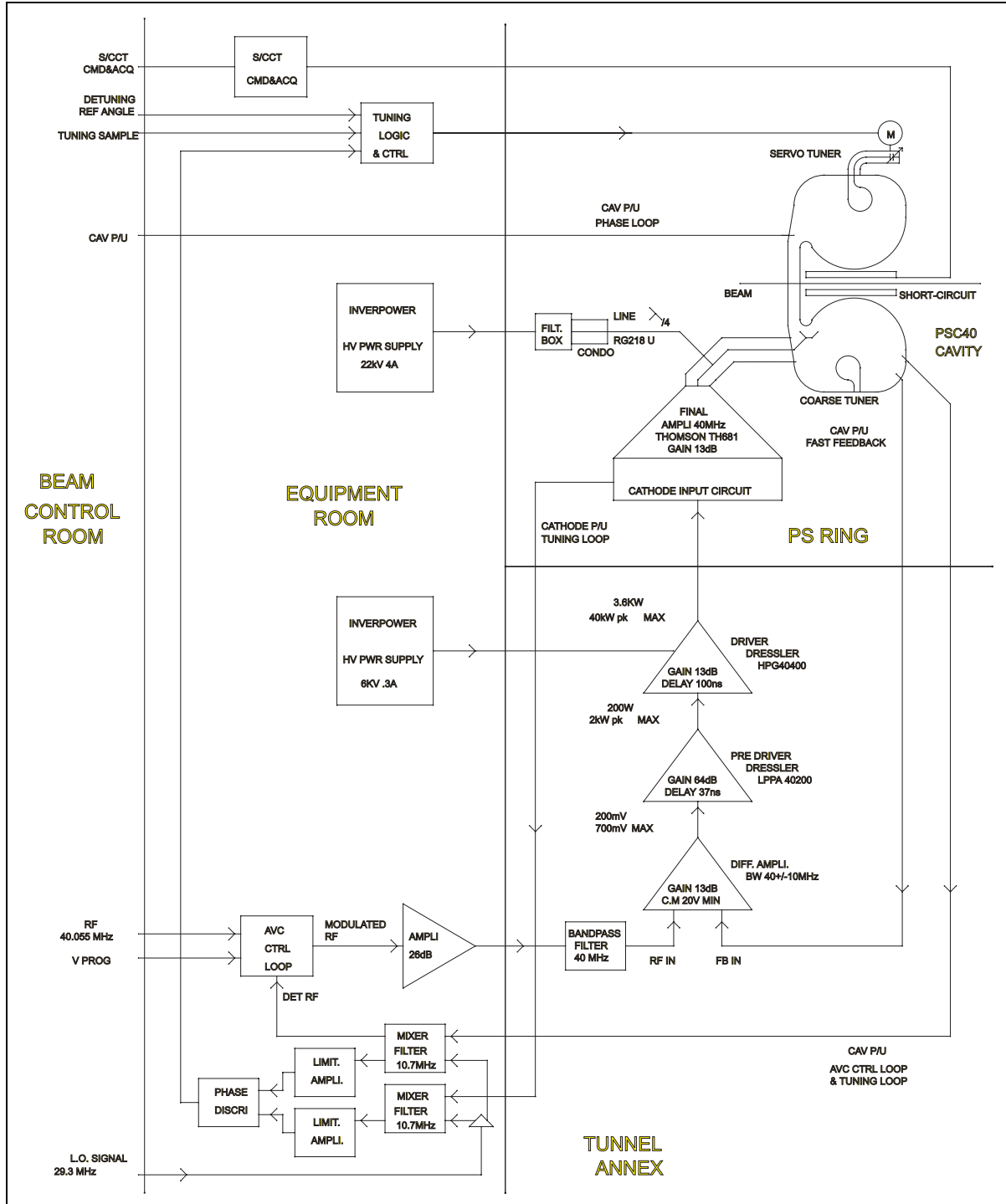


Fig. 47: Simplified block diagram of the 40 MHz system. The final stage of the power amplifier is mounted directly onto the cavity. The driver amplifiers are located in the tunnel annex, situated approximately 10 m from the cavity.

7. TRANSVERSE EMITTANCE CONSERVATION AND MEASUREMENT

7.1 Emittance conservation issues

The conservation of the transverse emittance for the LHC beam throughout the injection chain is an important issue mainly for the following reasons. The performance of a collider is determined by the luminosity,

$$L = \frac{k_b N_b^2 f_{\text{rev}} \gamma}{4\pi \epsilon_n \beta},$$

which is proportional to the number of events per second and thus has to be maximised. This favours a large particle number per bunch N_b and a small normalised emittance ϵ_n . However, space charge effects at low energies work against this by limiting the achievable beam brightness N_b/ϵ_n . The strategy is therefore to produce the highest possible brightness beam at low energy and then to transport it through the injector chain by carefully avoiding any performance loss due to emittance blow-up. More detailed considerations can be found in Chapter 1.

The proton injection chain for the LHC consists of the Linac2, the PSB, the PS and the SPS. The 50 MeV beam coming from the LINAC is injected into the four vertically stacked PSB rings using a multi-turn injection. At 1.4 GeV, the four rings are consecutively ejected towards the PS, filling half the PS circumference. After injection of a second batch from the PSB, the beam is accelerated to 26 GeV/c in the PS and ejected towards the SPS. The emittance budgets along the injection chain for the different LHC beams are summarised in Table 21.

Table 21
LHC initial, nominal and ultimate proton beam intensities and emittances.

	Linac	PSB	PS	SPS
Commissioning				
p/LHC bunch			$1.7 \cdot 10^{10}$	$1.7 \cdot 10^{10}$
p/pulse	180 mA	$1.80 \cdot 10^{11}/\text{ring}$	$1.4 \cdot 10^{12}$	$4.1 \cdot 10^{12}$
$\epsilon_n (= (\beta\gamma)_{\text{rel}} \cdot \sigma^2/\beta)$	1.0	0.6 (shaving?)	0.8	0.9 (scraping?)
Nominal				
p/LHC bunch			$1.1 \cdot 10^{11}$	$1.1 \cdot 10^{11}$
p/pulse	180 mA	$1.15 \cdot 10^{12}/\text{ring}$	$9.2 \cdot 10^{12}$	$2.7 \cdot 10^{13}$
ϵ_n	1.0	2.5	3.0	3.5
Ultimate				
p/LHC bunch			$1.7 \cdot 10^{11}$	$1.7 \cdot 10^{11}$
p/pulse	180 mA	$1.80 \cdot 10^{12}/\text{ring}$	$1.4 \cdot 10^{13}$	$4.1 \cdot 10^{13}$
ϵ_n	1.0	2.5	3.0	3.5

The multi-turn injection into the PSB and strong space charge effects lead naturally to the largest emittance blow-up in the injection chain. It has to be optimised to achieve a beam with the required high brightness (small emittance). This emittance should then be conserved throughout the injection chain. Therefore, besides the control of resonances and instabilities, the beam-transfers between PSB, PS and SPS are the major concerns. When transferring a beam between two machines, there are three main sources for rms emittance blow-up:

- injection mis-steering:
$$\frac{\Delta\epsilon}{\epsilon} = \frac{1}{2\epsilon} \left(\frac{\Delta x / \sqrt{\beta}}{\sqrt{\beta} \Delta x' + \alpha \Delta x / \sqrt{\beta}} \right)^2,$$
- betatron mismatch
$$\frac{\Delta\epsilon}{\epsilon} = \frac{1}{2} \frac{\beta}{\beta + \Delta\beta} \left(\frac{\Delta\beta / \beta}{\Delta\alpha + \alpha \Delta\beta / \beta} \right)^2,$$

- dispersion mismatch
$$\frac{\Delta\epsilon}{\epsilon} = \frac{\sigma_p^2}{2\epsilon} \left(\frac{\Delta D / \sqrt{\beta}}{\sqrt{\beta}\Delta D' + \alpha\Delta D / \sqrt{\beta}} \right)^2.$$

In the formulae above, α and β are the Twiss-functions in the matched case and $\Delta\alpha$ and $\Delta\beta$ are the deviations due to the mismatch, the same applies for the dispersion function D and D' ; $\sigma_p = (\Delta p/p)_{\text{rms}}$ is the standard deviation of the relative momentum spread. It should be noted that the emittance blow-up due to mis-steering and dispersion mismatch is inversely proportional to the initial emittance. Thus, these two error sources are particularly important for the LHC beam due to its small design emittance.

7.1.1 Transfer PSB to PS:

The foreseen maximum emittance blow-up between PSB ejection and PS ejection is $0.5 \mu\text{m}$ (Table 21, nominal). Assuming that $0.2 \mu\text{m}$ are assigned to effects during acceleration in the PS, the remaining $0.3 \mu\text{m}$ can be split into three equal parts for the blow-up sources mentioned above and one can quote typical values for maximum tolerable steering and matching errors between the two machines. The centre of the straight section 45 in the PS (location of the fast injection kicker) was chosen as reference point for the calculations⁶. The Twiss-parameters are $\beta_x = 20.3 \text{ m}$, $\beta_z = 11.9 \text{ m}$, $\alpha_x = \alpha_z = 0$, $D_x = 3 \text{ m}$, $D'_x = 0$. It was assumed that the errors are only in position, beta-function and Dispersion and are zero for the derivatives. The maximum tolerable mis-steering or mis-matches are quoted in Table 22.

Table 22
Maximum tolerable steering/matching errors for the transfer PSB to PS:
each effect alone causes an increase in ϵ_n of $0.1 \mu\text{m}$.

PS-section 45 centre	horizontal	vertical
Beta-function	20.3 m	11.9 m
Dispersion	3.0 m	-
Injection mis-steering	$\Delta x = 0.9 \text{ mm}$	$\Delta z = 0.7 \text{ mm}$
Betatron mismatch	$\Delta\beta = 5.7 \text{ m}$	$\Delta\beta = 3.4 \text{ m}$
Dispersion mismatch	$\Delta D = 0.7 \text{ m}$	-

The optics presently in use for the transfer between PSB and PS is not well matched in terms of dispersion. Up to now, this fact was not important but for the LHC beam, with a small transverse emittance and a large momentum spread ($\sigma_p = 1.25 \cdot 10^{-3}$), it becomes relevant. To improve on this side, a modified optics [62] that significantly reduces the dispersion mismatch (while preserving the betatron matching) is being tested and verified with a view to use it in the future.

In the case of the PSB the fact that there are four rings which need to be recombined imposes additional difficulties. To minimise the injection oscillations in the PS it is required to individually correct the trajectories of the four bunches. The number of independent correction elements is in theory sufficient, but in practice it is not straightforward to equalise the trajectories from different rings to better than $\pm 1 \text{ mm}$. Furthermore, the reproducibility of the trajectories is not guaranteed and therefore an injection damper will be installed in the PS to provide bunch-by-bunch correction of these residual injection errors (see below).

As far as betatron matching is concerned, the vertical dipoles in the recombination section create optical differences between the rings which cannot be corrected with the present hardware. The effect is small but if required it can be reduced by installing a correction quadrupole [63].

⁶ It should be noted that for the calculation of the emittance blow-up due to mis-steering and dispersion mismatch the unnormalised emittances have to be used.

7.1.2 PS injection damper

A mis-steering of less than 1 mm at PS injection leads to a significant emittance increase of the LHC-type beams (see Table 22). The four beams from the PSB, recombined to one and sent in two batches to the PS, undergo some unavoidable mis-steering because (i) small time-dependent variations of elements such as power converters or RF feedback loops lead to degrading beam orbits; (ii) the eight horizontal and vertical kicker magnets in the PSB-PS beam transport suffer from overshoot and flat-top ripple with frequencies of up to ~ 15 MHz (this latter effect cannot be corrected with steering dipoles). For these reasons, two injection oscillation dampers, one for each plane, are being built for the PS. They feature travelling-wave kicker magnets of 6.25 and 12.5 Ω characteristic impedance with a bandwidth of ~ 20 MHz. Two 3 kW power amplifiers will drive each kicker, which would then be capable of reducing a 3 mm initial injection oscillation to ~ 0.5 mm within 100 μs (50 turns). Recent beam observations suggest that these systems, with an overall bandwidth of ~ 20 MHz, would be quite suitable to also tackle transverse head-tail instabilities during the PS cycle, even at lower power. As the prototype kickers and power amplifiers are not yet finalised and further machine experiments are required to fully understand all aspects of the instabilities, the parameters given here are preliminary.

7.1.3 Transfer PS to SPS:

The beam optics of the TT2/TT10 transfer lines, linking PS and SPS has been reviewed and as a result the dispersion and the betatron matching could be improved [64]. In addition to that, orthogonal tuning knobs, to minimise the unavoidable residual mismatch were developed [65]. To minimise the blow-up due to injection mis-steering, a new damping system will be installed in the SPS [66].

7.2 Beam diagnostic upgrades in view of LHC beams

The high-brilliance LHC-type beams require close observation of possible emittance blow-up during acceleration in Linac2, PSB and PS and during transfers from one machine to the next. In view of these low-emittance beams several diagnostics instruments have been substantially upgraded while a few new ones have been built in order to cope with new diagnostic requirements.

The PSB has received 2 new Secondary Emission Monitor grids (SEM-grids) close to the injection septum. In the 1999/2000 shutdown the SEM-grids in the measurement line will be upgraded and a fast blade scanner as well as 8 new wire scanners for profile measurements in the 4 rings will be installed. The PS measurement targets have been upgraded and new electronics has been developed for their remote control. In addition, tests are being made in view of the development of a non-destructive profile measurement to measure beam profiles during the entire PS acceleration cycle.

7.2.1 SEM-grids at PSB injection

During the 97/98 shutdown 2 new SEM-grids have been installed in the PSB ring 3 in front of the injection septum. One of the SEM-grids sees the beam arriving from Linac2 while the other is designed to observe several turns of the circulating beam.

The SEM-grid in the 50 MeV transfer line is of *standard* type integrating the pulse generated by secondary emission during a single passage. It has 48 wires in each plane with a wire distance of 1 mm. For economic reasons only the inner 24 wires are equipped with an amplifier / Analogue to Digital Converter (ADC) readout chain resulting in a resolution of 1 mm and a coverage of 24 mm. This SEM-grid is used in standard operation now.

The SEM-grid placed in the circulating beam uses a very fast (~ 100 ns rise-time) amplifier in conjunction with a 40 MHz ADC which converts the wire signals and saves the

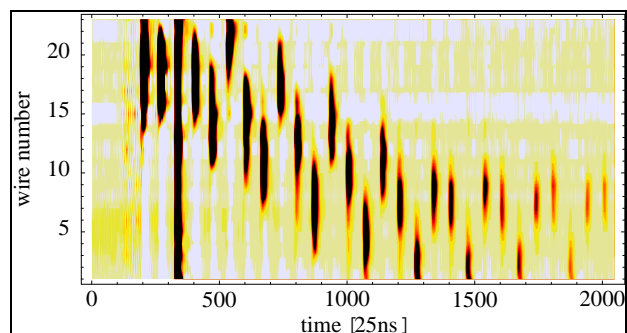


Fig. 48 SEMgrid profiles from several turns in Booster ring 3.

digital values in an associated 2 k-sample memory. With a revolution time of $2.4 \mu\text{s}$ at 50 MeV injection energy approximately 30 turns can be observed. It has 32 active wires placed at a distance of 2 mm covering a width of 64 mm. Only a horizontal wire plane ($50 \mu\text{m}$ wire diameter) is available.

A SEM-grid measuring beam profiles on a turn-by-turn basis can observe betatron mismatch. This method will be used with the SEM-grids in the PS. The PSB SEM-grids have been used for initial test measurements. During several MDs, position oscillations as well as width oscillations could be observed. Similar measurements on the PS SEM-grids are planned.

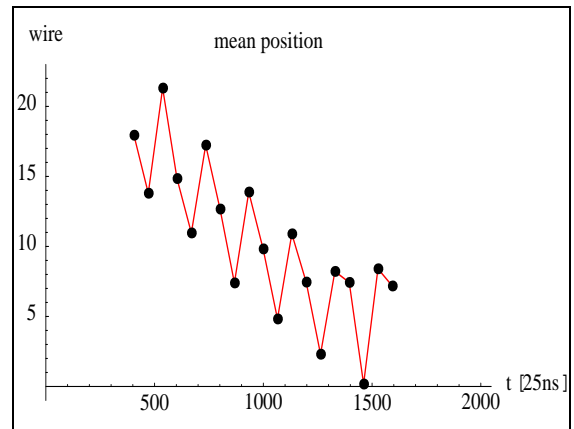


Fig. 49 Position oscillations measured on SEM-grid in Booster ring 3.

7.2.2 The PSB fast wire scanners

Since 1993, fast wire scanners are used successfully in the PS to measure transverse beam profiles to very high precision and it was natural to install these devices also in the PSB in order to get consistent measurements in both machines. It was known that wire scanners could be used for 1 GeV proton beams, but their performance at lower energies, especially at 50 MeV injection energy, was doubtful.

Before investing heavily in 10 new wire scanners (1 horizontal and 1 vertical for each of the 4 rings + 2 spares) the spare PS wire scanner was mounted in ring 1 of the PSB for investigation. During MDs in 97 and 98 its performance was tested and results compared to other measurements already available (BeamScope in the PSB, PSB measurement line and SEM-grids in TT2).

The PS wire scanner uses a scintillator and photomultiplier system in order to detect secondary particles created by the interaction of the circulating beam with the passing wire. This method works fine down to proton energies of a few hundred MeV but fails at very low energies (below the pion creation threshold). In order to cover the full PSB energy range we tried to measure the secondary emission current from the wire instead of detecting the secondary particle on the scintillator (Fig. 50).

We obtained very clean profiles even at 50 MeV proton energy. Comparison between profiles taken with the two detection methods showed no difference. Since the test measurements with the spare wire scanner yielded convincing results, the TRIUMF laboratory (Vancouver) has been charged to build 10 such devices of which 8 are scheduled to be installed during the 99/2000 shutdown.

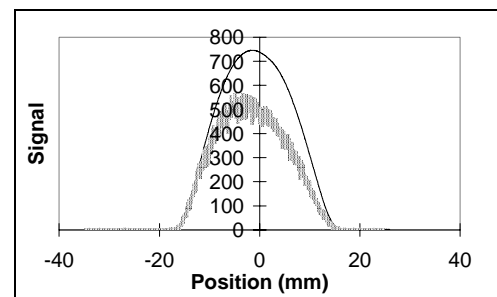


Fig. 50 Profile taken with photomultiplier (grey, noisy profile) and secondary emission at 50MeV.

7.2.3 The fast blade scanner

Until the fast wire scanners become available in all PSB rings, beam emittance is measured with the BeamScope. This device consists of a set of deflector magnets that drives the beam into a fixed aperture limitation. The beam is scraped away and the beam losses are detected on a DC Beam Current Transformer (DCBCT). Since this method modifies the beam orbit, which in turn is corrected by the RF feedback system, doubts existed about the validity of its results in particular for low emittance LHC-type beams.

A cleaner way of performing the same measurement is to leave the beam in its position and move the aperture limitation instead. This is done with the fast blade scanner prototype, a device that has also been constructed at TRIUMF. It consists of a fast moving blade ($\sim 10 \text{ m/s}$) which traverses the beam while the losses are observed with the DCBCT. The device is being tested at CERN and is also scheduled to be installed in PSB ring 1 during the 1999/2000 shutdown. It will allow comparison measurements with the BeamScope and the wire scanners.

7.2.4 The PSB measurement line

The PSB measurement line is equipped with 3 SEM-grids per plane, to measure the emittance of the beam sent to the PS. Their mechanisms are more than 20 years old and would need replacement. It was decided that instead of replacing them it would be favourable to have new, higher resolution grids installed permanently in the beam. The new grids will consist of a series of wires instead of ribbons to minimise the interaction with the beam. The number of wires per plane has been increased to 32 and the wire distance decreased to 1 mm for the outer SEM-grid and 0.5 mm for the central one. The analogue electronics chain will be replaced and the digital electronics will use VME ADCs instead of the old CAMAC scanning ADCs. The installation will be done during the 99/2000 shutdown.

7.2.5 The PS measurement targets

In addition to the wire scanners, the measurement targets can be used in the PS to measure beam sizes. The target consists of a fork with 2 fingers whose distance can be adjusted. The fork flips into the beam and beam losses are observed on the DCBCT.

The measurement targets, which can also be used for limiting the aperture, scraping the beam halo away, were only used manually up to now.

In order to remotely control the devices, the motors adjusting the distance of the fork fingers had to be replaced. New electronics had to be developed giving remote access to its internal parameters (fork finger distance, retention magnet, flip timing etc.)

In addition, an application program controlling the devices, reading the beam loss from the DCBCT and displaying the results in a user-friendly way was developed from scratch. The system is currently undergoing its final tests.

7.2.6 Non destructive profile measurement in the PS

Each of the previously described profile measurements is only capable of measuring the profile at a single instant within the acceleration cycle. It would be very desirable to be able to observe the beam profile evolution along the acceleration cycle in a continuous manner. This can only be done in a non-invasive way.

First test measurements are being made, using the light emitted from excitation of rest-gas molecules. In order to increase the light intensity, a gas (Xenon or Argon) is injected into the vacuum chamber thus creating a pressure bump. Test measurements with protons using the fast wire scanner have shown no significant beam blow-up up to pressures of 10^{-6} torr. This indicates that future measurements could be done parasitically as long as no heavy ions are accelerated in the machine (the lifetime of heavy ions is reduced drastically by bad vacuum due to stripping and recombination effects).

The main question to be answered before constructing a diagnostic device based on light emission from the rest-gas is the resolution that can be reached by such a detector.

7.3 Other beam diagnostics: new, improved, modified

Not only the emittance and profile measurement devices (Section 7.2), but many other beam measurement and diagnostics systems in the LHC pre-injector chain of accelerators (Linac2, PSB rings and PS) underwent a close scrutiny to highlight the problems and to propose solutions for the essential elements of the LHC filling scheme. While the changes required at the Linacs were minimal, close attention had to be paid to the existing systems in the PSB rings, PS and the beam transfer tunnel TT2. Many systems had to be improved and modified, essentially to cater for the new RF harmonics in both the PSB and the PS.

In 1993, the successful testing of the ideas behind the LHC filling scheme had shown that the existing PSB closed orbit measurement system was able to handle the new RF beam structures to a large extent, though perhaps not perfectly. No major changes have been carried out in this system for

the purposes of this study, however, it is envisaged that the PSB closed orbit system will undergo a hardware upgrade to perfectly match the beam characteristics in the PSB in the LHC era.

A completely new tune measurement system [67, 68] but based on the existing “Q-kickers” [69] for each of the four PSB rings has been developed, using synchronised beam excitation with a small-amplitude, one-turn kick and obtaining fast fourier transformation spectra using a DSP Board. The kicker pulser length is gated to the varying revolution period (1670 ns at injection to 570 ns at extraction) and similarly, the ADC is synchronised to sample the signals at four times the revolution frequency. The system is fully integrated into the standard VME based Controls System. Tune measurements may be performed every 10 ms in both planes for each of the 4 rings in the PSB, through the full acceleration ramp (50 MeV – 1.4 GeV) in the nominal 1.2 s PSB cycle (Fig. 51). Measurements have shown that the amplitudes of the transverse oscillations generated by the existing, small-amplitude pulser are sufficiently small not to affect the beam emittance. Hence, tune measurements may be carried out all the time without affecting the beam. However, if it is necessary to improve the measurements near 1.4 GeV, a new, controllable, larger amplitude kicker pulser is foreseen for implementation in the near future.

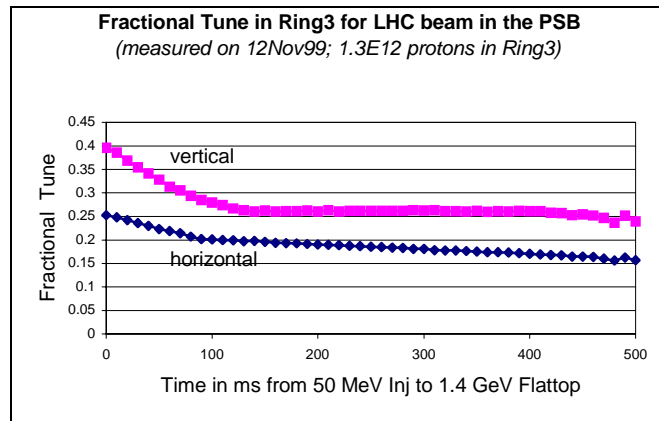


Fig. 51 PSB tune measurement.

For the PSB to PS transfer channel, the digital system used for the position pickups needed minor changes to cater for the new RF structure of the beam.

In the PS Ring, substantial work had to be carried out in the closed orbit and trajectory measurement system. The PS had traditionally a trajectory measurement system based on measurement of beam position over 2 consecutive turns near injection as well as at any instant in the acceleration cycle. Given the new RF harmonics and gymnastics in the PS required for LHC operation, considerable hardware and software additions and modifications were necessary. This has led to continuity with the traditional trajectory measurements as well as availability of additional capabilities as required for the double-batch injection, new beam structures and so forth, right up to, but not including measurements at the extraction of 84 bunches. The new trajectory and closed orbit system is fully integrated in the controls system and is spread over 3 networked VME crates [70-72].

For the beam current transformers in the PS Ring, the major implication has been the advent of double-batch filling from the PSB. However, most of the changes required are at the level of the timing and specific equipment (ADC channels, triggers and specific software) to provide additional measurement capabilities for this mode of operation. For example, the PS Ring DCBCT required an extra facility to permit measurement of the second batch, in addition to first one already injected on the same PS cycle. Similar changes are reflected in other systems like the one used in the PS for measuring beam current in each of the first six turns at injection for protons.

In the beam transfer line TT2 between the PS and SPS, two new electrostatic wide-band pickups have been developed and installed to observe the particular characteristics of the LHC type of beam (84 bunches, 4 ns width, 25 ns separation). The pickups are judiciously spaced apart in sections 208 and 228 (to determine position and angle of each of the 84 bunches) and have electrodes based on an earlier design for a special 200 kHz - 300 MHz wide-band pick-up in the section 98 of the PS ring. With new electronics purposely developed, the bandwidth of the pickups has been extended to ~ 6 kHz to 400 MHz. The signals from the electrodes as well as the sum signals are permanently connected to the analogue observation system and are routinely used for study purposes. The pickups also prove useful in observing other types of beams extracted from the PS to the TT2 transfer line, particularly the classical proton 5-turn extraction beam for the SPS. Further experience with this equipment has to be obtained before connecting it to the standard control system.

For beam current measurements in the TT2 transfer line, the LHC type of beam does not pose any particular problems. However, to supplement measurements from the existing fast beam current transformer TRA203, the lead ion transformers TRA372 and TRA379 have been modified to measure proton beams. These transformers, built for the lead ion operation from 1994 onwards, measure the stripping efficiency and are installed just at the switching of the beam from the PS controlled TT2 beam line to the SPS controlled TT10 beam line. A new transformer, TRA386, has been installed before the D3 beam dump at the end of TT2 to verify consistency of measurements under all operations. The fast beam current transformer measurements are now completely uniform with automatic range switching between the three ranges (up to $4 \cdot 10^{10}$, $4 \cdot 10^{10} - 1 \cdot 10^{12}$, $1 \cdot 10^{12} - 4 \cdot 10^{13}$ electric charges) and satisfying all known requirements for the SPS and LHC needs.

8. POSSIBLE FUTURE DEVELOPMENTS

8.1 Means to achieve the specified longitudinal beam parameters

8.1.1 Status of performance

Experiments have shown that the longitudinal beam characteristics are degraded at 26 GeV/c in the PS during the debunching-rebunching process (see Chapter 6). At the nominal intensity the longitudinal emittance blows-up by 40 % so that bunches end-up 20 % too wide in length and energy spread. An instability is responsible for this effect which could be caused by the high order resonances in the 114 MHz cavities used for lepton acceleration. Although the removal of these cavities is planned after the year 2000, the debunching-rebunching process will remain sensitive to perturbations and a more robust procedure is worthwhile considering.

Moreover the nominal scheme provides a train of 84 bunches without any gap for the rise-time of the fast ejection kicker [47], so that 3 bunches are either lost or subject to large transverse oscillations and subsequent filamentation in the SPS.

8.1.2 Multiple splitting

The proposal [48] is to avoid debunching and to change the number of bunches using multiple splitting operations as represented in Fig. 52.

Captured on harmonic 7 in the PS, the bunches are split in three at 1.4 GeV using appropriate amplitude and phase parameters on three groups of cavities operating on harmonics 7, 14 and 21, respectively. As predicted from simulation results (Fig. 53) and as observed during recent machine experiments in the PS (Fig. 54), that process preserves longitudinal emittance.

Bunched on harmonic 21, the beam is then accelerated up to 26 GeV/c where each bunch is split twice in two using the process which has been demonstrated in regular operation. A new 20 MHz 20 kV RF system is required at that stage. Finally each original bunch has been split in 12, and 84 bunches are created if all of the 7 buckets are filled.

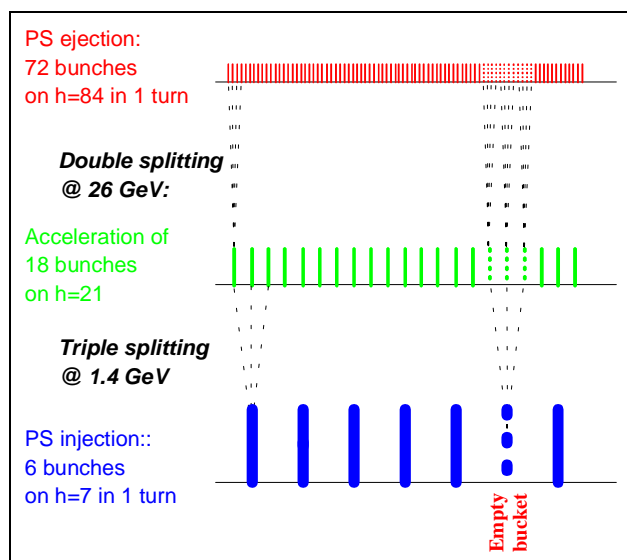


Fig. 52 Generation of the bunch train for LHC without debunching-rebunching.

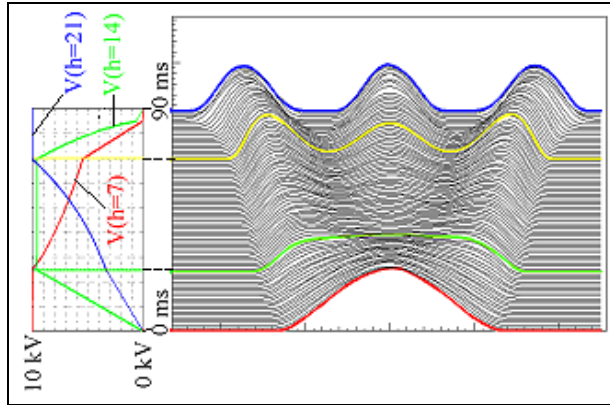


Fig. 53 Triple splitting in the PS (ESME simulation).

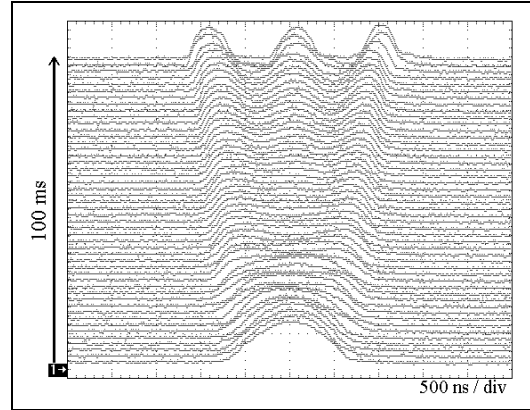


Fig. 54 Experimental observation of triple splitting in the PS.

The following features characterise that method:

- the beam is always under control of the rf, so that phase oscillation damping loops can be active;
- the beam is never debunched, so that the microwave instability threshold is less of a concern;
- the gap without particle corresponding to a missing bunch is preserved;
- since only 7 (instead of 8) bunches are needed from the PSB, the intensity per ring and the beam brightness have to be 15 % higher than for the original scheme.

Injecting only 6 bunches, the final bunch train contains 72 bunches and 12 consecutive empty buckets, providing a gap of ~ 320 ns (13×25 ns) for the rise-time of the ejection kicker. These data are summarised in Table 23.

Table 23
New / nominal PS complex operation for filling LHC.

	Nominal	“Multiple Splitting”
# bunches per PSB ring	1	1
# PSB cycles per PS cycle	2	2
# bunches from PSB per PS cycle	8	6
h at PS injection	8	7
Bunch splitting at 3.5 GeV/c	1=>2	1=>3
h between 3.5 and 26 GeV/c	16	21
# bunches between 3.5 and 26 GeV/c	16	18
Gymnastics at 26 GeV/c	Debunching-rebunching	Double bunch splitting (1=>4)
h at PS extraction	84	84
# bunches to SPS per PS cycle	81 (3 bunches “lost” due to PS extraction kicker rise time)	72
PS intensity at 1.4 GeV for $1.1 \cdot 10^{11}$ p/LHC bunch (“nominal”)	$9.2 \cdot 10^{12}$	$7.9 \cdot 10^{12}$
Intensity per PSB ring	$1.15 \cdot 10^{12}$	$1.32 \cdot 10^{12}$

Since the bunch train delivered by the PS has 9 bunches less than initially foreseen, the nominal LHC filling scheme is not efficient enough and new schemes had to be designed. Analysis [73] has shown that similar performance can be obtained for the experiments at the cost of a minor modification to the LHC injection kicker.

8.2 Other improvements

8.2.1 Bunching factor at low energy

The space charge effects at low energy limit the ultimate transverse beam brightness of the beam. The Laslett tune-shift being inversely proportional to the bunching factor B_f ($B_f = \text{mean beam current} / \text{peak beam current}$), the techniques which help reduce the peak beam current are beneficial for achieving and keeping small transverse emittances.

A classical solution is to use a second harmonic RF to decrease the longitudinal focussing for the particles at the core of the bunches and obtain “flat bunches”. This is in regular operation in the PSB since the end of the eighties, and it has also been implemented as part of the preparation of the PSB for LHC. However that technique is not applicable to the PS which does not have enough RF systems to support such a mode of operation.

Another solution is to modify the distribution of particles in the bunch and make it hollow, so that the line density has a flat top although using a single harmonic RF. If such characteristics are obtained at injection energy in the PSB, both the PSB and the PS will profit from reduced Laslett tune-shifts. Various methods have been tried and recent experimental results are very encouraging [74].

8.2.2 Special beam time structure for handling electron clouds in the LHC

Electron multipactoring has recently been diagnosed as a dominant contributor to the heat load to the LHC cryogenic system, potentially limiting drastically the machine performance [75]. Among the many actions envisaged to solve the problem, a number of them require the beam time structure to be modified, either doubling the distance between bunches or introducing more gaps in the bunch train.

The multiple splitting technique of Section 8.1 is extremely flexible. It offers several possibilities of changing the bunch train in ways which could not be achieved with the nominal debunching-rebunching procedure.

ACKNOWLEDGEMENTS

The authors express their gratitude for the continuous managerial support of A. Astbury, Director of TRIUMF, L. Evans, CERN LHC Project Leader, K. Hübner, CERN Director of Accelerators, and D.J. Simon, former CERN PS Division Leader. The way they removed problems in the spirit of mutual understanding made this CERN-TRIUMF joint venture so successful.

Amongst their many other colleagues in TRIUMF and the CERN Divisions EST, LHC, PS, SL and ST, the authors would like to especially acknowledge the help of J.M. Cravero, M. Corcelle, L. Ellstrom, D. Evans, H. Fiebiger, W. Fritschi, M. Georges, M. Haase, P. Harmer, M. Hourican, B. Keeley, E. Knight, M. Lindroos, A. Lombardi, A. Marmillon, S. Milner, F. Pedersen, R. Scrivens, G. Simonet.

APPENDIX: LIST OF RELEVANT PARAMETERS

Machine/Parameter	Unit	Commissioning	Nominal / common	Ultimate	Comments
RFQ					Four-vanes type
Input energy	keV		90		
RF frequency	MHz		202.5		
Output energy	keV		750		
Output intensity during pulse	mA		200		
Beam pulse length	μ s		120		
Transverse emittances ϵ_n	μ m		0.6		$\epsilon_n = (\beta\gamma) \sigma^2 / \beta_{twiss}$
$\Delta p/p$ (2σ)	10^{-3}		17.5		
Repetition time	s		1.2		
LINAC 2					Alvarez type
Input energy	MeV		0.75		
Number of tanks			3		10/30/50 MeV
RF frequency	MHz		202.5		
Output energy	MeV		50		
Output intensity during pulse	mA		180		
Beam pulse length	μ s		>30		100 μ s achieved
Transverse emittances ϵ_n	μ m		1.2		Equal both planes
$\Delta p/p$ (2σ)	10^{-3}		1.5		
Repetition time	s		1.2		
PSB (4 rings)					
Radius	m		25		¼ of PS
Number of lattice periods			16		lattice B-F-D-F-B
Max. β_x, β_y, D (dispersion)	m		7.6, 19.0, 1.5		
γ_r			~4.1		
Injection energy	MeV		50		
Main magnet field	T		0.1256		
Main magnet current	A		584		
Number of inj. turns		~1	~2	~3	Hor. betatron stacking
Q_x/Q_y		4.27/5.50	4.26/5.40	4.27/5.45	Subject to optimisation
revolution period	μ s		1.67		
RF h=1 system voltage/turn	kV		8		1 cavity/ring
Frequency	MHz		0.6-1.8		
h=2 system voltage/turn	kV		8		1 cavity/ring for bunch flattening
Frequency	MHz		1.2-3.9		
Number of bunches/ring			1		
Ejection energy	GeV		1.4		
Momentum	GeV/c		2.141		
Main magnet field	T		0.867		
Main magnet current	A		4030		
Q_x/Q_y			4.17/5.23		
Revolution time	ns		572		
Bunches/ring			1		
Beam intensity/ring	10^{12}	0.18	1.15	1.8	= 10.5 LHC bunches
ϵ_n	μ m	0.6	2.5	2.5	
Bunch length	ns		190		
$\Delta p/p$ (2σ)	10^{-3}		2.5		
Bunch area	eVs		1.45		
Bunch area/LHC bunch	eVs		0.14		
Repetition time	s		1.2		
Number of pulses to fill PS			2		

Machine/Parameter	Unit	Commissioning	Nominal / common	Ultimate	Comments
PS Radius Number of lattice periods Number of superperiods Number of magnets Max. β_x , β_y , D (dispersion) γ_r	m		100 25 10 100 22.3, 22.6, 3.0 6.1		(FD)O(DF)O Combined function
Injection energy Momentum Main magnet field Main magnet current Q_x/Q_y Revolution period Flat bottom length # PSB batches per injection Repetition time (LHC cycle)	GeV GeV/c T A μ s s s		1.4 2.14 0.101 406? 6.15/6.28 2.288 1.2 2 3.6		Subject to optimization Each batch fills 1/2 PS
RF accelerating system Number of cavities Max. voltage/turn Frequency range	 kV MHz		 12 240 3-10		Relevant for LHC beam Ferrite-loaded
RF fixed-frequency systems 40 MHz numb. of cavities Voltage/turn 80 MHz numb. of cavities Voltage/turn	 kV kV		 2 600 3 900		Bunch spacing 25 ns Bunch shortening 4 ns
Longitudinal parameters # bunches after injection RF harmonic at injection			8 8		
bunch splitting momentum # bunches after splitting Bunch area Bunch area/LHC bunch	GeV/c eVs eVs		3.56 16 1.0 0.19		h=8 => 16 Controlled blow-up
debunch-rebunch moment. Duration of process After rebunch.: # of bunches Bunch length $\Delta p/p$ (2σ) Bunch area Bunch rotation: bunch length $\Delta p/p$ (2σ) Bunch area	GeV/c ms ns 10^{-3} eVs ns 10^{-3} eVs		26 150 84 12 0.7 0.35 4 2.2 0.35		h=84
Ejection energy Momentum Main magnet field Main magnet current Revolution time	GeV GeV/c T A μ s		25.1 26 1.256 5140? 2.1		
Beam intensity p/pulse Intensity/LHC bunch ϵ_n PS pulses per SPS cycle	10^{12} 10^{11} μ m 3	1.4 0.17 0.8	9.2 1.1 3 3	14.3 1.7 3	84 LHC bunches

REFERENCES

- [1] P. Lefèvre, T. Petterson (Ed.), *The Large Hadron Collider, Conceptual Design*, CERN/AC/95-05(LHC), Oct. 1995.
- [2] F. Blas et al., *Conversion of the PS complex as LHC proton pre-injector*, Proc. PAC '97, p. 973, Vancouver, Canada, 1997.
- [3] P. Collier (editor), *The SPS as injector for LHC, conceptual design*, CERN-SL-97-07, DI, 1997.
- [4] The PS Staff, reported by K. Schindl, *Partial test of the PS complex as LHC proton pre-injector*, Proc. EPAC '94, p. 500, London, UK, June 1994.
- [5] K. Schindl, *Conversion of the PS complex as LHC proton pre-injector: Project proposal*, PS/DI/Note 94-17, 1994.
- [6] C.E. Hill, A.M. Lombardi, E. Tanke, M. Vretenar, *Present Performance of the CERN Proton Linac*, Proc. 1998 Linear Accelerator Conference, Chicago, ANL-98-28, p. 427, 1998.
- [7] C.E. Hill, A.M. Lombardi, W. Pirkl, E. Tanke, M. Vretenar, *Performance of the CERN Linac2 with a High Intensity Proton RFQ*, Proc. 1994 Linear Accelerator Conference, Tsukuba, p. 175, 1994.
- [8] E. Tanke, *Realignment of the Linac2 LEBT During the 1994/1995 Machine Shutdown*, CERN PS/Hi-Note 95-10 (MD), 1995.
- [9] J.L. Vallet, M. Vretenar, M. Weiss, *Field Adjustment and Beam Analysis of the High-Intensity CERN RFQ*, Proc. EPAC '90, p. 1234, Nice, France, 1990.
- [10] M. Vretenar, *Field Emission Measurements on RFQ2 and Recalibration of the Vane Voltage*, CERN PS/RF/Note 97-11 (MD), 1997.
- [11] A.V. Feschenko, A.V. Liiou, P.N. Ostroumov, O. Dubois, H. Haseroth, C. Hill, H. Kugler, A. Lombardi, F. Naito, E. Tanke, M. Vretenar, *Study of Beam Parameters of the CERN Proton Linac using a three dimensional Bunch Shape Monitor*, Proc. 1996 Linear Accelerator Conference, Geneva, CERN 96-07, 1996.
- [12] H. Ullrich, *Proposal for the upgrade of the Booster main magnet power supply*, CERN PS/PO/Note 95-02(tech.), 1995.
- [13] O. Bayard, *Description du filtre d'harmoniques sous station Jura*, CERN LABII/PS/OB/EEK/ Tech.Note-72 1, 1972.
- [14] J. Pedersen, *Technical specification for a 18 Mvar, 18 kV thyristor controlled reactor*, CERN ST-IE-PI/96-193, 1996.
- [15] H. Ullrich, *Rectifier double transformers for upgrading the Booster main magnet supply*, CERN PS/PO/Note 95-23 (Spec.), 1995.
- [16] T. Salvermoser, *New electronics for the regulation and timing of the Booster main power converter*, CERN PS/PO/Note 96-23 (Min.), 1996.
- [17] H. Ullrich, *12 phase thyristor power converters with passive and active filter modulated 0 to 300 A, 520 V*, CERN PS/PO/Note 95-24 (Spec.), 1995.
- [18] H. Fiebiger, F. Gendre, T. Salvermoser, *Modification of Booster magnet circuit grounding layout*, CERN PS/PO Note 97-07(Tech.), 1997.
- [19] M. Benedikt, C. Carli, *Operation of the CERN PS-Booster above 1 GeV - Saturation effects in the main bending magnets and required modifications*, CERN/PS 98-059 (OP), 1998.
- [20] T. Salvermoser, *Specification of a switch mode power supply*, CERN PS/PO/Note 98-54(Spec), 1998.

- [21] H. Fiebiger, F. Gendre, T. Salvermoser, H. Ullrich, *Commissioning Booster Trim Supply*, CERN Memo 19-3-99, 1999.
- [22] F. Völker, *Soft-Switched Mode DC Power Converters for the 1.4 GeV PSB Beam Transfer-line Magnets*, CERN PS/PO Note 96-01 (Spec), 1996.
- [23] F. Völker, *Soft-Switched Mode DC Power Converters for the 1.4 GeV PS-Booster Beam Transfer-line magnets*, CERN PS/PO Note 98-08 (Spec), 1998.
- [24] M. Georges, G. Simonet, *Les Nouvelles Alimentations des Lignes de Transfert PSB-PS et PSB-ISOLDE*, CERN PS/PO Note 98-44, 1998.
- [25] J.P. Royer, *High current with high precision flat-top capacitors discharge power converters for pulsed septum magnets*. CERN/PS/95-13 (PO), 1995.
- [26] J.P. Royer, *Technical specification of the capacitor discharge power supplies for septum magnet of the transfer line PSB-PS*, CERN PS/PO/SPEC94-08, 1994.
- [27] J.M. Cravero, J.P. Royer, *The new pulsed power converter for the septum magnet in the PS straight section 42*, CERN PS/PO/ note 97-03, 1997.
- [28] G.S. Clark, A.J. Otter, P. Reeve, *Magnets for the CERN PS Booster transfer line*, Proc. PAC '97, Vancouver, Canada, 1997.
- [29] M.J. Barnes et al., *New Magnets for the transfer line PSB-CPS*, CERN SL-Note-98-052 MS, 1998.
- [30] D. Evans, M.J. Barnes, B. Evans, R. Nussbaumer, *Rotating coil and data acquisition system for measuring CERN beam transferline quadrupole magnets*, Proc. of IMMW 10, Batavia, Illinois, USA, 1999.
- [31] M.J. Barnes, G.S. Clark, M. Sassowsky, *Three dimensional field calculations compared to magnetic measurements for CERN PSB-CPS transfer line magnets*, Proc. PAC '99, New York, USA, 1999.
- [32] A. Brückner, *Kicking protons, fast and cheap*, 1971 US Particle Accelerator Conference, Chicago, 1-3 March, 1971.
- [33] A. Brückner, *A non-linear step-pulse steepening delay line*, CERN Yellow Report 68-25, July 1968.
- [34] A. Fowler, *The PSB ejection bumper system for LHC*, CERN PS-CA Note 99-22, 1999.
- [35] B. Dumas et al., *PSB ME 10.-19.7.1996: Cooling water in tunnel +7°C*, PS/HL/Note 96-10 (ME), 1996.
- [36] W. Van Cauter, *Adaptation des systèmes de refroidissement et climatisation du Booster en vue du LHC*, CERN ST-CV/96.061/WVC/bm, June 1996.
- [37] R. Cappi, R. Garoby, S. Hancock, M. Martini, J.P. Riunaud, K. Schindl, H. Schönauer, *Beams in the PS complex during the LHC era*, CERN/PS 93-08 (DI), 1993.
- [38] U. Bigliani et al, *The RF Acc. Syst. for the CERN PS Booster*, IEEE Trans. Nucl. Sci. NS-18, No3, p.233, 1971.
- [39] J.E. Griffin, G. Nicholls, *A review of Some Dynamic Loss Properties of NiZn Accel. RF System Ferrite*, IEEE Trans. Nucl. Sci., Vol. NS-26, No.3, June 1979.
- [40] R. Garoby et al, *RF System for High Beam Intensity Acceleration in the CERN PS*, CERN/PS 89-28 (RF), 1989.
- [41] T. Bohl, T. Linnecar, E. Shaposhnikova, W. Sinclair, U. Wehrle, *Study of controlled longitudinal blow-up in the SPS using the 800 MHz rf system*, CERN SL-MD Note 221.
- [42] J. Bento, A. Blas, C. Carli, M. Chanel, J.P. Terrier, *PSB vacuum flanges impedance measurement*, to be published.

- [43] A. Hofmann, F. Pedersen, *Bunches with local elliptic energy distributions*, IEEE transactions on nuclear science, Vol. NS-26, No.3, June 1979.
- [44] F. Pedersen, F. Sacherer, *Theory and performance of the longitudinal active damping system for the CERN PS Booster*, CERN/PS/BR/77-8, February 1977.
- [45] R. Garoby, *Organisation and control of the PS low level RF in 1998*, CERN PS/RF/ Note 97-19, 1997.
- [46] R. Garoby, *A Non-Adiabatic Procedure in the PS to Supply the Nominal Proton Bunches for the LHC into 200 MHz RF Buckets in SPS*; CERN PS/RF/Note 93-17, Nov. 1993.
- [47] R. Garoby, *Longitudinal limitations in the PS complex for the generation of the LHC proton beam*, Particle Accelerators, Vol. 58, Numbers 1-4, pp. 121-136, 1997.
- [48] R. Garoby, *Status of the nominal proton beam for LHC in the PS*, Proceedings of the Workshop on LEP-SPS Performance, Chamonix 1999, pp. 94-98, 1999.
- [49] R. Garoby, *Requirements to the PS RF systems for filling the LHC with 25 ns spacing between bunches*; CERN PS/RF/Note 93-04, Mar. 1993.
- [50] A.J. Hatch, *Suppression of Multipactor in Particle Accelerators*; NIM 41, pp. 261–272, 1966.
- [51] W.D. Kilpatrick, *Criterion for Vacuum Sparking Designed to Include Both rf and dc*; Review of Scientific Instruments 28, No. 10, Oct. 1957.
- [52] R. Garoby, D. Grier, E. Jensen, A. Mitra, R.L. Poirier, *The PS 40 MHz Bunching Cavity*; CERN/PS/97-039, Proc. PAC '97, Vancouver, Canada, 1997.
- [53] E. Jensen, R. Hohbach, A.K. Mitra, R.L. Poirier, *Higher-Order Mode Damping of the CERN PS 40 MHz Cavity*; Proc. EPAC '96, Sitges, Spain, 1996.
- [54] A.K. Mitra: *Servo Tuner for 40 MHz Cavity*, CERN PS/RF/Note 96-20, Jul. 96.
- [55] A.K. Mitra, R.L. Poirier, E. Jensen, *Coarse and Fine Tuners for the CERN PS 40 MHz Buncher Cavity*; Proc. PAC '97, Vancouver, Canada, 1997.
- [56] I. Enchevich, R.L. Poirier, *Perpendicularly Biased Ferrite Tuner for the CERN LHC cavity*; TRIUMF Design Note TRI-DN-97-28, Dec. 1997.
- [57] A.K. Mitra, R.L. Poirier, R. Losito, *Measurements at TRIUMF on a 80 MHz Cavity Model for the CERN PS Upgrade for LHC*; Proc. PAC '97, Vancouver, Canada; 1997.
- [58] D. Grier, E. Jensen, R. Losito, A.K. Mitra, *The PS 80 MHz Cavities*; CERN/PS/98-021(RF), Proc. EPAC '98, Stockholm, Sweden, 1998.
- [59] A.K. Mitra, S. Rose, *Higher-Order-Mode Damping of the CERN 80 MHz Cavity*; TRIUMF Design Note TRI-DN-97-8, Apr. 1997.
- [60] R. Losito, *Design report for the capacitive tuners of the 80 MHz cavity*, CERN PS/RF/Note 96-32, Dec. 1996.
- [61] For some details of the mechanical construction see e.g.: N. Mezin, *Cavités RF 40 et 80 MHz pour PS-LHC*, http://www.cern.ch/CERN/Divisions/EST/MF/ACTIVITES/v_cavites_rf_ps_lhc.html
- [62] M. Martini, T. Risselada, K. Schindl, *Measurement of betatron and dispersion matching between Booster and PS*, CERN PS/AP Note 91-13, CERN, 1991.
- [63] M. Benedikt, A. Jansson, M. Sassowsky, *Proposal for a quadrupole correction magnet in the Booster recombination section*, PS/OP/Note 99-18, CERN, 1999.
- [64] K. Hanke et al, *Measurement and optimisation of the PS-SPS transfer line optics*, Proc. PAC '99., p. 1282, New York, USA, 1999.
- [65] G. Arduini, K. Hanke, *Tuning knobs for the PS-SPS transfer line*, Proc. PAC '99, p. 1284, New York, USA, 1999.

- [66] W. Höfle, *Towards a transverse feedback system and damper for the SPS in the LHC era*, Particle Accelerators, Vol. 58, 1997.
- [67] A. Chapmann-Hatchett, V. Chohan, E.T. D'Amico, *Tune Measurement for the CERN Proton Synchrotron Booster Rings using DSP in VME*, Proc. PAC '99, New York, USA, 1999.
- [68] M. Gasior, J.L. Gonzalez, *New Hardware of the tune measurement system for the Proton Synchrotron Booster Accelerator*, CERN PS/BD/Note 99-10, Sept. 1999.
- [69] H. Koziol, *Q-measurement on the PS Booster*, CERN MPS/INT/BR 74-14, 1974.
- [70] J.L. Gonzalez, *Specification for VME CODD Synchronisation*, CERN PS/BD/Note 98-05(Tech.), July 1998.
- [71] T. Baglin, *High Sensitivity Amplifiers for PS Pick-ups*, CERN PS/BD/Note 98-06 (tech.), July 1998.
- [72] M. Ludwig, *The Synchronisation for the PS Closed Orbit Measurement System: Real time software development and implementation*, CERN PS/BD/Note 99-03(tech.), March 1999.
- [73] J.M. Jowett, *Collision Schedules and Bunch Filling Schemes in the LHC*, LHC Project Note 179.
- [74] A. Blas, S. Hancock, S. Koscielniak, M. Lindroos, F. Pedersen, *New Technique for Bunch Shape Flattening*, Proc. PAC 99, New York, USA, 1999.
- [75] V. Baglin et. al., *Beam-induced electron cloud in the LHC and possible remedies*, LHC Project Report 187, 1998.